UNIVERSITY OF CALIFORNIA,
IRVINE

Biomass Burning Records in Northern High Latitude Ice Cores

DISSERTATION

submitted in partial satisfaction of the requirements
for the degree of

DOCTOR OF PHILOSOPHY

in Earth System Science

by

Mackenzie Marie Grieman

Dissertation Committee:
Professor Eric S. Saltzman, Chair
Professor Claudia I. Czimczik
Professor Ellen R.M. Druffel
Professor James T. Randerson

2016

DEDICATION

To my parents, Fred and Janet Grieman

TABLE OF CONTENTS

LIST OF FIGURES

LIST OF TABLES

ACKNOWLEDGMENTS

I would like to thank my adviser, Eric Saltzman, for his invaluable guidance throughout my Ph.D. He not only supported this work, but taught me how to be a scientist. This work would have not been possible without the support of the past and present members of the Saltzman research group: Murat Aydin, Tom Bell, Mike Lawler, Kristal Verhulst, Jack Porter and Mindy Nicewonger. I also cannot thank Cyril McCormick enough for the numerous times he helped me troubleshoot issues in the lab. He makes what seems impossible in the lab possible. I would also like to thank Ricky Jimenez and Steffi Rohland for all of their help analyzing samples. I would also like to acknowledge all of my collaborators at the National Ice Core Laboratory, the Desert Research Institute, the Alfred Wegener Institute, and the Paul Schurrer Institute. I would particularly like to thank Joe McConnell, Michael Sigl, Olivia Masselli, Nathan Chellman, Thomas Opel, and Sabina Bruetsch-Sutter. I would also like to acknowledge the students in my cohort, who were my support in my first year, particularly Tyler Sutterley and Ashley Payne, who taught me how to code. None of this would have been possible without my family, Fred, Janet, and Zach Grieman, who have supported me in all of my endeavors.

This research was supported by a generous donation from the Jenkins Family to the Department of Earth System Science, University of California, Irvine and by the Antarctic Glaciology program of the National Science Foundation (ANT-0839122; 240 PLR-1142517). It furthermore contributes to the Eurasian Arctic Ice 4k project (grant OP 217/2- 241 1 by Deutsche Forschungsgemeinschaft awarded to T.O.). I would also like to acknowledge Copernicus Publications for permission to include excerpts from my previous publication in this thesis.

CURRICULUM VITAE

Mackenzie Marie Grieman

EDUCATION

Doctor of Philosophy in Earth System Science **2016**
University of California, Irvine *Irvine, California*

Master of Science in Earth System Science **2012**
University of California, Irvine *Irvine, California*

Bachelor of Arts in Public Policy Analysis **2009**
emphasis in Chemistry
Pomona College *Claremont, California*

RESEARCH EXPERIENCE

Graduate Research Assistant **2010–2016**
University of California, Irvine *Irvine, California*

REFEREED JOURNAL PUBLICATIONS

Grieman, M. M., Greaves, J., Saltzman, E. S., "A method for analysis of vanillic acid in polar ice cores," *Climate of the Past*, (2015). doi:10.5194/cp-11-227-2015.

CONFERENCE PRESENTATIONS

Grieman, M., Saltzman, E., McConnell, J., Fritzsche, D., Opel, T. A 3000-year Siberian ice core record of vanillic acid and *p*-hydroxbenzoic acid. *Poster, AGU Fall Meeting 2014.*

Saltzman, E., Grieman, M., McConnell, J., Cole-Dai, J. Aromatic acids from biomass burning in the WAIS Divde ice core. *Poster, AGU Fall Meeting 2014.*

Grieman, M., Saltzman, E., McConnell, J., Cole-Dai, J., Vanillic acid and *p*-hydroxybenzoic acid in the WAIS Divide ice core. *Poster, WAIS Divide Science Meeting 2014.*

Grieman, M., Saltzman, E., Jimenez, R., McConnell, J., Fritzsche, D. Analysis of Vanillic Acid in Polar Ice Cores as a Biomass Burning Proxy. *Talk, AGU Fall Meeting 2013.*

ABSTRACT OF THE DISSERTATION

Biomass Burning Records in Northern High Latitude Ice Cores

By

Mackenzie Marie Grieman

Doctor of Philosophy in Earth System Science

University of California, Irvine, 2016

Professor Eric S. Saltzman, Chair

Biomass burning plays a major role in climate variability, atmospheric chemistry, carbon cycling, and atmospheric dynamics. In order to understand the drivers of biomass burning and how fire activity will change in the future, it is necessary to investigate how it has varied in the past. Proxy records are needed for understanding the forcing and feedbacks related to fire that are required for developing algorithms for biomass burning in Earth System models. Progress in this field has been limited due to a lack of well-dated proxy records documenting regional variability in burning on millennial and centennial time scales.

In this dissertation, new ice core proxies are utilized to examine past trends in biomass burning. These proxies are organic chemicals (vanillic and *p*-hydroxybenzoic acids) produced by the incomplete combustion of lignin and commonly found in biomass burning aerosols. New analytical techniques utilizing high performance liquid chromatography, ion chromatography, and mass spectrometry were developed to measure ultra-trace levels of these compounds in polar ice cores. The abundance of these chemicals was measured in Arctic ice cores from Siberia, Greenland, and Svalbard.

The 3,000-year Siberian record shows strong multi-centennial variability in burning with a signal to noise ratio unprecedented in previous proxy burning records. This Siberian ice-core record shows that extended periods of elevated wildfire emissions in Siberia occurred

simultaneously with changes in the strength of the Asian Monsoon and the episodic pulsing of ice-rafted debris in the North Atlantic Ocean known as the Bond Events. This is the first clear observational evidence linking wildfire activity to large-scale climate change on millennial timescales.

The 1,700-year Greenland and 750-year Svalbard records exhibit levels of these organic compounds that are considerably lower than those in Siberia, likely reflecting greater distance from the source regions. The variability of the two cores is similar, but quite different from the Siberian record. These differences suggest that the Siberian ice core records regional trends in fire, rather than an average across the high latitude northern hemisphere.

This study represents the first millennial scale ice core records of these organic aerosol tracers. The results show significant spatial and temporal variability that should add significantly to our understanding of the relationship between biomass burning and climate change. Further work will be needed to understand fully these signals and to use such information to compare these biomass burning signals to Earth system models.

Chapter 1

Introduction

Includes excerpts from:

M. M. Grieman, J. Greaves, E. S. Saltzman, "A method for analysis of vanillic acid in polar ice cores," *Climate of the Past*, (2015).

1.1 Overview

Biomass burning is a major influence on atmospheric chemistry, the global carbon cycle, and climate. Fire influences climate by changing the albedo of the land surface and releasing greenhouse gases and aerosols (*Randerson et al.*, 2006). The IPCC has reported that extreme fire event risk will increase in the future due to global climate change. However, the drivers, effects, and climate feedbacks related to fire are still poorly understood and biomass burning is not well represented in climate models (*Solomon et al.*, 2007). One of the factors limiting the development of such models is a lack of historical reconstructions of variability in biomass burning on long time scales and over large geographic regions. Such records are needed in order to relate burning to large scale climate variability.

The existing data on historical rates and patterns of biomass burning are limited. The two most commonly used tools to investigate burning rates are fire scars on tree rings and

charcoal in lake sediments. These proxies record local, rather than regional, conditions and typically exhibit a high degree of spatial variability. Fire scar records only span the past few centuries. Sedimentary charcoal records extend over millennial time scales, but have limited time resolution and age control. Ice cores have the potential to provide biomass burning signals on millennial time scales that are regional in nature and well-dated. Inorganic ions have been used as burning proxies in ice cores with some success (*Whitlow et al.*, 1994; *Gambaro et al.*, 2008; *McConnell et al.*, 2007; *Eichler et al.*, 2011). However, such compounds have multiple sources and may reflect processes other than biomass burning.

This study takes a new approach to examine past biomass burning by exploring the abundance of aromatic organic acids in polar ice cores. These chemicals are uniquely produced by the combustion of biomass by the pyrolysis of lignin. The first goal of this study was to determine if these chemicals were present in ice core samples and preserved over long periods of time. The second goal was to compare the variability of these compounds to that from other biomass burning tracers. Finally, the new ice core records will be examined in terms of past changes in climate to assess the impact of climate change on biomass burning on centennial and millennial time scales. If successful, this approach has the potential to produce well-dated, high resolution regional burning records that could help to understand the long-term drivers of fire and improve parameterization of fire in climate models.

1.2 Approach

The overall goal of this study was to assess the value of organic tracers in ice cores as proxy records of biomass burning. There were three specific goals: 1) to determine if organic tracers are present in Arctic ice cores, 2) if they are present, to evaluate whether the levels of the tracers are preserved over time, and 3) if they are preserved, then to investigate the relationship between climate and burning. In this study, new analytical methods were developed

for measuring organic acids in ice cores employing liquid chromatography with electrospray ionization and mass spectrometric detection (HPLC/ESI/MS/MS and IC/ESI/MS/MS). The development of new methods was aimed at greatly reducing the sample size, sample handling, and time required for analysis. This is important as developing ice core records requires the analysis of large numbers of samples. The methods developed in this study would also improve analysis of these compounds in natural waters and aerosols. The new analytical methods were developed using laboratory standards and Arctic ice core samples.

The Akademii Nauk ice core from northern Siberia, the Tunu ice core from northeastern Greenland, and the Lomonosovfonna ice core from Svalbard were analyzed in this study. Northern Siberia contains two-thirds of the world's boreal forests (*Eichler et al.*, 2011) and is an ideal location to examine biomass burning products from woody vegetation. The Svalbard and Greenland ice cores were analyzed to determine if the signals observed in the Siberian ice core were regional in nature or characteristic of the whole Arctic. The results from these ice cores are compared to sedimentary charcoal records and other climate proxies to determine if there is a systematic relationship between burning and climate.

1.3 Background

1.3.1 The significance of fire in the earth system

Fire emits carbon-containing chemical species, including carbon dioxide (CO_2), carbon monoxide (CO), methane (CH_4), and particulate matter (black carbon). Biomass burning currently emits about 1/3 as much carbon as is produced from fossil fuel combustion. Fire also releases about 40% of the black carbon emissions (*Hessl*, 2011). CO and CH_4 react with hydroxyl radicals (OH) to reduce the oxidative efficiency of the troposphere (*Crutzen and Andreae*, 1990). CO_2, CH_4, and particulate matter cause changes in climate. On a regional

scale, black carbon heats the troposphere and hinders vertical convection, which inhibits rain-cloud formation and precipitation. Biomass burning also changes the albedo of the land surface. For instance, a forested area that has been cleared by fire and replaced with pasture is more reflective (*Bowman et al.*, 2009).

Each ecosystem is adapted to a specific fire regime. Fire regimes are defined by fuel type, temporal characteristics, spatial range, and impacts (*Bowman et al.*, 2009). Knowledge about fire regimes is important for understanding carbon cycling and ecological change. Net carbon exchange through an ecosystem depends on a balance between net primary production and heterotrophic respiration. This balance can be shifted if there is a change in net primary production or respiration (*Gower et al.*, 2001).

Fire is a major disturbance of net primary production in boreal forest ecosystems (*Gower et al.*, 2001). Boreal forest fires are characterized as surface, crown, and ground fires based on their intensity (*Stocks et al.*, 2001; *Ryan*, 2002). Most large trees survive surface fires. Stand-replacing crown fires are high intensity fires and result in loss of vegetation (*Stocks et al.*, 2001). These fires alter the balance between carbon emissions and net primary production for several decades because it can take over 100 years of regrowth for carbon stocks to return to pre-fire levels in the region affected (*Kasischke et al.*, 1995).

Arctic tundra fires have the potential to release large amounts of carbon into the atmosphere because Arctic tundra contains pools of soil carbon that have accumulated over millennia. The impact of fire on carbon storage in Arctic tundra is not well-known because Arctic tundra fires are rare (*Mack et al.*, 2011). For instance, lake sediment cores show no evidence of fire in the Anaktuvuk River region in Alaska in the last 5,000 years (*Mack et al.*, 2011). Fires in tundra ecosystems are a growing concern due to Arctic warming. Under warmer or drier climate conditions, tundra can burn more frequently. A fire occurred in the Anaktuvuk region for the first time in 5,000 years in 2007 (*Mack et al.*, 2011). Northcentral Alaska burned every 144 years on average from 14,000-10,000 years ago likely due to drier conditions

(*Higuera et al.*, 2008).

Over longer time scales, the locations of boreal forests and tundra can shift location due to climatological changes that trigger changes in fire frequency. These vegetation changes alter the balance between atmospheric carbon and terrestrial carbon stocks for a longer period of time (*Kasischke et al.*, 1995). For instance, pollen records show that ecosystems can shift in a particular location within a millennium (*Eichler et al.*, 2011). Determining how fire regimes and ecosystems have changed over longer timescales is important for accounting for changes in carbon storage as the climate changes in the future.

1.3.2 Biomass burning proxies: types, limitations, and major results

Proxy-based records are used to reconstruct past biomass burning. Biomass burning proxies include fire scars on trees rings, charcoal accumulation in lake sediments, and gases and aerosols in ice cores (Figure 1.1). These proxies each have their own strengths and limitations, and reflect burning on a wide range of spatial/temporal scales. Dating uncertainties, emissions from sources other than biomass burning, atmospheric reactivity, transport processes, and post-depositional processes limit the interpretation of biomass burning proxies.

Charcoal particle accumulation in lake sediments is the most commonly used paleofire proxy. Charcoal records are local, representing fires on watershed scales. Compilations of lake charcoal records have been used to produce regional, hemispheric, and global biomass burning records (*Power et al.*, 2008). One of the major findings from these composite records is that burning declined globally 1-1750 CE (*Marlon et al.*, 2008). This decline is likely related to gradual cooling in the Northern Hemisphere in the Late Holocene (*Marlon et al.*, 2008). The value of charcoal as a proxy is limited by the small spatial scale of the source region, the limited coverage of records for many regions, and uncertainty in the dating. Dating control

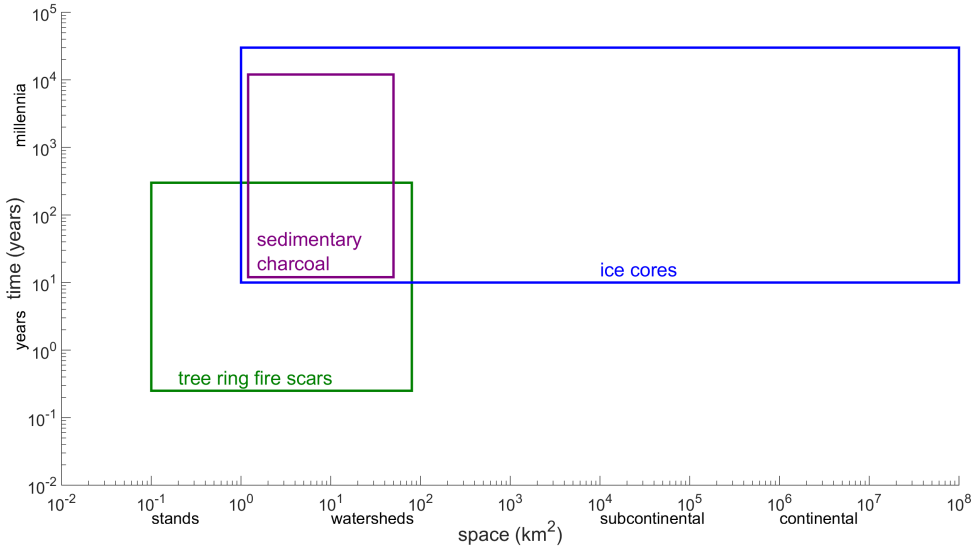

Figure 1.1: Spatial and temporial scales of biomass burning proxies. Adapted from *Kehrwald et al.* (2013).

of these charcoal records is typically obtained from interpolation between a relatively few ^{14}C dates (*Power et al.*, 2008).

Biomass burning emissions histories have been inferred from variations in the stable isotopic composition of ice core methane (*Ferretti et al.*, 2005; *Sapart et al.*, 2012). Methane is emitted from agricultural, geologic, microbial, and biomass burning sources. The contribution from burning is obtained by assigning end-member isotopic compositions to the various sources. A strength of this approach is that methane isotope records integrate global biomass burning signals because methane has an atmospheric lifetime of about ten years. Late Holocene methane isotopic records show that burning was high globally from 1-1000 CE, declined from 1000-1700 CE, and increased again after 1700 CE (*Ferretti et al.*, 2005; *Mischler et al.*, 2009). Cooler and wetter conditions likely drove the decline in burning from 1000-1500 CE (*Ferretti et al.*, 2005).

Aerosol-borne chemicals preserved in ice cores are also used as biomass burning proxies. Aerosol tracers in ice cores represent biomass burning over large regions, can be sampled at high temporal resolution, and provide evidence of fires at high latitudes and altitudes,

where lake sediments are scarce (*Kehrwald et al.*, 2010). Past fire events have been detected in Greenland ice from enrichment of ammonium, formate and oxalate, and the transport of these chemicals to Summit, Greenland in biomass burning plumes has been documented (*Fuhrer et al.*, 1996; *Legrand et al.*, 1992; *Dibb et al.*; *Jaffrezo et al.*, 1998; *Savarino and Legrand*, 1998). Ammonium in Greenland ice cores indicates that burning increased in North America for 1-2 century-long periods over the past millennium (*Savarino and Legrand*, 1998; *Whitlow et al.*, 1994; *Laj et al.*, 1992; *Rubino et al.*, 2015). The interpretation of inorganic ion levels in ice cores as biomass burning signals is challenging because inorganic ions have sources other than biomass burning. Ammonium emissions sources into the atmosphere include animal excreta, synthetic fertilizers, the ocean, biomass burning, crops, natural vegetation soils, industrial processes, fossil fuels, and other anthropogenic sources (*Bouwman et al.*, 1997). Attribution of these chemicals to burning requires detection of increased levels over some natural, and often variable, baseline.

A new ice core burning proxy is levoglucosan, an aerosol-borne anhydrous sugar exclusively produced by burning of cellulose. Levoglucosan is generated from combustion of all types of cellulose-containing plant matter, and is therefore not specific to a particular plant type or ecosystem (*Simoneit et al.*, 1999). Levoglucosan has been detected in aerosols over Summit, Greenland, and in Eastern Siberian, Greenland, and Antarctic ice (*Kehrwald et al.*, 2012; *Gambaro et al.*, 2008; *Kawamura et al.*, 2012; *Zennaro et al.*, 2014). Levoglucosan levels in an ice core from Greenland peaked between 1500-1700 CE (*Zennaro et al.*, 2014). There has been some debate in the literature about the atmospheric reactivity of levoglucosan, and its suitability as a quantitative tracer for aerosol source apportionment (*Hoffmann et al.*, 2010; *Hennigan et al.*, 2010; *Slade and Knopf*, 2013). Levoglucosan is a promising tracer because it comprises a major fraction of the carbonaceous mass of biomass burning aerosols. However, it is also highly challenging to measure due to its low levels in polar ice cores.

1.3.3 Organic acids as vegetation-specific records

Laboratory and field studies have shown that fine particulates emitted from wood smoke are comprised of a wide range of aromatic compounds. The chemistry of these biomass burning aerosols is related to the structure of the precursor lignin material combusted (*Simoneit*, 2002). These lignin-derived methoxylated phenols, aldehydes, and acids have been used as tracers for the contribution of biomass burning to ambient aerosols on a local or regional basis (*Nolte et al.*, 2001). Such compounds are incorporated into polar ice cores and may contain information about climate-related variability in biomass burning and about the type of plant material combusted.

Lignin is a group of aromatic polymers that make cell walls of biomass rigid, impermeable, and protected from microbial decay. Lignin is derived from the hydroxyl-cinnamyl alcohols (i.e. monolignols): coniferyl alcohol and sinapyl alcohol, and smaller amounts of *p*-coumaryl alcohol. When these aromatic building blocks are incorporated into the lignin structure, they are characterized as guaiacyl (from coniferyl alcohol), syringyl (from sinapyl alcohol), and *p*-hydroxylphenyl (from *p*-coumaryl alcohol) units. The structures of these units only differ by the number of methoxy groups (-OCH_3) substituted on their benzene rings: 0 (*p*-hydroxylphenyl units), 1 (guaiacyl units), or 2 (syringyl units) groups (Figure 1.2). Gymnosperm (softwood) lignin is composed of guaiacyl units and smaller amounts of *p*-hydroxylphenyl units. Angiosperm (hardwood) lignin is made of guaiacyl and syringyl units (*Vanholme et al.*, 2010). Grass lignin contains small amounts of all three types of lignin units (*Simoneit*, 2002).

When lignin is oxidized, vanillyl (V), syringyl (S), cinnamyl (C) (*p*-coumaric and ferulic acids), and *p*-hydroxyl (P) phenols are produced. The relative abundances of these products can indicate the type of vascular plant burned because the different types of lignin units produce these types of phenols. Vanillyl and *p*-hydroxyl phenols are produced by the oxidation

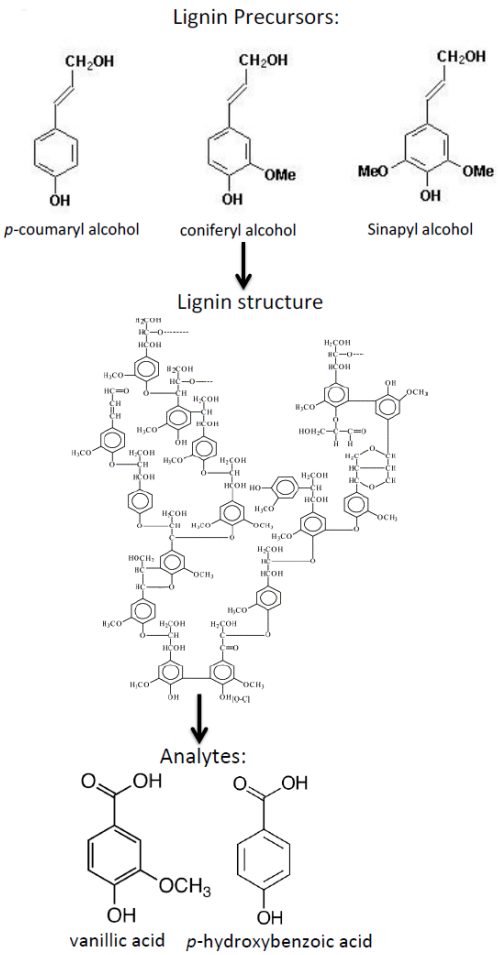

Figure 1.2: Lignin building blocks (top), basic lignin structure (middle), pyrolysis products measured in this study (bottom).

of both angiosperms and gymnosperms. Gymnosperms produce more vanillyl phenols than *p*-hydroxyl phenols (P/V < 1). Angiosperms produce about the same amounts of vanillyl and *p*-hydroxyl phenols (P/V ≈ 1) (*Hedges and Parker*, 1976). When gymnosperms are oxidized, syringyl-type phenols are not produced (S/V $= 0$) (*Hedges and Mann*, 1979; *Oros and Simoneit*, 2001a). Angiosperms produce more syringyl phenols than vanillyl and *p*-hydroxyl phenols (S/V > 1, S/P > 1) (*Hedges and Mann*, 1979; *Hedges and Parker*, 1976; *Opsahl and Benner*, 1995; *Oros and Simoneit*, 2001b). Cinnamyl phenols are produced by the oxidation of nonwoody gymnosperm and angiosperm tissues. Therefore, cinnamyl and vanillyl phenols are present when both angiosperms and gymnosperms are oxidized, but vanillyl phenols are

produced in greater quantities (C/V < 1) (*Hedges and Mann*, 1979).

To date there have been few measurements of such compounds in polar ice cores. *McConnell et al.* (2007) measured vanillic acid in ice cores from west central Greenland for 1788-2000 CE. *Kawamura et al.* (2012) measured vanillic acid, dehydroabietic acid, and *p*-hydroxybenzoic acid in an ice core from eastern Siberia for the past 300 years. The vanillic, *p*-hydroxybenzoic, and dehydroabietic acid records are all elevated from 1950-2000 CE (*Kawamura et al.*, 2012). In this study, vanillic acid and *p*-hydroxybenzoic acid acid were measured. These compounds were chosen to try to identify the type of plant material burned because each acid is likely a product of a different lignin unit (Table 1.1).

Table 1.1: Lignin precursors, units, oxidation products, and likely plant source material.

# of methoxy groups	lignin precursor	lignin unit	phenol product	likely plant material	analyte
0	p-coumaryl alcohol	p-hydroxyl-phenyl	p-hydroxyl	gymnosperms (minor amounts), angiosperms, grasses	p-hydroxybenzoic acid
1	coniferyl alcohol	guaiacyl	vanillyl	gymnosperms, angiosperms, grasses	vanillic acid
2	sinapyl alcohol	syringyl	syringyl	angiosperms, grasses	syringic acid

1.4 Transport

Aerosol transport into the Arctic from lower latitudes is weaker in the summer than in the winter. The atmosphere is dry and thermally stable in the Arctic in the winter. The dry, stable atmosphere leads to reduced wet deposition and long aerosol lifetimes. In the summer, the atmosphere is less stratified at lower altitudes because inversions at the surface are weaker

(*Stohl*, 2006). Biomass burning occurs in the summer when removal mechanisms (i.e. wet and dry deposition) are more efficient. However, the high number of particles produced by biomass burning suppresses local wet deposition. Particles from biomass burning can therefore reach the Arctic in the summer (*Stohl*, 2006).

FLEXPART model trajectories suggest that the strongest biomass burning aerosol signal in the summer is transported to the Arctic from Siberia (Figure 1.3; 48°-66°N, 60°-140°E). The FLEXPART model is a Lagrangian transport and dispersion model that is used to simulate long-range atmospheric transport. Twenty-five percent of FLEXPART modeled trajectories from Siberia reached the Arctic in 3 days, and 50% of trajectories reached the Arctic in 10 days. Russian fires in 2003 contributed 40-56% of the mass of BC deposited in the spring and summer above 75°N (*Generoso et al.*, 2007). Lidar data from the Arctic Research of the Composition of the Troposphere from Aircraft and Satellites (ARCTAS) mission indicate that biomass burning plumes from Russian forest fires in 2008 contributed to aerosol loadings over the North American Arctic (*Matsui et al.*, 2011; *Warneke et al.*, 2010).

The second strongest sources of biomass burning aerosol to the Arctic are western Canada and Alaska, requiring 10 days for transport using the FLEXPART model (*Stohl*, 2006). Biomass burning aerosols also increased in Barrow (Alaska), Alert (Canada), Summit (Greenland), and Zepplin/Ny Alesund on Spitsbergen (Svalbard) as a result of fires in Alaska and Canada in 2004 (*Stohl et al.*, 2006). Biomass burning at lower latitudes strongly influences black carbon levels in the Arctic.

1.4.1 Representation of fire in climate models

Wildfire extent and frequency is related to both climate and vegetation. Simulating fire on long time scales requires fully coupled process models that include both climate and ecosystems, as well as fire dynamics and emissions (*Thonicke et al.*, 2010). General circulation

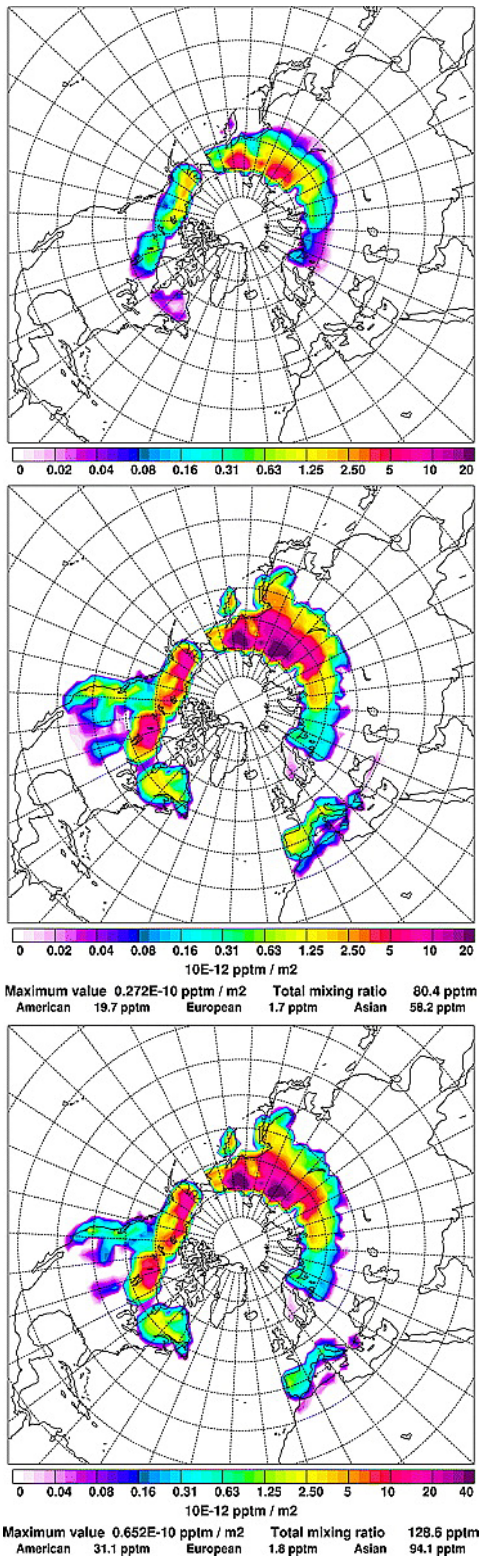

Figure 1.3: Potential source contributions of aerosols that remain in the Arctic (>70°N) for at least 5 days from boreal forest fires with transport times of 3 days (top) and 30 days (middle). Particles with transport time of 30 days reaching altitudes below 1000 m in the Arctic (bottom). The FLEXPART model was run for the years 1999-2005. Figure from *Stohl* (2006).

models (GCMs) have been used to simulate global fire frequency based on climatic factors for the past, present, and future (*Hessl*, 2011; *Brown et al.*, 2004; *Pechony and Shindell*, 2010). Process-based fire regime models coupled to vegetation models have been used to simulate regional fire frequency (*Thonicke et al.*, 2010). To date, most fire modeling has been carried out in an uncoupled mode, using climate models to simulate air temperature, precipitation, humidity, wind speed and direction, cloudiness, sea level pressure, and sea surface temperature (*Dai et al.*, 2004). These climatic factors are used to project future fire frequency under various carbon dioxide emissions scenarios (*Hessl*, 2011; *Brown et al.*, 2004). Under a scenario with doubling carbon dioxide emissions, fire season length, fire intensity, and burned area are all projected to increase in the Western United States, the Mediterranean, Canada, and Russia (*Hessl*, 2011).

Thonicke et al. (2010) coupled the Spread and Intensity of Fire (SPITFIRE) process-based fire regime model to a Dynamic Global Vegetation Model (DGVM) to determine regional fire regime changes. DGVMs determine global vegetation distribution by simulating growth and competition between plant functional types. The SPITFIRE model uses outputs of percentages of plant functional types from the DGVM to estimate different fuel classes. SPITFIRE model estimates of the global distribution of fire were used to explain regional MODIS satellite fire observations for the late 20^{th} century (*Thonicke et al.*, 2010).

Pechony and Shindell (2010) modeled global fire trends over the past 1,000 years using the Goddard Institute for Space Studies (GISS) GCM to simulate past climatic change and a History Database of the Global Environment (HYDE) dataset of land use and population change to simulate human impact. This study is one of the only fire modeling studies simulating fire over the past 1,000 years. They used their model to explain the *Marlon et al.* (2008) charcoal history of burning (Figure 1.4). *Pechony and Shindell* (2010) conclude that global burning trends can be explained by climatic change prior to industrialization. Coupling this GCM method to a vegetation model could improve predictions of biomass

burning trends regionally. A coupled model could be used to explain fire trends in proxy records, which would improve predictions of fire frequency into the future.

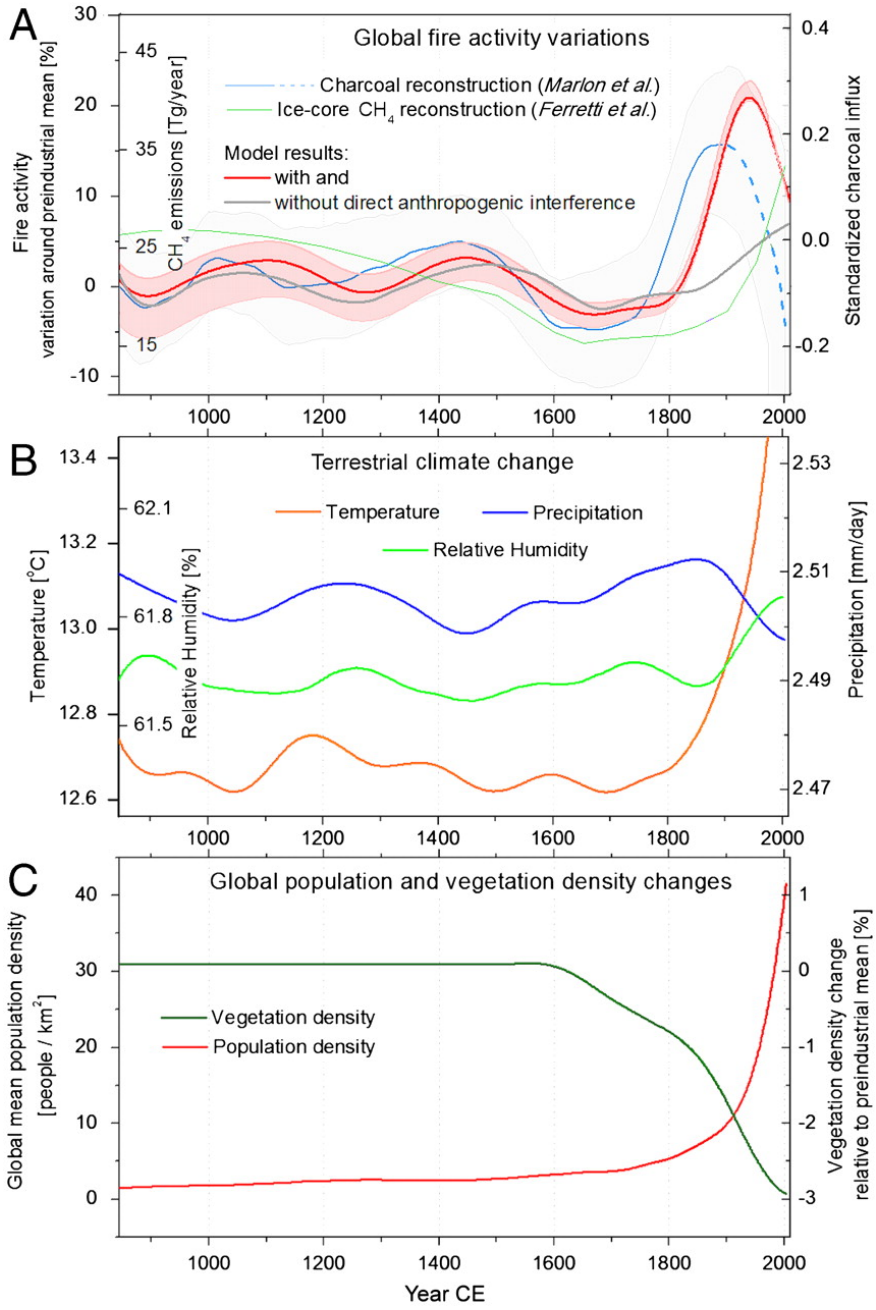

Figure 1.4: Relationship between global fire activity and climate. (A) Modeled fire activity with (red) and without human influence (gray), ice core methane history (green), and global charcoal reconstruction (blue), (B) modeled annual means of terrestrial temperature (orange), precipitation (blue), and relative humidity (green), (C) Global mean population (red) and vegetation (green) densities. Figure from *Pechony and Shindell* (2010).

Chapter 2

Analytical methods for analysis of aromatic acids in ice cores

Includes excerpts from:

M. M. Grieman, J. Greaves, E. S. Saltzman, "A method for analysis of vanillic acid in polar ice cores," *Climate of the Past*, (2015).

2.1 Overview

This study focuses on the analysis of two aromatic acids, vanillic acid (VA) and *p*-hydroxybenzoic acid (*p*-HBA) in polar ice cores. Previous measurements of these compounds in aerosols, natural waters, and ice core samples were carried out by gas chromatographic separation with mass spectrometric detection (GC-MS) (*Nolte et al.*, 2001; *Simoneit et al.*, 2004; *Fu et al.*, 2008; *Kawamura et al.*, 2012). GC-MS has the disadvantage of requiring large samples (80-250 mL) and extensive sample handling. Sample preparation includes preconcentration by rotary evaporation, solvent extraction, heated derivatization to form trimethylsilyl derivatives, and dissolution in hexane. This study developed new analytical methods capable of more sensitive and rapid analysis of aromatic acids.

High performance liquid chromatography with tandem mass spectrometric detection (HPLC-

ESI/MS/MS) is a relatively new technique that has potential to reduce sample size and sample handling. Relatively little previous work has been done using this method to analyze phenolic compounds in environmental samples. *Zangrando et al.* (2013) used HPLC-ESI/MS/MS to detect VA and other phenolic compounds in Arctic aerosol samples. *McConnell et al.* (2007) detected VA in a Greenland ice core using a continuous flow melter and ESI/MS/MS.

This chapter presents the two methods developed in this study for analysis of VA in ice cores: HPLC-ESI/MS/MS and anion exchange chromatography (IC) with ESI/MS/MS detection. The IC-ESI/MS/MS method showed higher sensitivity of VA detection than the HPLC-ESI/MS/MS method. The IC-ESI/MS/MS method was used for analysis of VA in all of the ice cores in this study. This method was also used for analysis of *p*-HBA in the Siberian and Svalbard ice cores.

2.2 HPLC-ESI/MS/MS Method

2.2.1 Instrumentation

The HPLC-ESI/MS/MS method was developed using a ThermoFinnigan TSQ Quantum System. The system consists of an autosampler, a high performance liquid chromatograph (HPLC), and an electrospray ionization-triple quadrupole mass spectrometer (ESI-MS/MS). The Xcalibur data system (TSQ Tune 1.2, Xcalibur 2.0, ThermoFinnigan Corp.) was used for instrument control and data acquisition. The electrospray ionization source was operated using the following conditions: -3 kV spray voltage, 38 psi sheath gas pressure, and 15 psi auxiliary gas pressure. The mass spectrometer was operated using a mass resolution of m/z 0.7. High concentration vanillic acid solutions (1-10 ppm) were introduced directly into the ESI/MS/MS via syringe pump (NE-300, New Era) for instrument tuning and signal

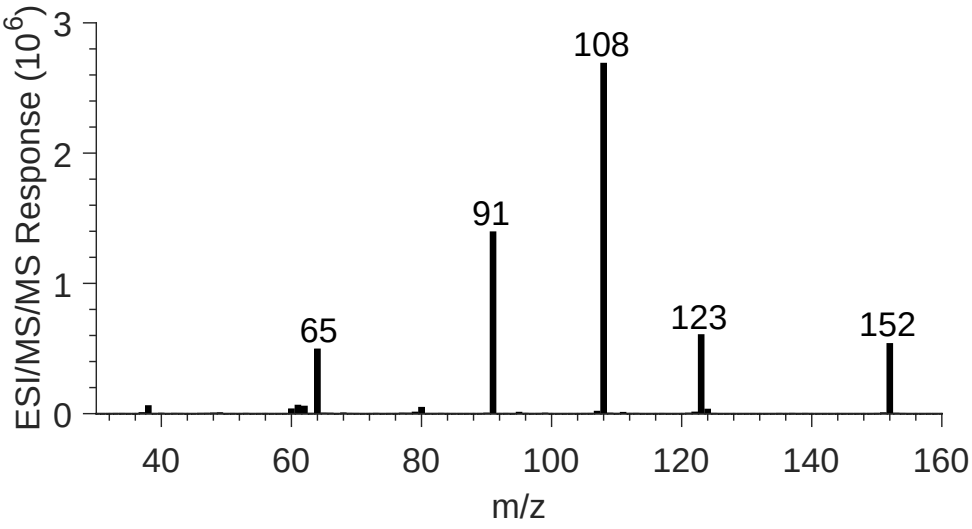

Figure 2.1: ESI-MS/MS product scan of vanillic acid using 30 eV collision energy.

optimization. Vanillic acid was detected using the mass spectrometer in the negative ion mode, with an ion inlet cone temperature of 350 °C.

2.2.2 Method optimization

Collision energy

MS/MS detection of vanillic acid was optimized using product scans with varying collision energies. Solutions containing 1 ppm vanillic acid in a 75 : 25% water: methanol mixture were delivered directly to the electrospray source using the syringe pump. The vanillic acid $[M\text{-}H]^-$ (m/z 167) was used as the precursor mass and the collision gas pressure was 1.5×10^{-4} psi of Ar. Figure 2.1 shows a product scan at a collision energy of 30 eV. The major product fragments under these conditions are: $C_4H(O)$ (m/z 65), C_6H_3O (m/z 91), $C_6H_3(O)OH$ (m/z 108), $C_6H_3(OCH_3)OH$ (m/z 123), and $C_6H_3(O)(COO)OH$ (m/z 152).

Figure 2.2 shows the fragmentation pattern as a function of collision energy over the range of 0–40 eV. Maxima were found at a collision energy of 15 eV for fragments at m/z 152

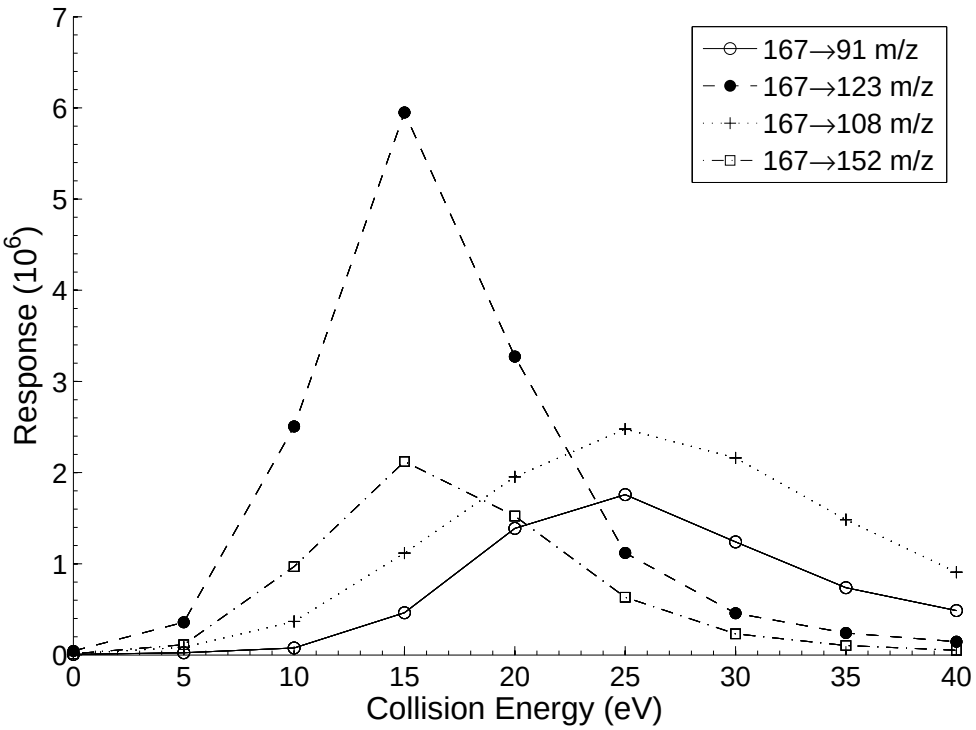

Figure 2.2: Instrument response to a 1 ppm vanillic acid solution at varying collision energies using the 167→91 m/z, 167→123 m/z, 167→108 m/z, and 167→152 m/z mass transitions.

(loss of CH_3) and m/z 123 (loss of CO_2). Maxima were observed at 25 eV for fragments at m/z 108 (loss of CH_3 and CO_2) and m/z 91 (loss of COOH and OCH_3). The highest response overall was obtained for the m/z123 fragment at 15 eV. However, solvent noise at the 167→123 transition was too high to allow detection of vanillic acid in ice core samples. The optimal signal to noise was obtained at the 167→108 transition at a collision energy of 30 eV. These conditions were used in this study.

2.2.3 Chromatography

The Surveyor autosampler was programmed to inject 100 μL of sample onto a reversed phase Kinetex 2.6 μm particle size XB-C18 100A analytical column (100 mm × 2.2 mm, Phenomenex). The mobile phase was an isocratic solution of 25 % methanol in water, flowing

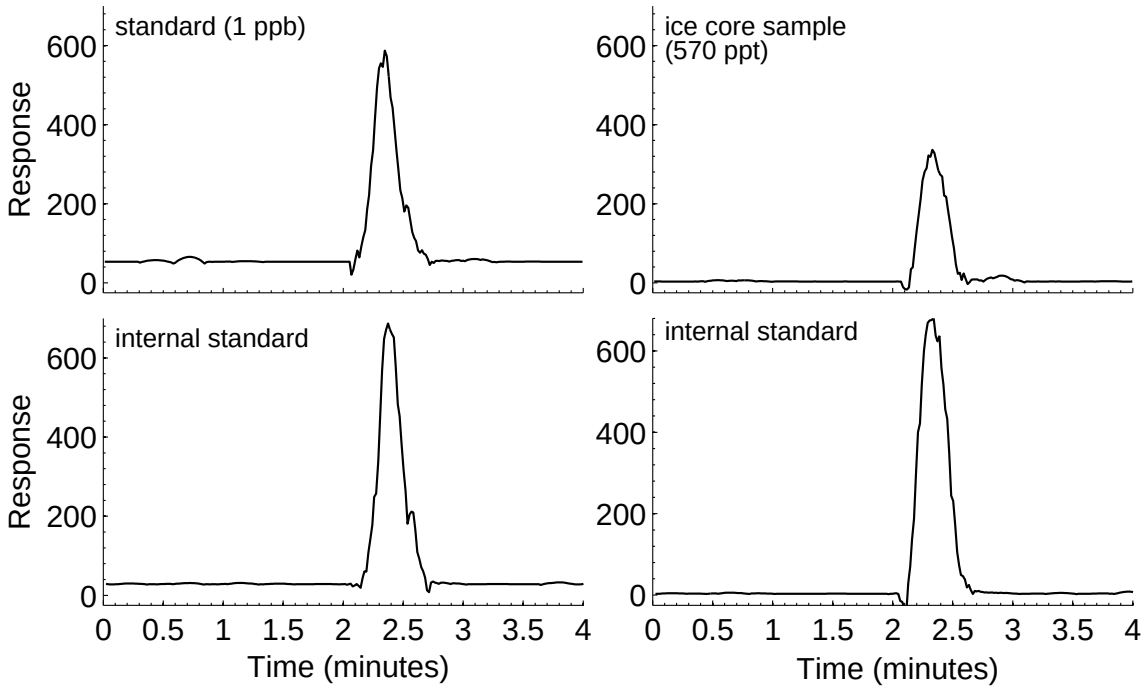

Figure 2.3: HPLC/MS/MS vanillic acid chromatograms. Left: 1 ppb vanillic acid standard in Milli-Q water (^{12}C, 167→108 m/z) (upper) with 1 ppb internal standard (^{13}C-labeled vanillic acid, 168→108 m/z) (lower). Right: Akademii Nauk ice core sample containing 570 ppt vanillic acid (325 m depth, 286 CE) (^{12}C, 167→108 m/z) (upper) with 1 ppb internal standard (^{13}C-labeled vanillic acid, 168→108 m/z) (lower).

at 200 μL min^{-1}. All of the column effluent was directed to the electrospray ionization source. Vanillic acid is eluted from the column with a retention time of 2.5 min and a peak width at half height of 0.2 min. Chromatograms of standard mixture of a 1 ppb vanillic acid standard (167→108) and a 1 ppb ^{13}C-labeled vanillic acid isotope standard (168→108) are shown in Figure 2.3 (left side).

2.2.4 Standardization and limit of detection

Standards were prepared using vanillic acid (4-hydroxy-3-methoxybenzoic acid, 97% purity, Sigma-Aldrich). The internal standard was ^{13}C-labeled vanillic acid (Carboxyl-^{13}C, 99% purity, Cambridge Isotope Laboratories). Stock solutions of 0.1% vanillic acid and ^{13}C-labeled vanillic acid were prepared monthly in high-performance liquid chromatography

(HPLC)-grade methanol (J. T. Baker). Intermediate 1 ppm standards were prepared daily in methanol. Working standards ranging from 0 to 2 ppb were prepared by dilution in ultrapure water (Millipore Milli-Q) directly in 2 mL Surveyor autosampler vials. The uncertainty in the accuracy of these standards is estimated to be ± 4 % based on the stated purity of the reagent grade vanillic acid and the estimated uncertainty in our preparation of working standards. Samples and standards were spiked with ^{13}C-labeled vanillic acid (2 μ L of 1 ppm internal standard in 2 mL) to generate a 1 ppb internal standard.

Calibration curves were constructed by analyzing vanillic acid standards ranging in concentration from 0 to 3 ppb. The calibration curves were based on the ratio of peak areas of the vanillic acid and isotope-labeled vanillic acid signals at their respective mass transitions, $167 \rightarrow 108$ and $168 \rightarrow 108$. Using linear least-squares regression, the slope of the calibration curve was $1.2 \pm 0.025\,\mathrm{ppb}^{-1}$ and the intercept was 0.035 ± 0.047 ($n = 414$). The detection limit is approximately 0.077 ppb, defined as 3 times the standard deviation of vanillic acid levels in distilled water blanks spiked with internal standard. The level of ^{12}C vanillic acid in the ^{13}C vanillic acid internal standard was below the limit of detection.

2.2.5 Matrix effects

Polar ice core samples are complex mixtures of organic and inorganic compounds. It is important to quantify matrix effects that might suppress or enhance analyte response in an ice core sample compared to that in a pure water standard. This was done by comparing the response of the isotope-labeled internal standard in ice core samples to that in pure water. The response to the isotope-labeled standard in ice core samples was identical to that in pure water standards. This clearly demonstrates the absence of significant matrix effects in the Akademii Nauk ice core samples analyzed in this study.

2.2.6 Ice core sample analysis

The ice core samples used to test the analytical method were obtained from the Akademii Nauk ice core (*Fritzsche et al.*, 2005). The ice core samples analyzed for this study covered the time period 200-350 CE, based on a provisional timescale [McConnell, personal communication]. Samples were melted using a continuous melter, and collected in 8 mL HDPE vials using a peristaltic pump and fraction collector (*McConnell et al.*, 2001).

The procedure used for analysis of ice core samples was as follows: 1 ppb of ^{13}C-labeled vanillic acid was added to each ice core sample and standard. Occasional blanks without internal standard were also analyzed. A blank and/or standard was analyzed after every fifth ice core sample. Samples were typically analyzed in batches of 50-70 samples day^{-1} and typically calibration curves were based on all of the standards and blanks analyzed on the same day. An example of a chromatogram from an Akademii Nauk ice core sample is shown in Figure 2.3 (right side). The results of duplicate analysis of ice core samples are shown in Figure 2.4. The relative standard deviation of duplicates is about 30% for levels above the detection limit and below 0.600 ppb ($n = 167$).

The vanillic acid was measured in 34 Akademii Nauk ice core samples, covering the time period of 200-350 CE (Figure 2.5). Each sample represents approximately 1 year. Vanillic acid concentrations ranged from below the detection limit to 0.698 ppb, with an overall mean of 0.226 ± 0.189 ppb (1σ) and a median of 0.156 ppb.

There are few reports of previous ice core measurements of vanillic acid. The vanillic acid levels reported in the literature are generally similar to those measured here. *Kawamura et al.* (2012) reported vanillic acid levels ranging from below detection (0.005 ppb) to 0.125 ppb for samples from the Ushkovsky ice core on the Kamchatka Peninsula covering the time period 1690-1997. *McConnell et al.* (2007) reported vanillic acid levels from 0.001 to 0.350 ppb in ice core samples from west-central Greenland ranging in age from AD 1788 to 2002.

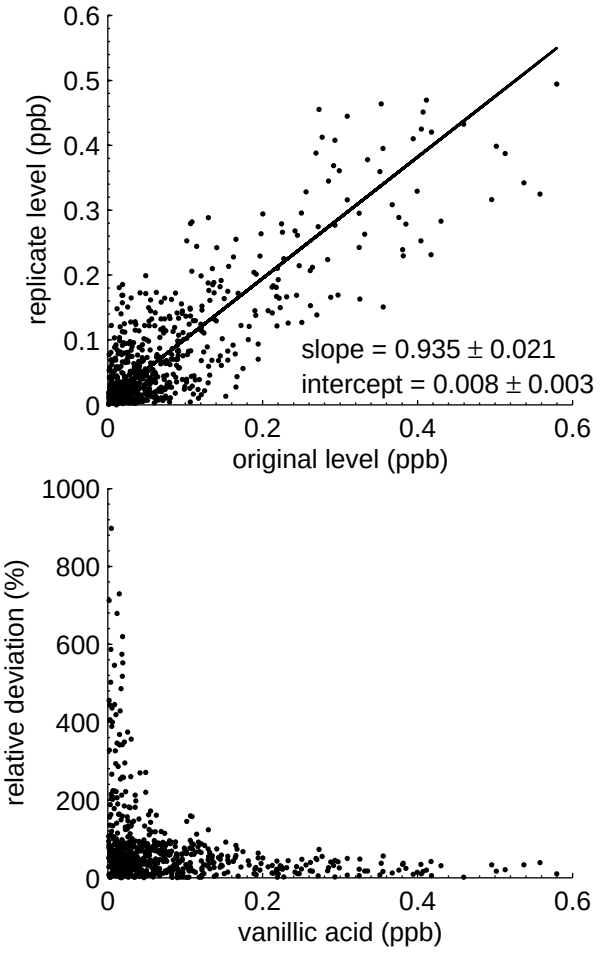

Figure 2.4: Precision of HPLC-ESI/MS/MS vanillic acid measurements as a function of concentration. Upper plot — replicate measurements of Akademii Nauk ice core samples. Lower plot — vanillic acid measurement (ppb) against relative deviation (%, Δ level/total mean) of the replicates.

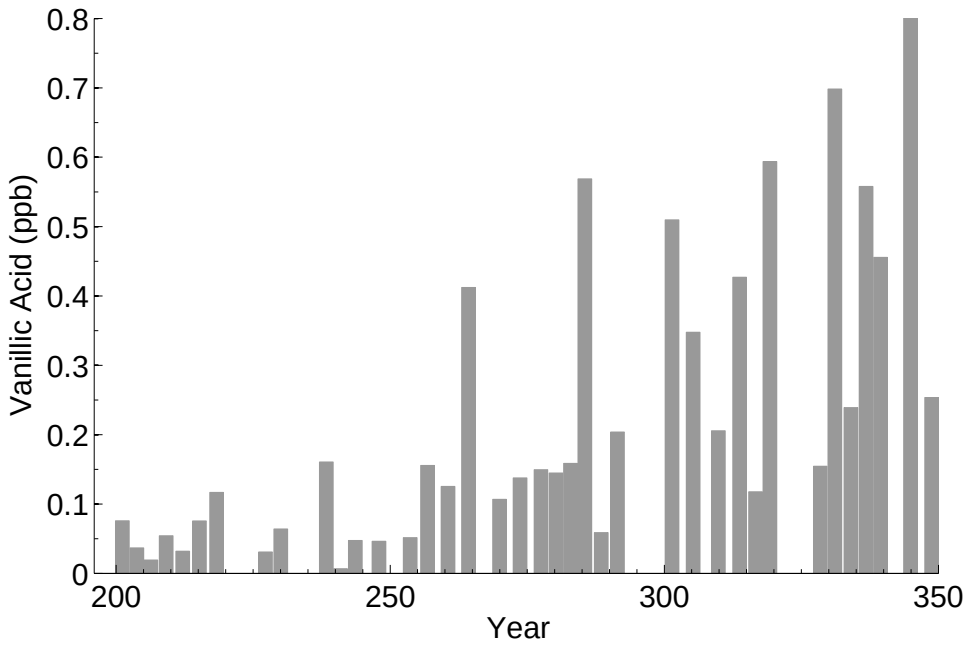

Figure 2.5: Vanillic acid concentrations in Akademii Nauk ice core samples plotted against ice age for the years AD 200–350.

2.3 IC-ESI/MS/MS Method

The maximum sample loop size that can be used with the HPLC technique is 100 μL. In order to achieve greater sensitivity, a higher volume must be focused on the analytical column without peak broadening. Anion exchange chromatography (IC) replaced HPLC as the separation technique prior to mass spectrometric detection. Ion chromatography allows for a sample loop size of up to 1 ml. This volume increase provides a 10x increase in sensitivity for a given concentration if the flow rate of the eluent remains at 200 $\mu L/min$.

The IC-ESI/MS/MS experimental system consisted of a Dionex AS-AP autosampler, Dionex ICS-2100 integrated reagent-free ion chromatography system, and ThermoFinnigan TSQ Quantum System. The separation was carried out on an IonPac AS18-Fast 2 m analytical column with a 40 mM potassium hydroxide eluent at a flow rate of 200 μL/min. Cations were removed from the column effluent using a Dionex electrolytically regenerated suppressor (AERS 500). Methanol was added to the eluent stream downstream of the suppressor

in order to maintain a stable electrospray (70 μL/min, J.T. Baker LC-MS grade). The electrospray source was operated at the same conditions as the HPLC method. The analytes were detected using a collision energy of 30 eV at the following mass transitions: vanillic acid, m/z 167→108; *p*-hydroxybenzoic acid, m/z 137→93; and syringic acid, m/z 197→153. External standards were prepared using commercial vanillic, *p*-hydroxybenzoic, and syringic acids (Sigma-Aldrich). Stock solutions of 100 ppb were prepared weekly and diluted daily to prepare working standards ranging from 0.1-2 ppb.

Syringic, vanillic, and *p*-hydroxybenzoic acids were detected at retention times of 11.3, 11.9, and 12.4 minutes, with peak widths at half height of 0.4 minutes (Figure 2.6). Limits of detection were estimated as 0.05, 0.01, 0.05 ppb, respectively, defined as 3x the standard deviation of the blank in MilliQ water.

2.4 Method comparison

Both methods developed in this study are capable of detecting VA in ice core samples. VA was measured in a Siberian ice core, covering 1-1000 CE, using both methods (Figure 2.7). The similarity between the VA records using two different chromatographic techniques confirms the identity of the VA peak. The IC method is more sensitive than HPLC method due to the 10x increased volume of the sample injection without peak broadening. Both methods have peak widths at half height of 0.4 minutes. The VA LOD using IC for separation is 8x lower than the VA LOD using HPLC for separation. The IC-ESI/MS/MS method was used to measure VA and *p*-HBA in all of ice cores in this study.

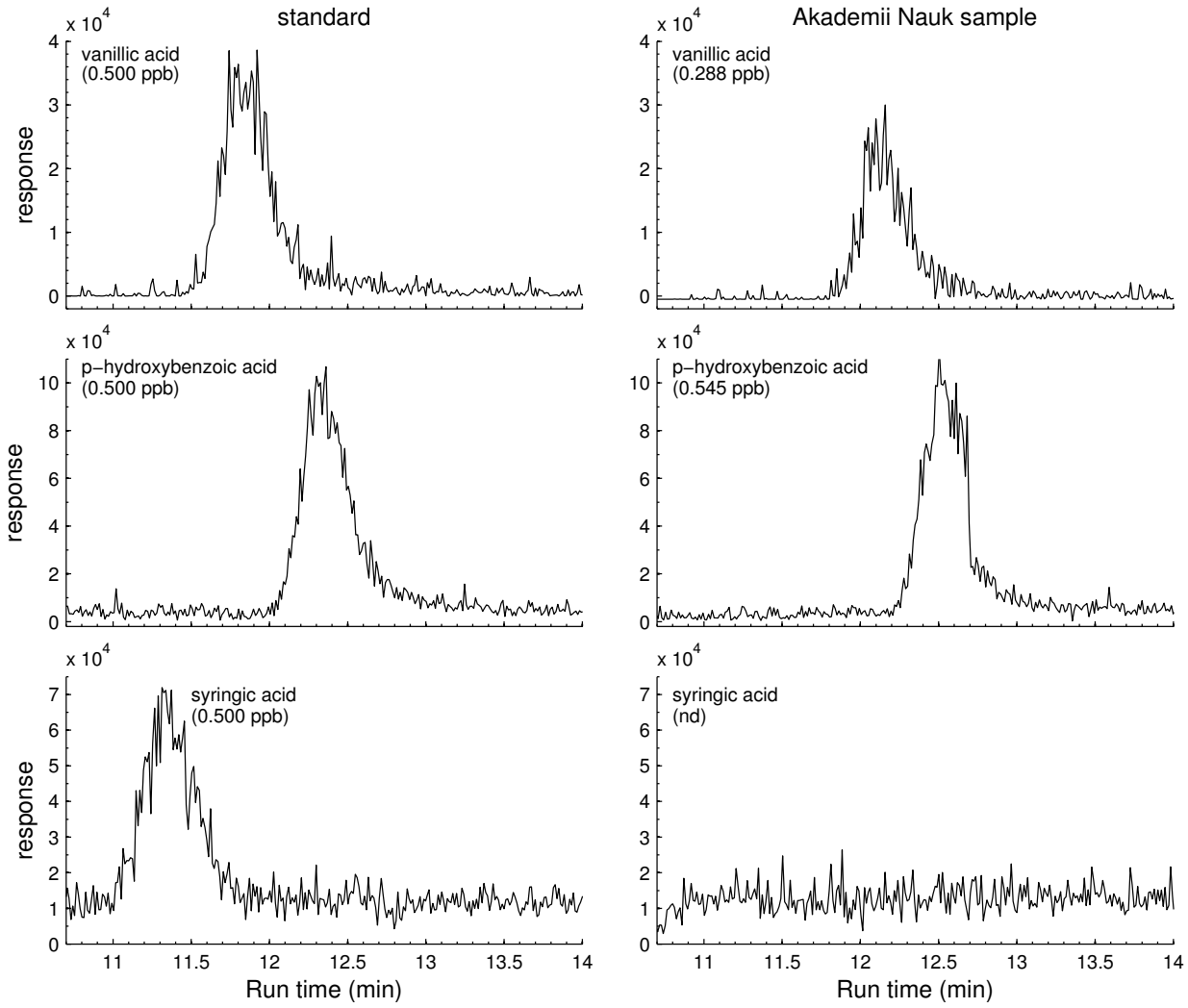

Figure 2.6: Left: Chromatograms of 0.500 ppb vanillic acid, *p*-hydroxybenzoic acid, and syringic acid standards. Right: Chromatograms of an Akademii Nauk ice core sample (219 m, AD 1450) containing 0.288 ppb vanillic acid and 0.545 ppb *p*-hydroxybenzoic acid.

2.5 Future method development

Phenolic compounds produced from biomass burning are important because they are unique to burning and could potentially be used to determine the types of plant material burned. These compounds can therefore be used to determine how biomes changed historically. The IC-ESI/MS/MS method described in this chapter could be optimized to detect several of these compounds.

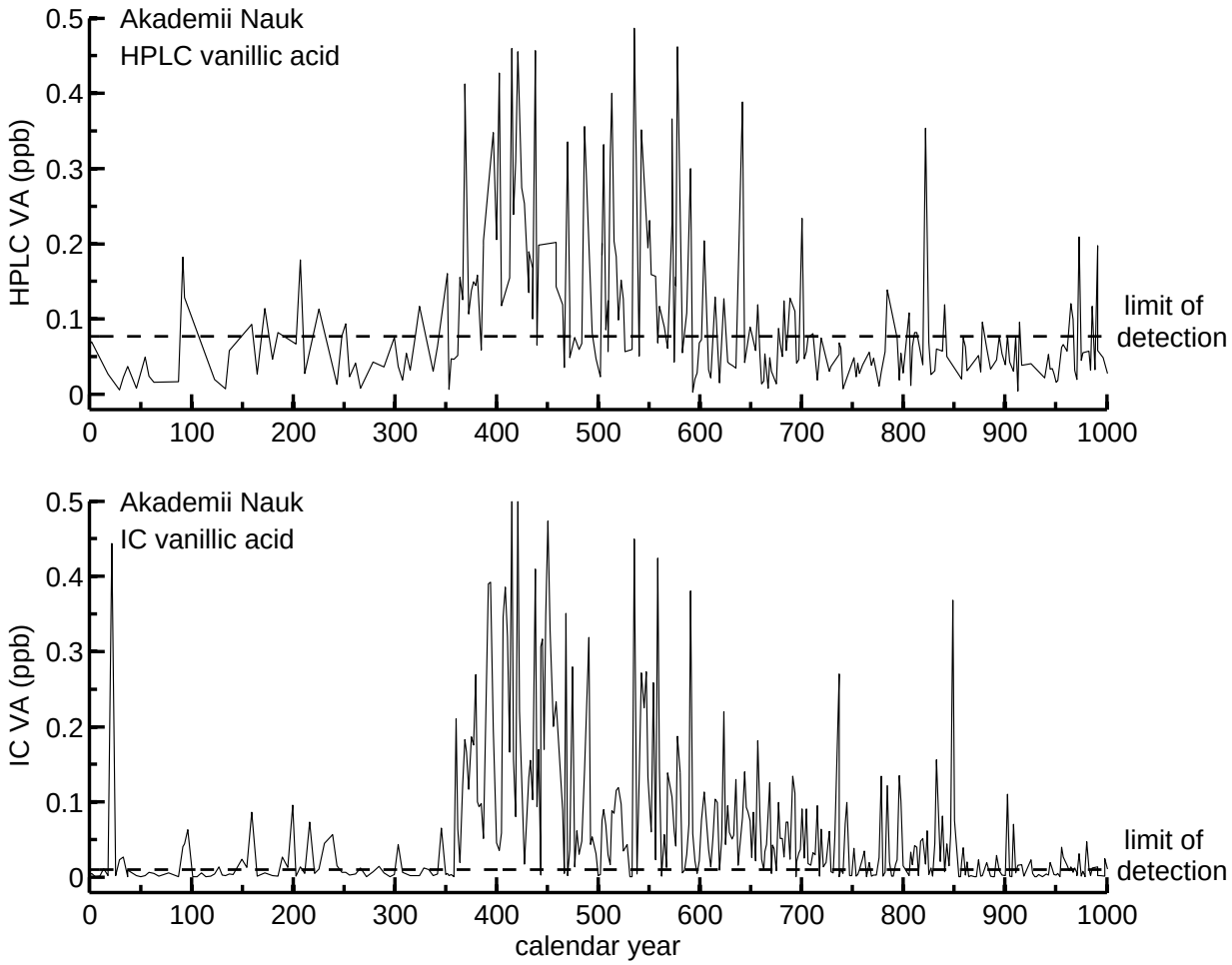

Figure 2.7: Vanillic acid concentrations in Akademii Nauk ice core samples plotted against ice age for the years AD 1-1000 using HPLC-ESI/MS/MS (top) and IC-ESI/MS/MS (bottom).

This method could also be adapted to detect levoglucosan. Levoglucosan is produced by the pyrolysis of cellulose by several plant types. It is emitted in greater quantities than lignin pyrolysis products (*Oros and Simoneit*, 2001a,b; *Oros et al.*, 2006). A column that interacts well with sugars would have to be used in place of the column used in the current method. The Dionex CarboPac SA10 Carbohydrate column is designed to separate simple sugars. This column could be used to increase the sensitivity of levoglucosan analysis in ice core samples by reducing levoglucosan peak broadening.

Chapter 3

Siberian ice core record of biomass burning

3.1 Overview

In this chapter, measurements of vanillic acid (VA) and *p*-hydroxybenzoic acid (*p*-HBA) are presented in an ice core from the Akademii Nauk ice cap in the Russian Arctic. The ice core samples analyzed span the past 3,000 years (1195 BCE-1998 CE). This is the first millennial-scale ice core record of these biomass burning-specific organic acids. This unique ice core record of variability in biomass burning shows major features in the *p*-HBA and VA records that are broadly similar, with multi-century periods of elevated levels superimposed on a baseline that is near or below detection.

3.2 Ice core sample collection and dating

The ice core analyzed in this study was drilled on the Akademii Nauk ice cap (5,575 km^2, 800 m a.s.l), on the Severnaya Zemlya archipelago in the Eurasian Arctic (Figure 3.1; 80°31'N, 94°49'E). The ice core was drilled to the bedrock with a total depth of 723.91 m (*Fritzsche et al.*, 2005). The Akademii Nauk ice cap has a mean annual accumulation rate of 0.46 meters water equivalent per year and a mean annual temperature of -15.7 °C (*Fritzsche et al.*, 2002, 2005; *Weiler et al.*, 2005).

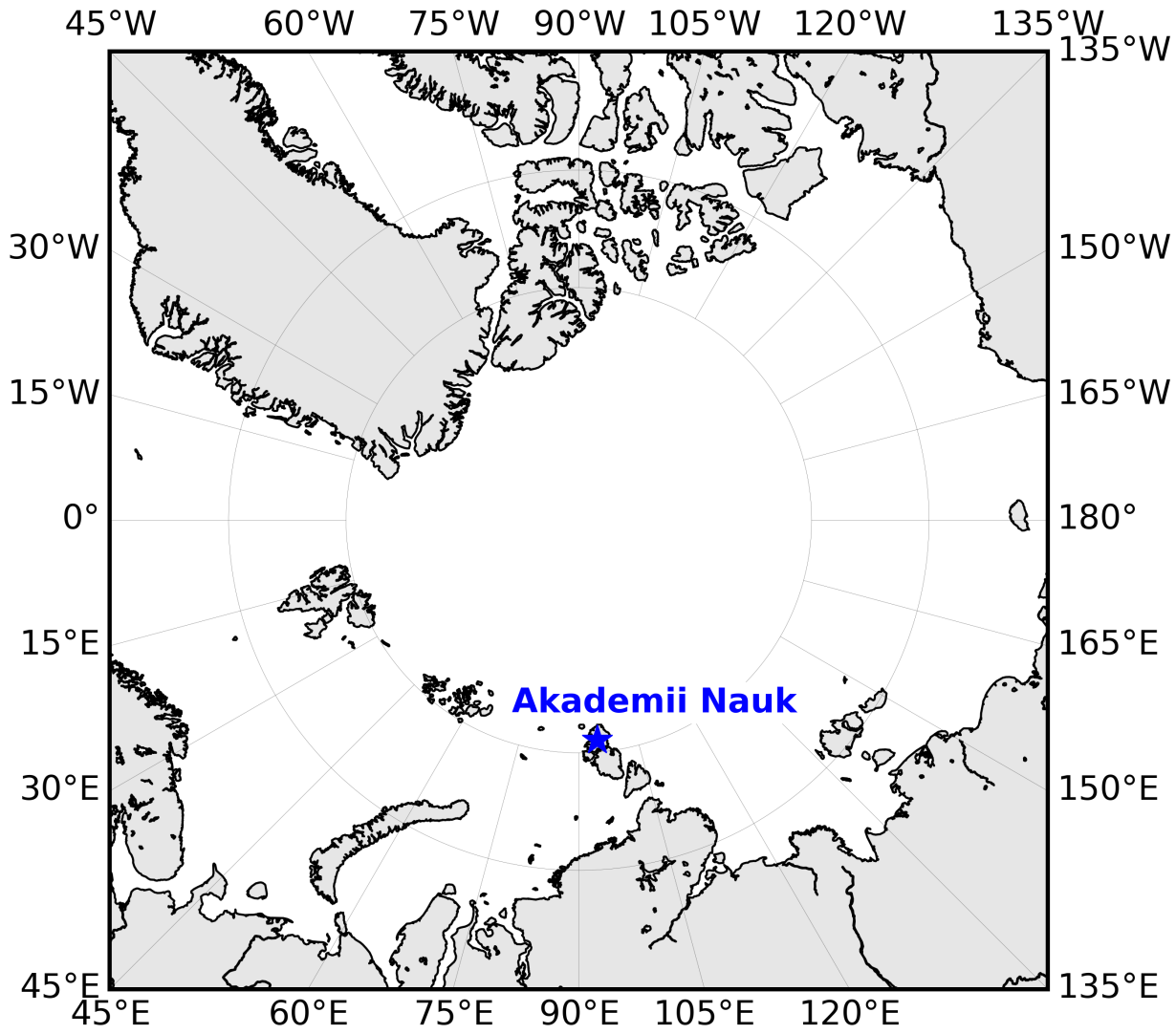

Figure 3.1: Akademii Nauk ice core drilling site 80°31'N, 94°49'E).

The analyses in this study were made on subsamples of meltwater from the ice core. Discrete samples from 0-129 m were melted at the Alfred Wegener Institute from a 30 mm-thick horizontal section of the core, at a frequency of roughly two samples per year. These samples were previously analyzed for major ions (*Fritzsche et al.*, 2005). Samples from 129-671 m were melted at the Desert Research Institute by the continuous melting of a 2.3 cm x 2.3 cm cross section of the core (*McConnell et al.*, 2001). Subsamples for this work were collected from the melt stream via fraction collector at a frequency of roughly one sample per year.

An age scale for the upper 411 m of the core (900-1998 CE) was developed based on annual layer counting of stable water isotopes, on volcanic sulfate signals, and on correlation of high resolution multi-element continuous flow measurements on this and other Arctic ice cores (*Opel et al.*, 2013; *Sigl et al.*, 2013). For the lower part of the ice core (411-724 m), the high-resolution multi-element correlation-based time scale was used (Figure 3.2). There is a significant difference between this timescale and an earlier published Akademii Nauk timescale based on a geophysical flow model (*Opel et al.*, 2013).

3.3 Results and discussion

3.3.1 Measurements and data processing

Analysis of vanillic acid and *p*-hydroxybenzoic acid was carried out using anion exchange chromatography with electrospray ionization and tandem mass spectrometric detection in the negative ion mode (IC/ESI-MS/MS). This method is described in Chapter 2.

In this study, 56% of the vanillic acid (VA) samples were below the detection limit (n = 3,294), and 76% of the hydroxybenzoic acid (*p*-HBA) samples were below the detection limit (n = 2,585). The frequency distributions of the VA and *p*-HBA ice core measurements are not normally distributed, but are skewed towards lower concentrations (Figure 3.3).

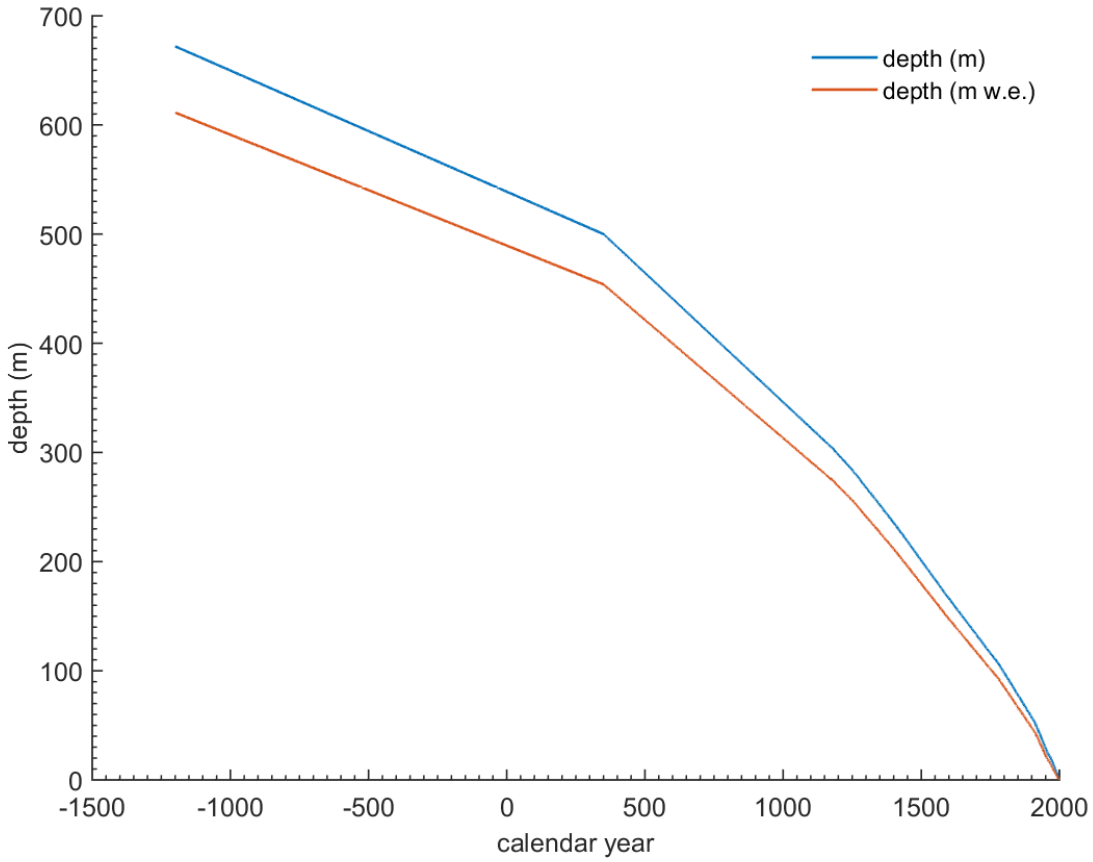

Figure 3.2: Akademii Nauk depth-age scale used in this analysis. The age scale is based on volcanic sulfate signals and correlation of high-resolution multi-element continuous flow measurements on this and other Arctic ice cores (*Sigl et al.*, 2013). This timescale yields a basal age that is ∼500 years longer than an earlier published AN timescale based on a geophysical flow model (blue - meters of ice, orange - meters water equivalent) (*Opel et al.*, 2013).

Logarithmic transformation of the data resulted in a more symmetric distribution. The Box-Cox power law transformation was less successful at normalizing the data. In the Box-Cox transformation, the data are raised to the exponent (λ = -5 to 5) that transforms the data into the most normal distribution.

All transformed data were normalized using the mini-max transformation and the z-score (*Marlon et al.*, 2008). In the mini-max transformation, each data point is subtracted from the minimum of the dataset. The result is then divided by the range of the dataset (maximum-minimum). After the mini-max transformation, each transformed data point is subtracted from the mean of the transformed dataset and then divided by the standard deviation to determine the z-score.

The geometric means of VA and *p*-HBA were $0.0087^{+0.037}_{-0.0071}$ and $0.019^{+0.048}_{-0.014}$ ppb ($\pm 1\sigma$), respectively. Outliers were excluded from the datasets prior to the log transformation. Outliers were defined as VA and *p*-HBA levels greater than $\pm 2\sigma$ above the median (0.0075 ppb and 0.021 ppb, respectively). This process excluded 0.43% of the VA data and 2.6% of the *p*-HBA data.

Both LOESS smoothing (*Marlon et al.*, 2008) and 40-year binned averaging were applied to identify centennial/millennial-scale variability in the log-transformed VA and *p*-HBA records. The LOESS method is a way of fitting a smoothed curve between localized subsets of data. LOESS is a localized method because the fit is weighted by the data closest to each individual point. The size of the subset of data used to weight each data point depends on the "span" setting. If the span is less than 1, then the weighting of each point to the fit is proportional to 1-(distance/maximum distance)^3)^3. If the span used is too small, then an insufficient amount of data will be used for the fit, resulting in a large variance. If the span used is too large, then the data will be over-smoothed. For this analysis, a span of 0.013 was used. The smoothed records resulting from both treatments exhibit the same centennial/millennial-scale features (Figure 3.4). The exponentials of the log-transformed 40-year bin averaged

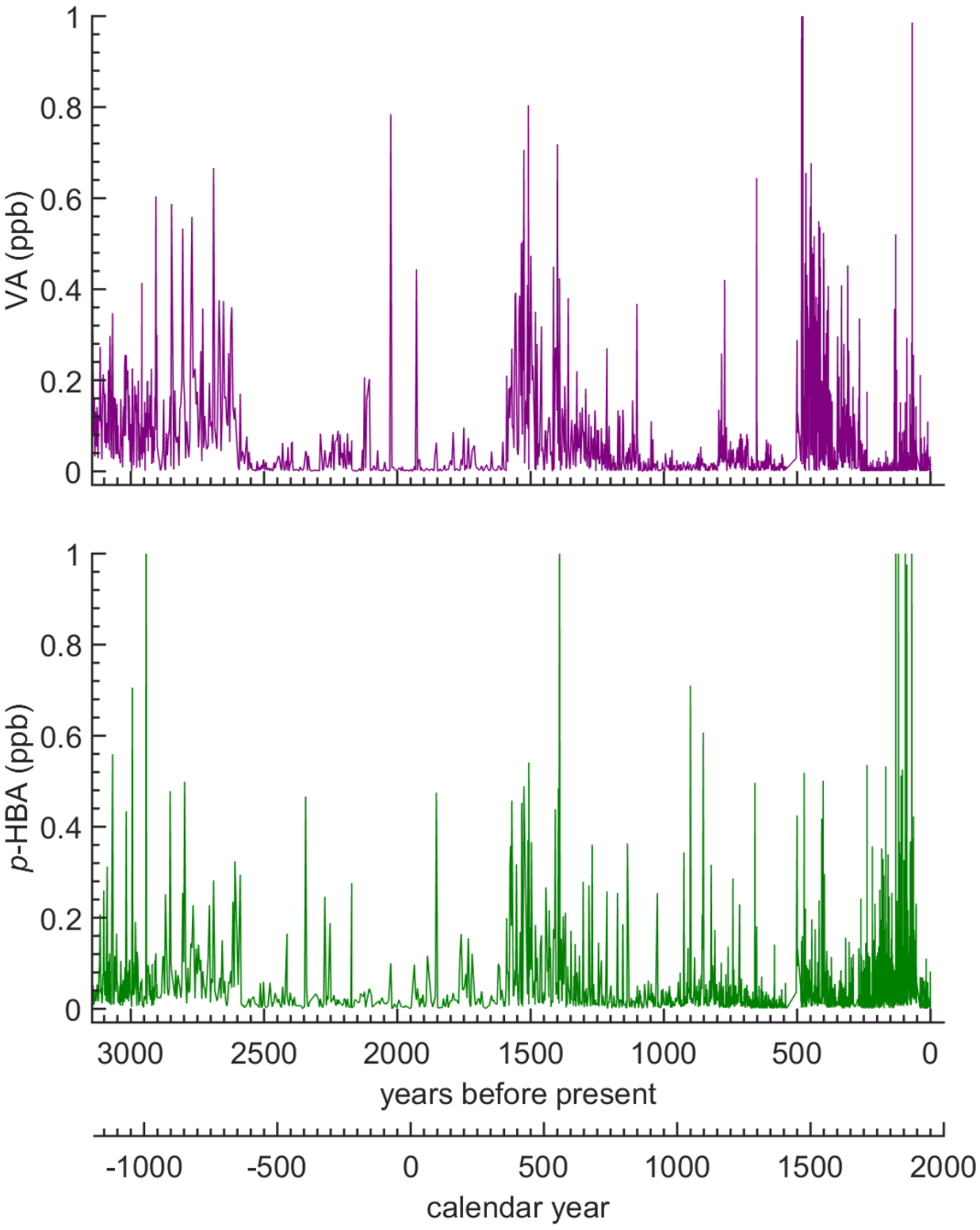

Figure 3.3: Akademii Nauk vanillic acid (top) and *p*-hydroxybenzoic acid (bottom) ice core records.

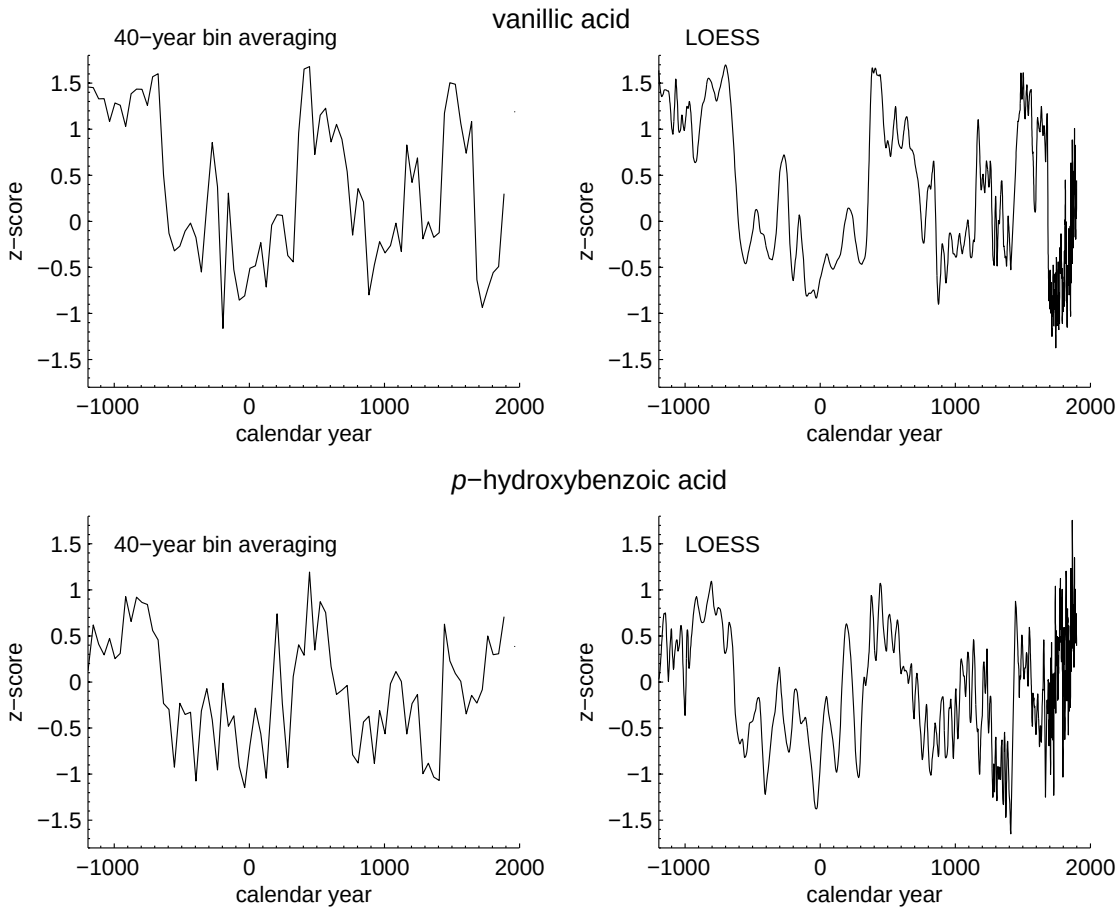

Figure 3.4: Akademii Nauk vanillic acid (top) and *p*-hydroxybenzoic acid (bottom) using 40-year bin averaging (left) and LOESS smoothing (span = 0.013) (right). Outliers were omitted prior to analyses. Data were normalized using the mini-max transformation and the z-score.

VA and *p*-HBA records are used here for interpretation of temporal variability and trends (Figure 3.5). The exponentials of log-transformed 40-year bin averaged VA and *p*-HBA records. The exponential was used to present the data in mass units (ppb).

3.3.2 The raw data

VA and *p*-HBA exhibit both short-term and long-term variability. Variability is evidenced by several data points elevated above the baseline throughout the records (Figure 3.3). Long

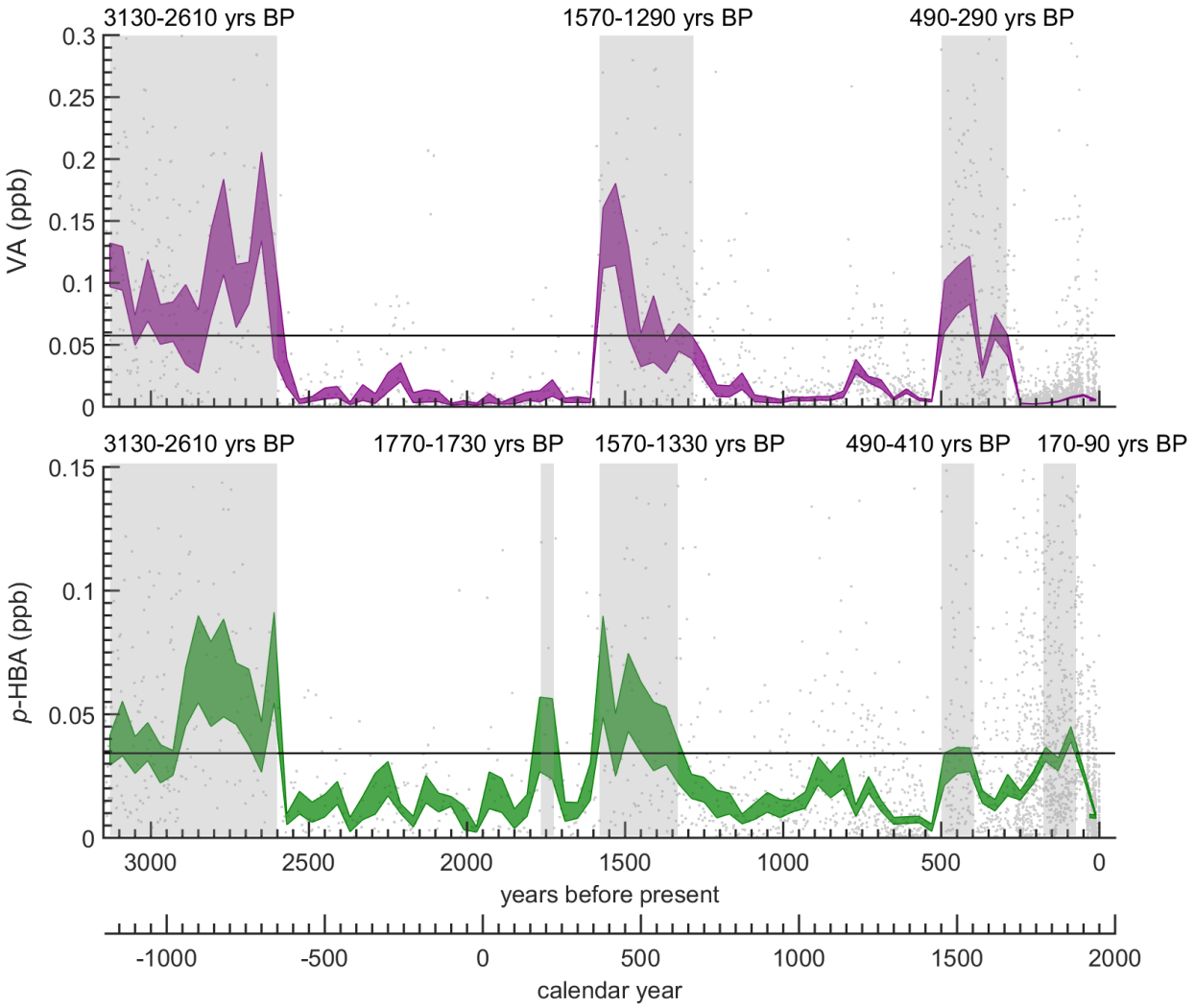

Figure 3.5: Akademii Nauk vanillic acid (top) and *p*-hydroxybenzoic acid (bottom) ice core records. Fills are exponentials of ± 1 standard errors of 40-year bin averages of the log-transformed data. Data above the line are in the upper quartile of the averaged dataset. Gray bars are periods of elevated vanillic acid or *p*-hydroxybenzoic acid. Elevated periods are defined as periods when averaged data are in the upper quartile of the transformed dataset.

periods of several data points above the baseline reveal multi-decadal and multi-century periods of elevated VA or *p*-HBA. Sporadic data points above the baseline between these periods of long-term variability show short-term periods of elevated VA and *p*-HBA. Long-term periods of elevated VA and *p*-HBA are defined using the 40-year bin averages of the datasets.

3.3.3 Long-term temporal variability and trends

The measurements reveal evidence of three multi-century periods of elevated VA and *p*-HBA, which presumably indicate extended periods of elevated biomass burning in northern Asia (Figure 3.5). Periods with averages in the upper quartile (75^{th} percentile) of the 40-year bin averaged log-transformed dataset are defined as periods of elevated VA or *p*-HBA. These periods in the VA record are from 3,130-2,610 ± 40 years before present (BP), 1,570-1,290 ± 40 years BP, and 490-290 ± 40 years BP (1180-660 BCE, 380-660 CE, and 1460-1660 CE). Present is defined as 1950 CE. Elevated periods in the *p*-HBA record are from 3,130-2,610 ± 40 years BP, 1,770-1,730 ± 40 years BP, 1,570-1,330 ± 40 years BP, 490-410 ± 40 years BP, and 170-90 ± 40 years BP (1180-660 BCE, 180-220 CE, 380-620 CE, 1460-1540 CE, and 1780-1860 CE). Three of the elevated periods in the datasets overlap. VA and *p*-HBA are both elevated from 3,130-2,610 ± 40 years BP, 1,570-1,330 ± 40 years BP, and 490-410 ± 40 years BP (1180-660 BCE, 380-620 CE, and 1460-1540 CE).

The levels of aromatic organic acids during these periods are enriched many-fold over the background levels in between. The vanillic acid peaks range from below detection to about 0.2 ppb, using the 40-year bin averaged log-transform of the dataset. This value is a 2200% increase from the geometric mean of the dataset (0.0087 ppb). The *p*-hydroxybenzoic acid peaks range from below detection to 0.071 ppb, using a 40-year bin averaged log-transform of the dataset. This value is a 270% increase from the geometric mean of the dataset (0.019 ppb). All of the peaks in these datasets are large deviations from the mean.

3.3.4 Interpreting the record

The 3 kyr record of VA and *p*-HBA in the Akademii Nauk ice core reflects the combined effects of variations in emissions, atmospheric transport, and depositional processes (i.e. wet vs. dry deposition). The levels of these compounds may also be influenced by changes in snow accumulation rate (leading to variable dilution of the signals) and possible post-depositional modification due to chemical reactions or volatility (*Grannas et al.*, 2004). In this section, the extent to which these various processes likely influence the Akademii Nauk record is discussed. It is, of course, impossible to unravel all of these effects definitively with data from a single ice core. As the first millennial-scale record of these tracers, this dataset is valuable as the first record available for assessing the influences of these processes in the long-term.

Here we interpret these aromatic acids as evidence of extensive wildfire emissions. The only potential alternative might be direct biogenic emissions, perhaps associated with some disturbance such as drought or widespread infestation, but there is no evidence in the literature of aromatic acid emissions associated with such phenomena.

VA and *p*-HBA are aromatic organic acids. VA has a boiling point of 353.4°C. *p*-HBA decomposes upon boiling. These species are semivolatiles that may reside either in the gas or condensed phase depending on aerosol water content, pH, and the concentration of cations that can form stable complexes with these acids. Photochemical oxidation of semivolatile organics like VA and *p*-HBA is also linked to volatility. Photochemical models suggest that such compounds are prone to rapid oxidation by OH in the gas phase, but are shielded from oxidation in the aerosol phase.

The gas phase atmospheric lifetimes of organic aerosols are dependent on the rate of their reaction with the hydroxyl radical (*Donahue et al.*, 2013). The rate constants of the vanillic acid and *p*-hydroxybenzoic acid reactions with the hydroxyl radical in the atmosphere are

$1.22\text{x}10^{-11}$ cm^3/molec-sec and $1.3\text{x}10^{-11}$ cm^3/molec-sec, respectively. Based on these rate constants, the atmospheric lifetime of vanillic and *p*-hydroxybenzoic acids in the gas phase is ∼11 hours. They are shielded from oxidation in the condensed phase, which means that their atmospheric lifetimes are longer (*Donahue et al.*, 2013). If the oxidation of organic aerosol by the hydroxyl radical is dependent on the size of the particle, then a 500 nm particle has an atmospheric lifetime of ∼5.8 days and a 200 nm particle has an atmospheric lifetime of ∼3 days (*Donahue et al.*, 2013). Long-range transport of vanillic acid has been observed in atmospheric aerosol in the Arctic in both coarse and fine (submicron) particles, suggesting both long-range and regional transport (*Zangrando et al.*, 2013).

Vanillic acid and *p*-hydroxybenzoic acid are likely more stable after deposition under high accumulation rate conditions because they are vulnerable to photochemically-induced reactions in the snowpack (*Grannas et al.*, 2007). If post-depositional processes affected vanillic acid and *p*-hydroxybenzoic acid levels in the ice core, then there would be a relationship between vanillic acid or *p*-hydroxybenzoic acid flux and accumulation rate. The large dynamic range of the VA and *p*-HBA signals make it very unlikely that changes in accumulation rate influence the observed trends. The age-depth relationship for Akademii Nauk is linear in the upper part of the core, to about 140 m, indicating relatively constant average accumulation over the period from 1700-2000 CE. Below about 140 m, the rate of increase in age increases with depth, consistent with a model of layer thinning due to ice flow with relatively constant accumulation (Figure 3.1) (*Opel et al.*, 2013). There is no evidence of very large changes in accumulation that would be required in order to generate the VA and *p*-HBA peaks observed in the ice core.

Changes in aerosol or snow chemistry could influence partitioning and hence, the trends observed in the ice core. If this was the case, one might expect to find a positive correlation to the abundance of seasalt Na^+ or terrestrial-derived Ca^{2+} (higher pH) or negative correlations to volcanic sulfate (lower pH). No such correlations are observed in the Akademii Nauk ice

core (Figure 3.6). Therefore, aerosol/ice core chemistry is likely not the primary control on the trends in VA and *p*-HBA.

The Akademii Nauk site experiences frequent seasonal melting (particularly during the past century). Soluble compounds have undergone redistribution on time scales of roughly 5 years due to percolation of meltwater (*Fritzsche et al.*, 2005; *Opel et al.*, 2013). For this reason, we interpret only major multidecadal features rather than interannual variability. The timing of higher/lower melt layer percentages in the upper part of the ice core do not correlate with timing of elevated periods in the vanillic acid record (Figure 3.7; T. Opel, personal communication).

The observed variations in abundance of VA and *p*-HBA in the Akademii Nauk ice core most likely reflect variations in the atmospheric levels and deposition of biomass burning-derived aerosols. The levels and relative abundance of the two compounds may also reflect changes in the nature of the biomass fuels and/or combustion conditions (temperature, oxygen levels, etc.). The timing of the VA and *p*-HBA peaks is consistent throughout most of the records. A linear fit comparison between the 40-year bin-averaged log-transformed datasets gives an r-squared value of 0.47 and a p-value < 0.000001 (Figure 3.8). The similarity in VA and *p*-HBA strongly suggests that the two compounds are derived from a common source for much of the record.

Comparing the records to other proxy records (e.g. charcoal and other ice core proxies) and identifying the plant type burned can help to determine the source of burning. The large millennial-scale vanillic acid and *p*-hydroxybenzoic acid peaks are quite different from the enrichment patterns typically found for inorganic ice core burning tracers such as ammonia, nitrate, or black carbon, where relatively small fire signals are superimposed on a high background from other natural sources (Figure 3.9) (*Eichler et al.*, 2011; *Fuhrer et al.*, 1996; *Savarino and Legrand*, 1998; *Taylor et al.*, 1996; *Whitlow et al.*, 1994). Ammonium and nitrate are derived from biogenic and other sources in addition to biomass burning. Statistical

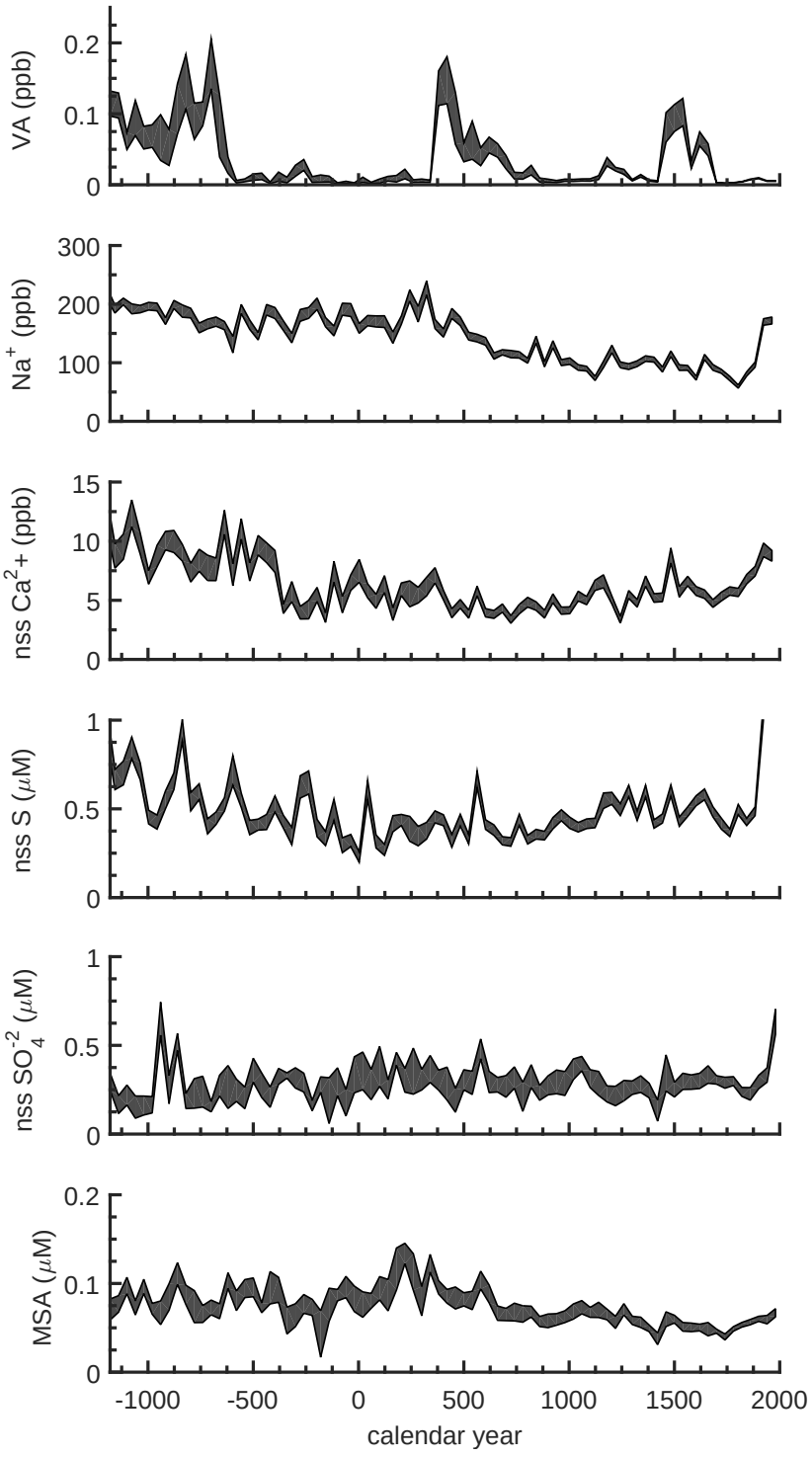

Figure 3.6: Akademii Nauk ice core chemistry over the past 3,000 years. Data are 40-year bin-averaged (gray fill is ± 1 standard error of log transform) measurements from the Akademii Nauk ice core over the past 3,000 years. From top: 1) vanillic acid measurements from this study, 2) sodium (J. McConnell, personal communication) 3) non-seasalt calcium (J. McConnell, personal communication), 4) non-seasalt sulfur (J. McConnell, personal communication), 5) non-seasalt sulfate (this study), and 6) methanesulfonate (this study).

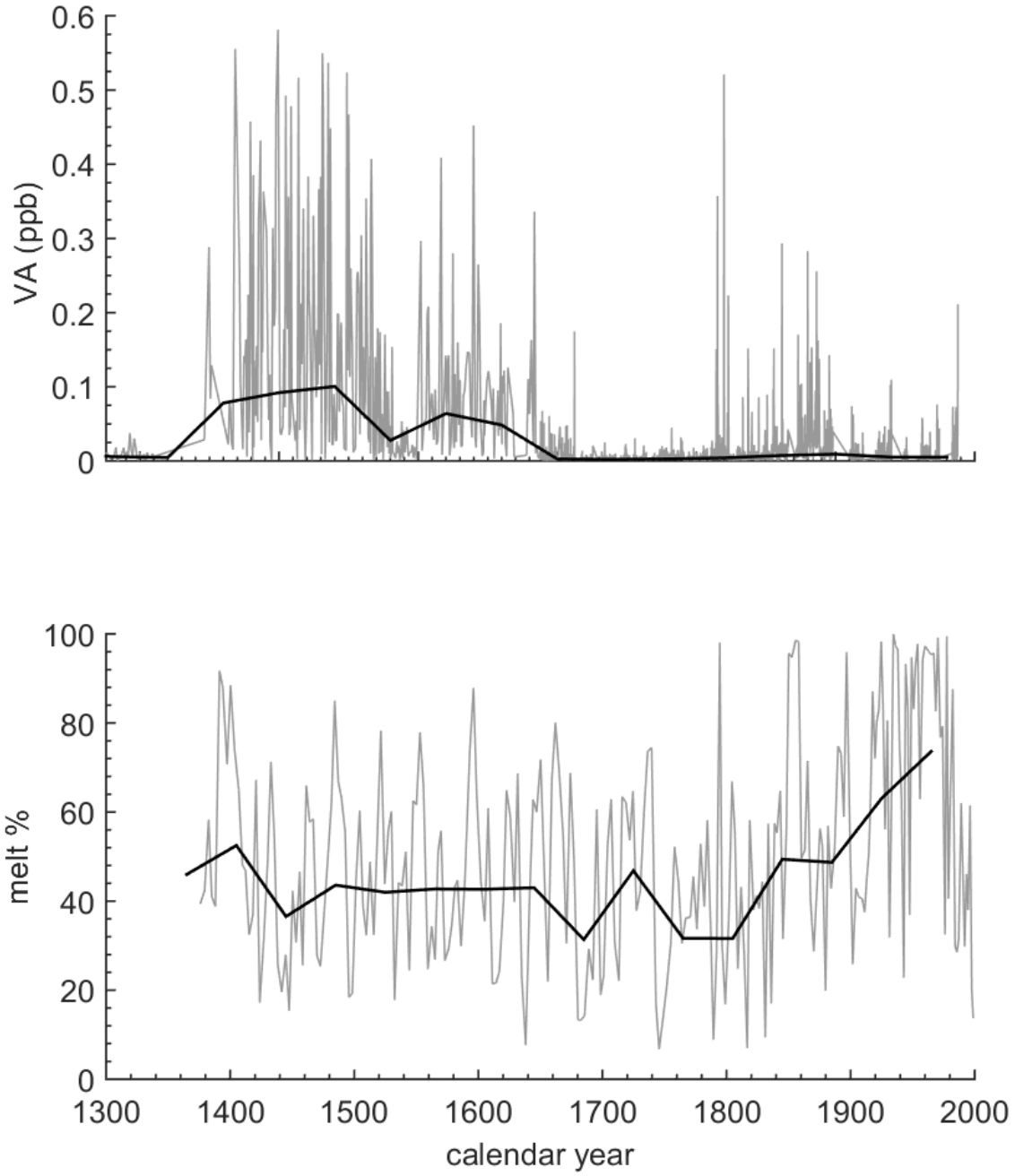

Figure 3.7: Akademii Nauk vanillic acid (top) and melt layers (bottom, T. Opel, personal communication). The solid black lines on both plots are 40-year bin-averages of the log transform.

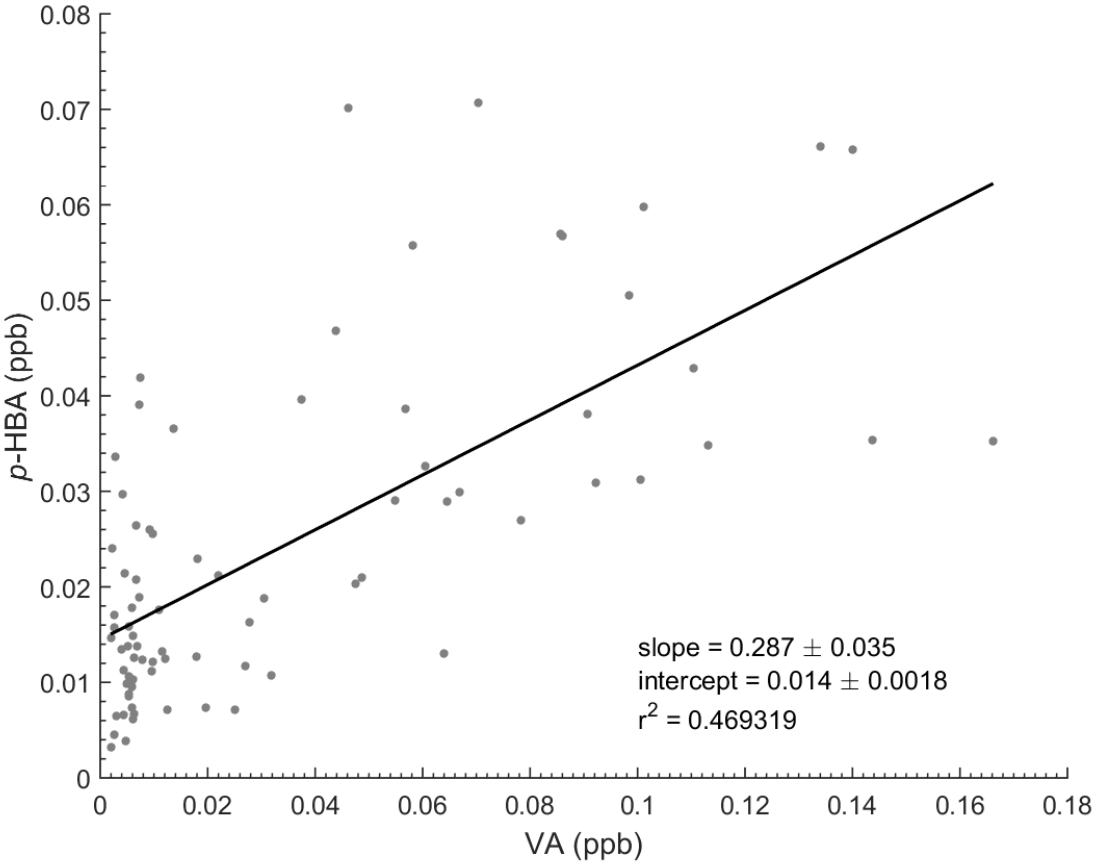

Figure 3.8: Linear fit of the 40-year bin averaged log-transform of VA against the 40-year averaged log-transform of *p*-HBA.

analysis is necessary to determine the biomass-burning signal from these compounds. Black carbon is interpreted as a biomass-burning signal prior to industrialization in the literature (*McConnell et al.*, 2007; *Chylek et al.*, 1995). The differences between the VA and *p*-HBA records and the black carbon record could suggest that the VA and *p*-HBA records are showing burning of particular types of biomass or that the atmospheric transport of VA and *p*-HBA is different from that of total black carbon.

3.3.5 Transport

VA and *p*-HBA are transported through the atmosphere from biomass burning locations to the Akademii Nauk ice core site. The HYSPLIT model was used in this study to determine possible source locations of biomass burning to the Akademii Nauk ice core site (*Stein et al.*, 2015; *Draxler et al.*, 1999; *Draxler and Hess*, 1998, 1997). Meteorological data (NCEP/NCAR Reanalysis) from 2008 for spring (trajectories beginning March 1, 2008-May 31, 2008), summer (trajectories beginning June 1, 2008-August 31, 2008), and fall (trajectories beginning September 1, 2008-November 30, 2008) were used for 10-day back-trajectories from the ice core site (80°N, 94°E) to possible biomass burning source locations (*Kalnay et al.*, 1996). Data can be accessed at: ftp://arlftp.arlhq.noaa.gov/pub/archives/reanalysis. One trajectory was run every 12 hours starting from 12:00 AM and 12:00 PM local time (UTC + 7 hours) each day for each three-month period (spring, summer, and fall). Back trajectories were run starting at 100 m and 500 m above ground level. 2008 was chosen as the year of study because it was a high fire year in Russia (*Matsui et al.*, 2011; *Warneke et al.*, 2010).

Trajectories started at 12:00 AM showed the same result as trajectories started at 12:00 PM. Trajectories generally stay in the Arctic over the 10-day period (Figure 3.10). Trajectories reach Northern Siberia and the northernmost regions of Canada in all three seasons starting at both 100 m and 500 m above ground level. The farthest reaching trajectories are in the

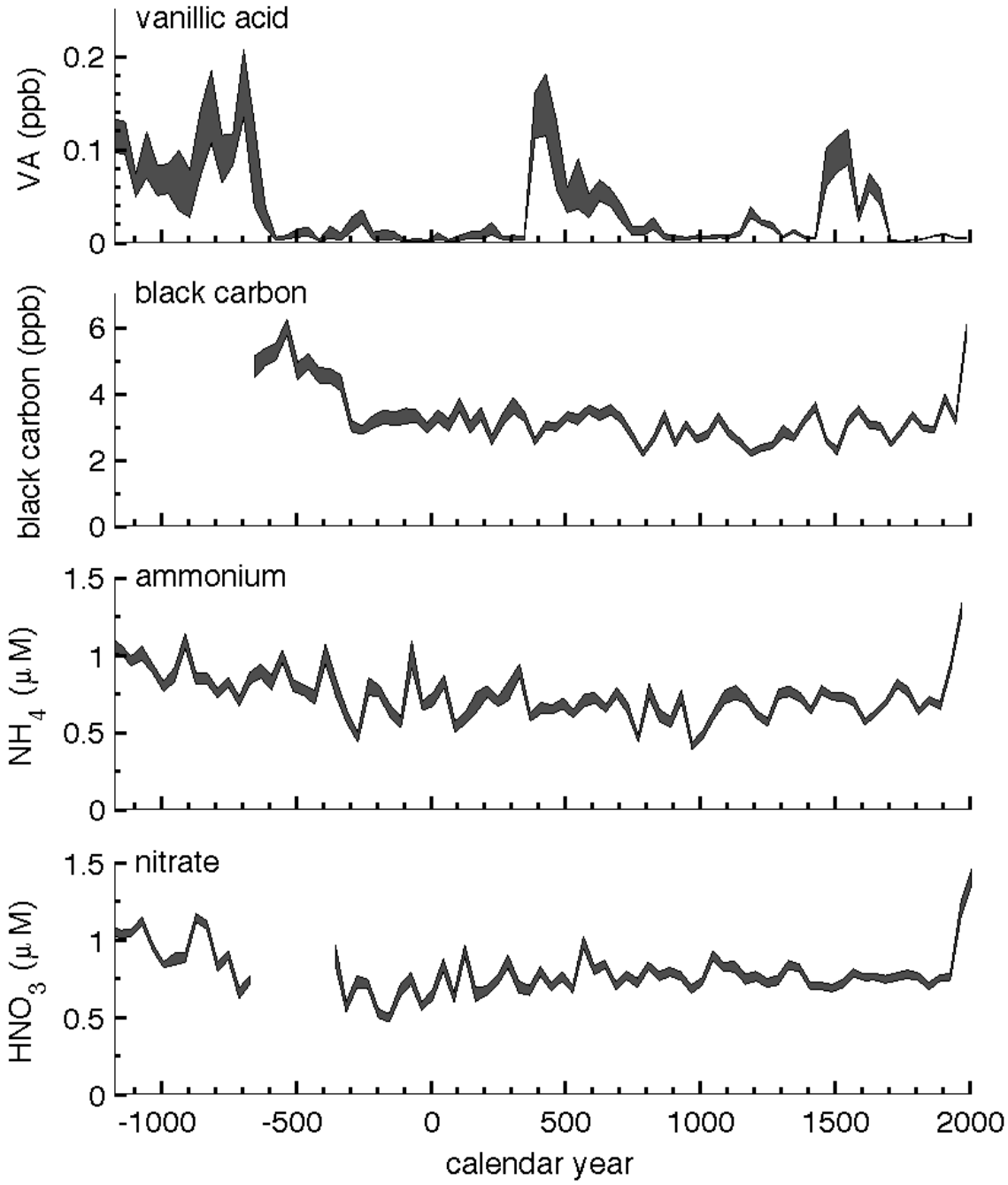

Figure 3.9: Burning tracers in the Akademii Nauk ice core over the past 3,000 years. Data are 40-year bin-averaged (gray fill is ± 1 standard error of log transform) measurements from the Akademii Nauk ice core over the past 3,000 years. From top: 1) vanillic acid measurements from this study, 2) black carbon (J. McConnell, personal communication) 3) ammonium (J. McConnell, personal communication), 4) nitrate (J. McConnell, personal communication).

fall, when several trajectories reach below 60° N in Siberia. This back-trajectory analysis suggests that Siberia is the most likely biomass burning source region of the Akademii Nauk ice core site.

3.4 Conclusion

The development of wildfire records from measurements of aromatic organic acids in polar ice cores has potential as a qualitative proxy for biomass burning on millennial time scales. Clearly, analysis of multiple ice cores is needed to validate the trends observed here and to differentiate between regional variations in emissions versus patterns of atmospheric transport. Molecules like aromatic acids also have the potential to provide information about the composition of the precursor lignin, and hence about the composition of the original ecosystems. Such records are needed in order to study millennial time scale relationships between climate and ecological changes.

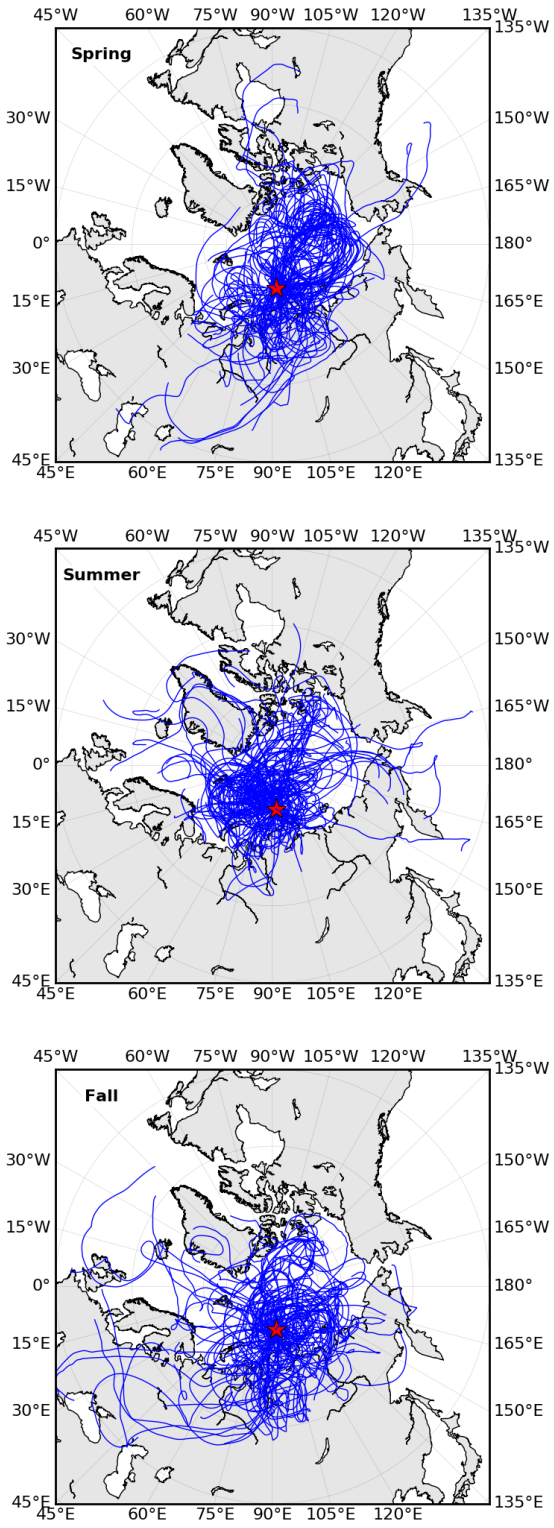

Figure 3.10: 10-day Air mass back-trajectories from the Akademii Nauk ice core site (red stars) starting at 12:00 PM from 500 m above ground level above ground level. From top: 1) spring (trajectories beginning March 1, 2008-May 31, 2008), 2) summer (trajectories beginning June 1, 2008-August 31, 2008), and 3) fall (trajectories beginning September 1, 2008-November 30, 2008).

Chapter 4

Northeastern Greenland ice core record of Biomass Burning

4.1 Overview

In this chapter, measurements of the aromatic biomass burning tracer vanillic acid (VA) in an ice core from Tunu in Northeastern Greenland covering the past 1,700 years (268-2013 CE) are presented. Elevated VA levels in the Tunu ice core are not large deviations from the baseline. These low VA levels complicate the interpretation of VA as a biomass burning signal. Elevation of VA from the baseline must be due to biomass burning rather than other influences, such as snow accumulation rate, transport, or post-depositional processes in order to interpret VA as a biomass burning signal. The Tunu ice core site has a variable accumulation rate. Comparison between the Tunu accumulation rate and Tunu VA suggests that accumulation rate changes could explain some of the variability in the Tunu VA record. Reversible deposition could also play a role VA variability in the Tunu ice core.

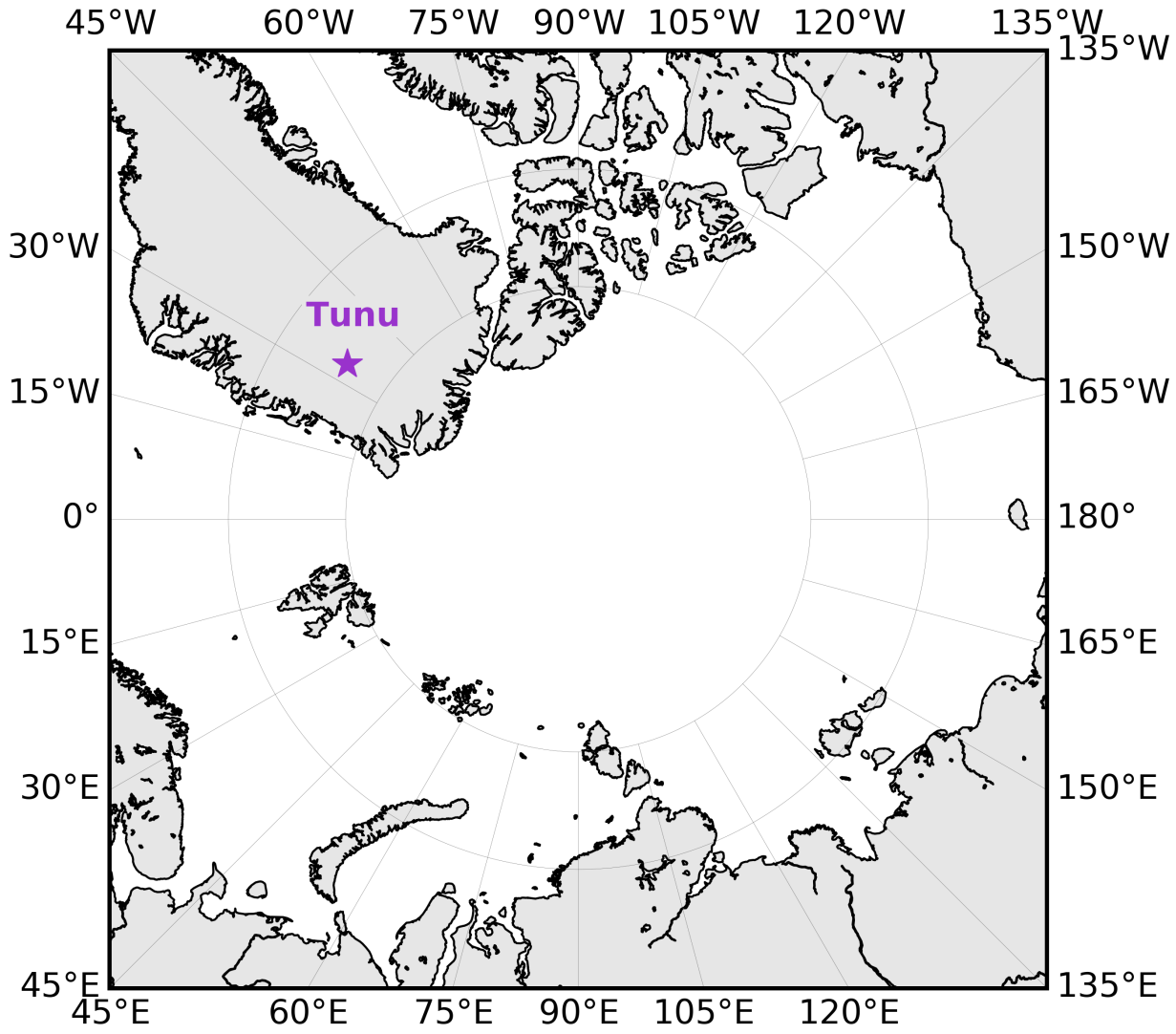

Figure 4.1: Tunu ice core drilling site (78.04°N, 33.88°W).

4.2 Ice core characteristics, dating, and sample collection

The Northeastern Greenland ice core was drilled in the Tunu region in May 2013 (Figure 4.1; 78.04°N, 33.88°W, 2000 m above sea level). The ice core was drilled to a depth of 212 m. The ice core site has a mean accumulation rate of 0.100 m water equivalent yr^{-1} (*Sigl et al.*, 2015).

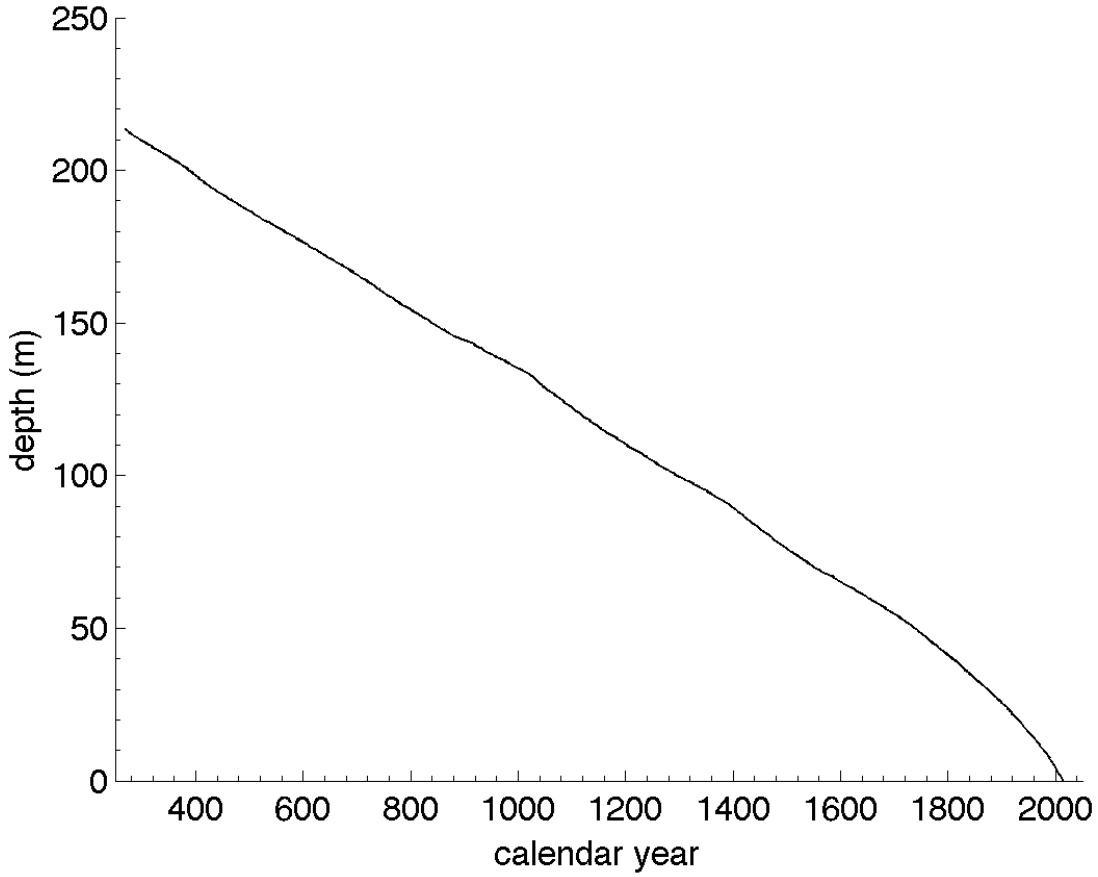

Figure 4.2: Tunu ice core depth-age scale (J. McConnell, personal communication).

An age scale for this ice core was developed based on the annual layer counting of its non-seasalt sulfur and sodium signals (Figure 4.2) (*Mernild et al.*, 2015). Annual layer counts were validated by matching volcanic horizons between this ice core and the NEEM ice core from northwest Greenland (NEEM-2011-S1) (*Mernild et al.*, 2015; *Sigl et al.*, 2013, 2015). The age uncertainty between these ice cores was < 2 years using these volcanic tie points (*Mernild et al.*, 2015; *Sigl et al.*, 2015).

4.3 Methods of sampling and analysis

Meltwater from the Tunu ice core was analyzed for vanillic acid using the IC/ESI-MS/MS method described in Chapter 2. *p*-Hydroxybenzoic acid could not be analyzed in this ice core because of interfering peaks at the same retention time in the blanks. Samples were obtained from the continuous melting of a 33 x 33 mm cross section subsample core at the Desert Research Institute (*McConnell et al.*, 2001; *Sigl et al.*, 2015; *Mernild et al.*, 2015). Discrete samples of the melt stream were collected via fraction collector at a frequency of roughly one sample every 2.5 years. The detection limit for vanillic acid in the Tunu samples was 0.0046 ppb, defined as 3x the standard deviation of MilliQ water blanks (n = 58).

4.4 Results and discussion

4.4.1 Measurements and data processing

In this study, 575 samples were analyzed for vanillic acid (Figure 4.3). The distribution of the measurements was skewed towards lower concentrations. Forty percent of the samples were below the detection limit.

The transformation and smoothing methods described in chapter 3 were used for interpretation of the Tunu ice core VA record. The mini-max transformation and the z-score were used to normalize the data *Marlon et al.* (2008). A more symmetric distribution resulted from logarithmic transformation of the data. The geometric mean was $0.0053^{+0.0069}_{-0.0030}$ ppb ($\pm 1\sigma$). The Box-Cox power law transformation was a less effective method of redistributing the data.

40-year bin averaging and LOESS smoothing were used to identify centennial-scale features in the record. LOESS smoothing is described in Chapter 3. Both smoothing methods show

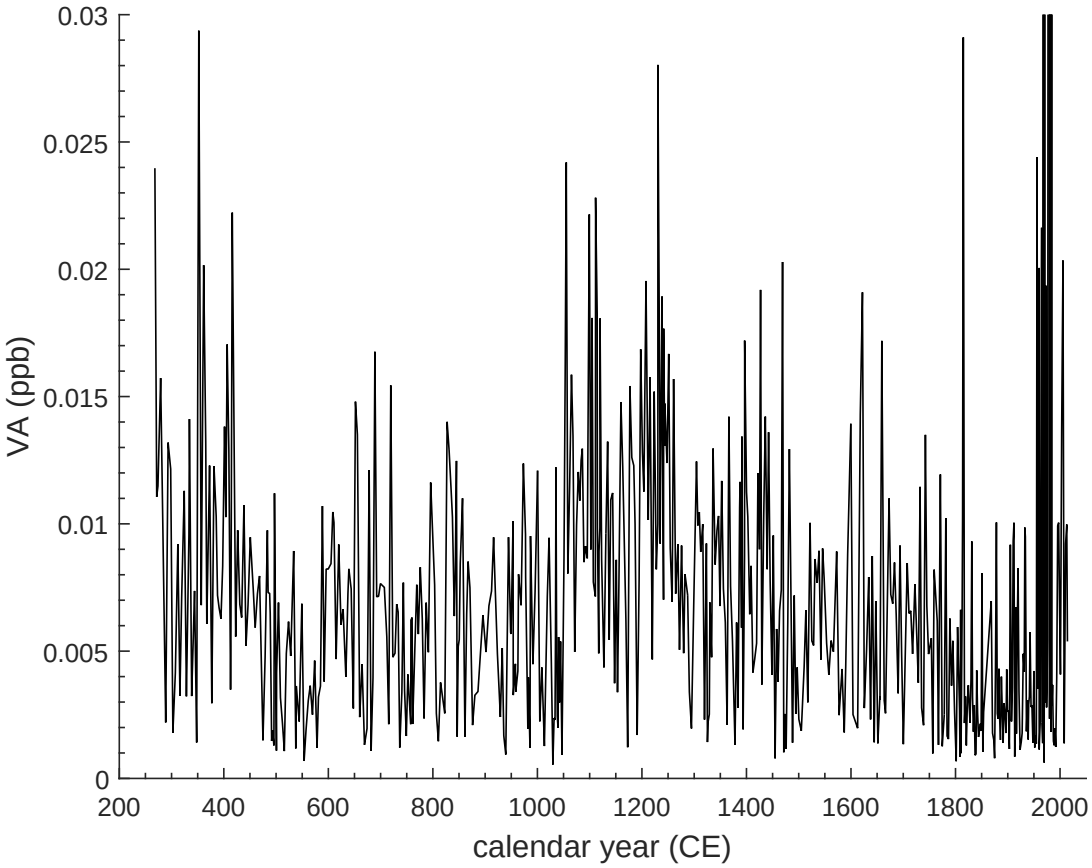

Figure 4.3: Tunu ice core vanillic acid (VA) record.

the same centennial features in the record (Figure 4.4). The 40-year bin averages of the log-transformed VA record are applied here for interpretation of temporal variability. The data ranges from below the detection limit to 0.014 ppb, using the 40-year bin averages of the log transforms.

4.4.2 Temporal variability and trends

The measurements show two multi-century periods of elevated vanillic acid. These periods are from 270-500 CE and 1050-1300 CE. These vanllic acid peaks range from below the detection limit to 0.012 ppb, using the 40-year bin averages of the log-transformed dataset. This value is only a 126% increase from the geometric mean of the dataset. These small deviations above the geometric mean of the dataset make these peaks more difficult to interpret as periods of elevated burning. VA is also elevated from 1900-2000 CE.

4.4.3 Interpretation of the record

The levels of organic aerosols in the Tunu ice core result from the combined influences of emissions, atmospheric transport, depositional processes, and post-depositional processes. The atmospheric reactivity of VA is described in Chapter 3.

The Tunu ice core has a variable accumulation rate. Changes in accumulation rate can affect the levels of VA in an ice core, depending on whether VA was wet deposited or dry deposited (*Saltzman et al.*, 1997). An aerosol is wet deposited if it is dropped onto the ice sheet as precipitation. An aerosol is dry deposited if reaches an ice sheet independently of precipitation. If VA is wet deposited, then the effect of changes in accumulation rate on the VA levels in the ice core will be minor. If VA is dry deposited, then changes in snow accumulation will cause variability in how concentrated the VA levels are in the ice core. When snow accumulation is high, the concentration of VA in the ice core is diluted.

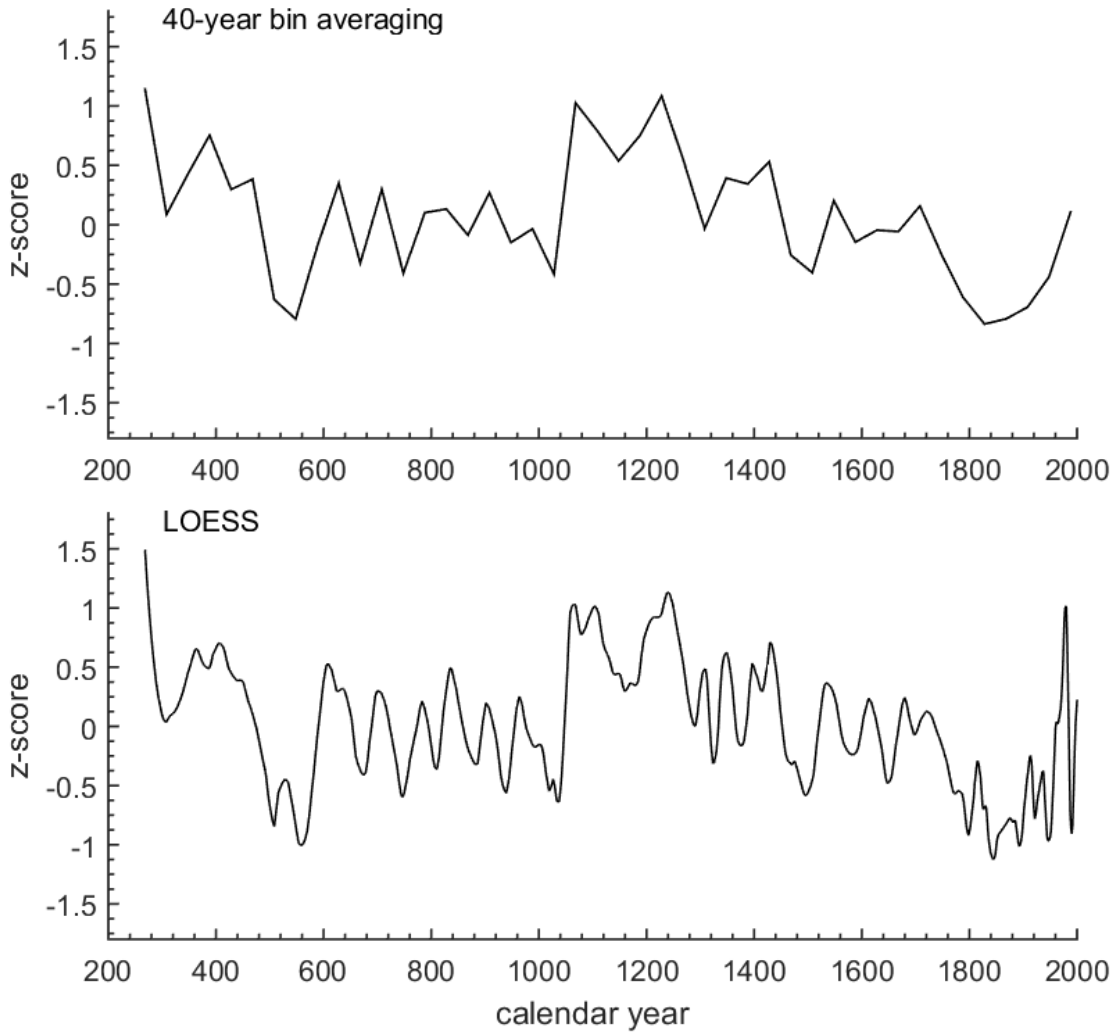

Figure 4.4: Tunu vanillic acid (top) using 40-year bin averaging (top) and LOESS smoothing (span = 0.04) (bottom) of the log transform. Data were normalized using the mini-max transformation and the z-score.

Accumulation is defined as precipitation and losses of water vapor due to sublimation. In the paleo record, accumulation is used as a proxy for paleo-precipitation because the historical precipitation rate is not known (*Saltzman et al.*, 1997).

In order to determine the effect of a variable precipitation rate on VA concentrations in the ice core, the depositional flux of VA was compared to the accumulation rate. The depositional flux (F) is defined as mass of VA per unit area in the ice core per year. It is calculated as follows:

$$F = C_{in\ ice}\ A_{H_2O}\ \rho_{ice}$$

where $C_{in\ ice}$ is the concentration of VA in the ice core (ppb), A_{H_2O} is the accumulation rate (m/yr), and ρ_{ice} is the density of the ice (*Saltzman et al.*, 1997). The density of the ice making up the ice core changes with depth as the layers in the ice core thin due to the pressure of the ice above the deeper layers. In this case, the water flux (kg/m^2/yr), determined based on a thinning function, which was used in place of A_{H_2O} and ρ_{ice} (Figure 4.5; Joe McConnell, personal communication).

The relative contributions of wet and dry deposition to the VA flux were calculated using the following:

$$F = (C_{air}\ V_d)\ +\ (C_{air}\ S\ P_{H_2O})$$

where C_{air} is the concentration of VA in the atmosphere, V_d is the dry deposition velocity for aerosols, S is the wet deposition scavenging ratio, and P_{H_2O} is the accumulation rate. S is defined as the ratio of the VA concentration precipitated out of the atmosphere and the VA atmospheric concentration (*Saltzman et al.*, 1997). If S, V_d, C_{air} and are constant, then there is a linear relationship between the VA flux and the accumulation rate (P_{H_2O}),

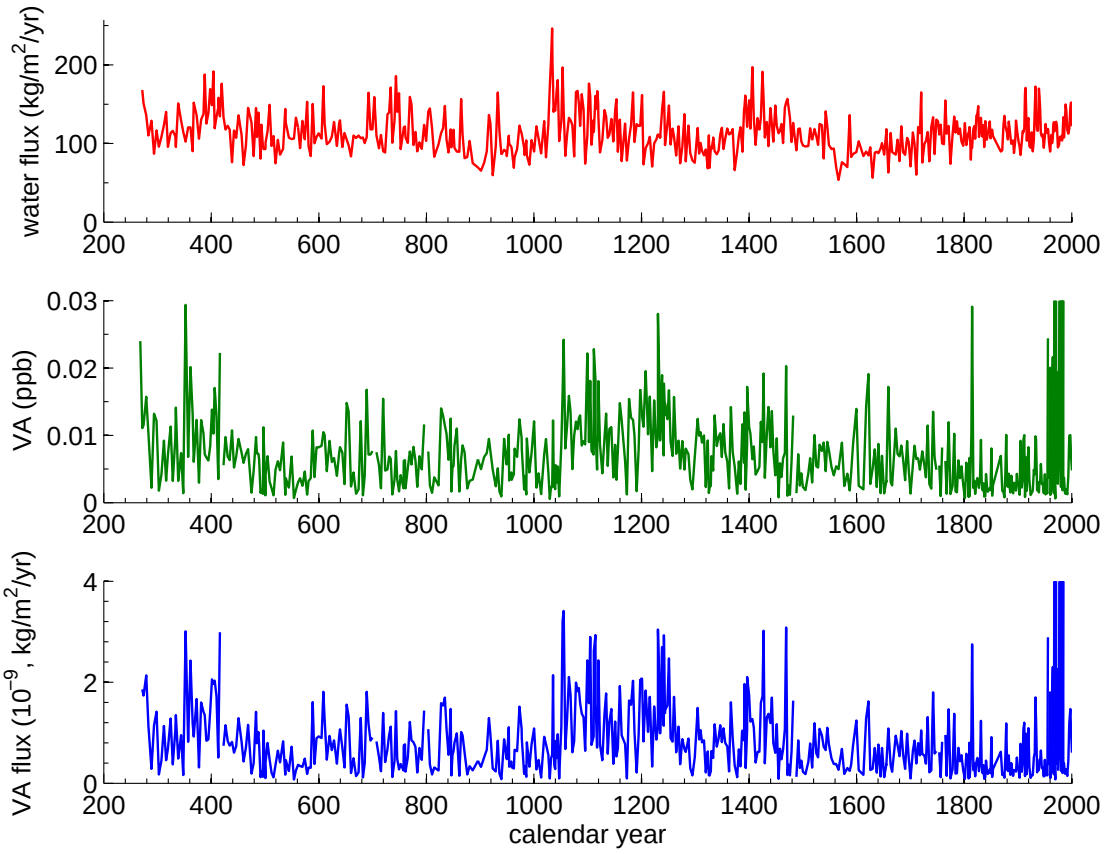

Figure 4.5: Relationship between Tunu ice core VA and water flux. Water flux (top), VA in the ice core (middle), VA flux (bottom).

as follows:

$$F = D \ + \ (W \ P_{H_2O})$$

where the slope (W) is the concentration of VA in the precipitation (i.e. the wet deposition component). The intercept (D) is the flux of the compound that is dry deposited (*Saltzman et al.*, 1997). Only VA measurements above the detection limit were used in the linear fit. VA levels greater than the mean VA level + 1 standard deviation were excluded from the linear fit. VA levels after 1600 CE were also excluded from the linear fit because the accumulation rate increases near 1600 CE. The intercept (D) is close to zero in the Tunu ice core (Figure 4.6). This intercept suggests that dry deposition was not an important contribution to the VA levels in the ice core.

This relationship between accumulation rate and flux would not necessarily be linear if S, V_d, or C_{air} are not constant over time. For example, C_{air} could change if the VA level increases in the atmosphere due to a burning event. The linear trend is still significant ($p < 10^{-6}$) if high levels of VA (> mean +1 standard deviation) before 1600 CE are included, but the r-squared value decreases from 0.30 to 0.21. These high values could represent high fire years. The accumulation rate declines from 1200-1300 CE, but VA flux increases (Figure 4.7). Biomass burning could have been elevated from 1200-1300 CE.

VA flux could also deviate from the linear trend if VA is reversibly deposited. VA is reversibly deposited if it is lost after deposition onto the ice sheet via sublimation or photochemical reaction. VA can only undergo photochemical reaction if it is exposed to sunlight. VA loss would therefore increase under low accumulation conditions when VA is not buried in the ice quickly. Under low accumulation conditions, lower VA flux values than expected from the linear trend would be present if VA is reversibly deposited.

The flux at low accumulation rates was compared to the expected flux based on the linear

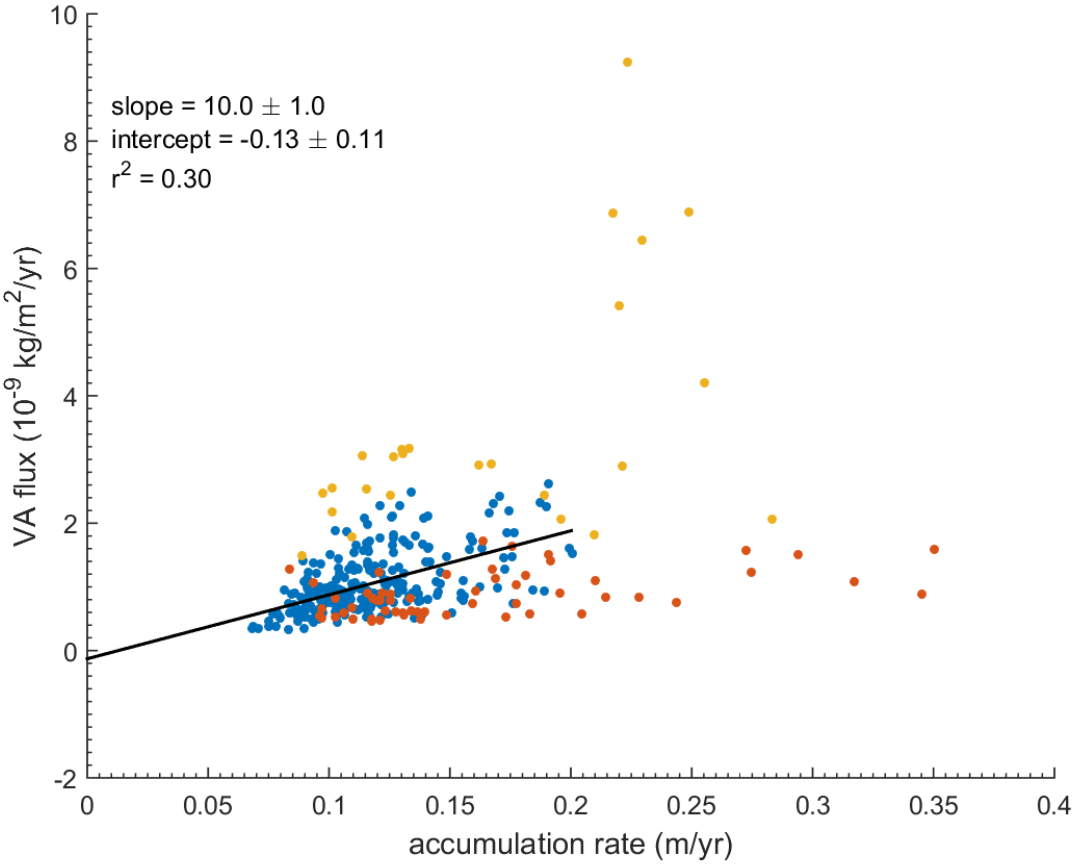

Figure 4.6: Relationship between accumulation rate and VA flux. Data below the detection limit. Data included in fit are below the mean +1 standard deviation of VA (ppb) and before 1600 CE (blue). Data above the mean +1 standard deviation of VA (ppb, yellow), and all other data after 1600 CE (orange) were excluded from the linear fit.

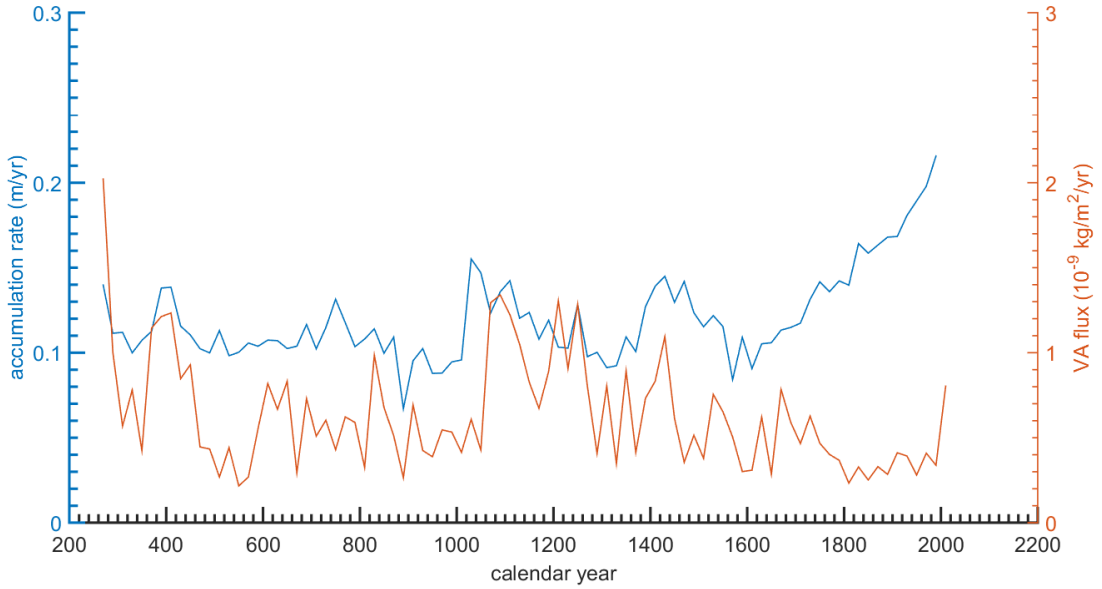

Figure 4.7: Tunu accumulation rate (blue) and VA flux (orange). Data are 40-year bin-averages of the log transforms.

trend to determine the likelihood of reversible deposition of VA. Low accumulation was defined as accumulation rates lower than the average accumulation rate before 1600 CE (0.12 m/yr). Lowest expected VA flux values were determined using the slope and the intercept of the linear fit (Figure 4.6). 70% of the expected VA flux values calculated were greater than the actual VA flux values (n = 216). This result suggests that reversible deposition could be an important process in the Tunu ice core.

The possible correlation between aerosol/snow chemistry and VA trends is described in Chapter 3. VA could be negatively correlated in a more acidic environment. These correlations are not observed in the Tunu ice core (Figure 4.8). Therefore, ice core chemistry is likely not an important driver of VA trends in the Tunu ice core.

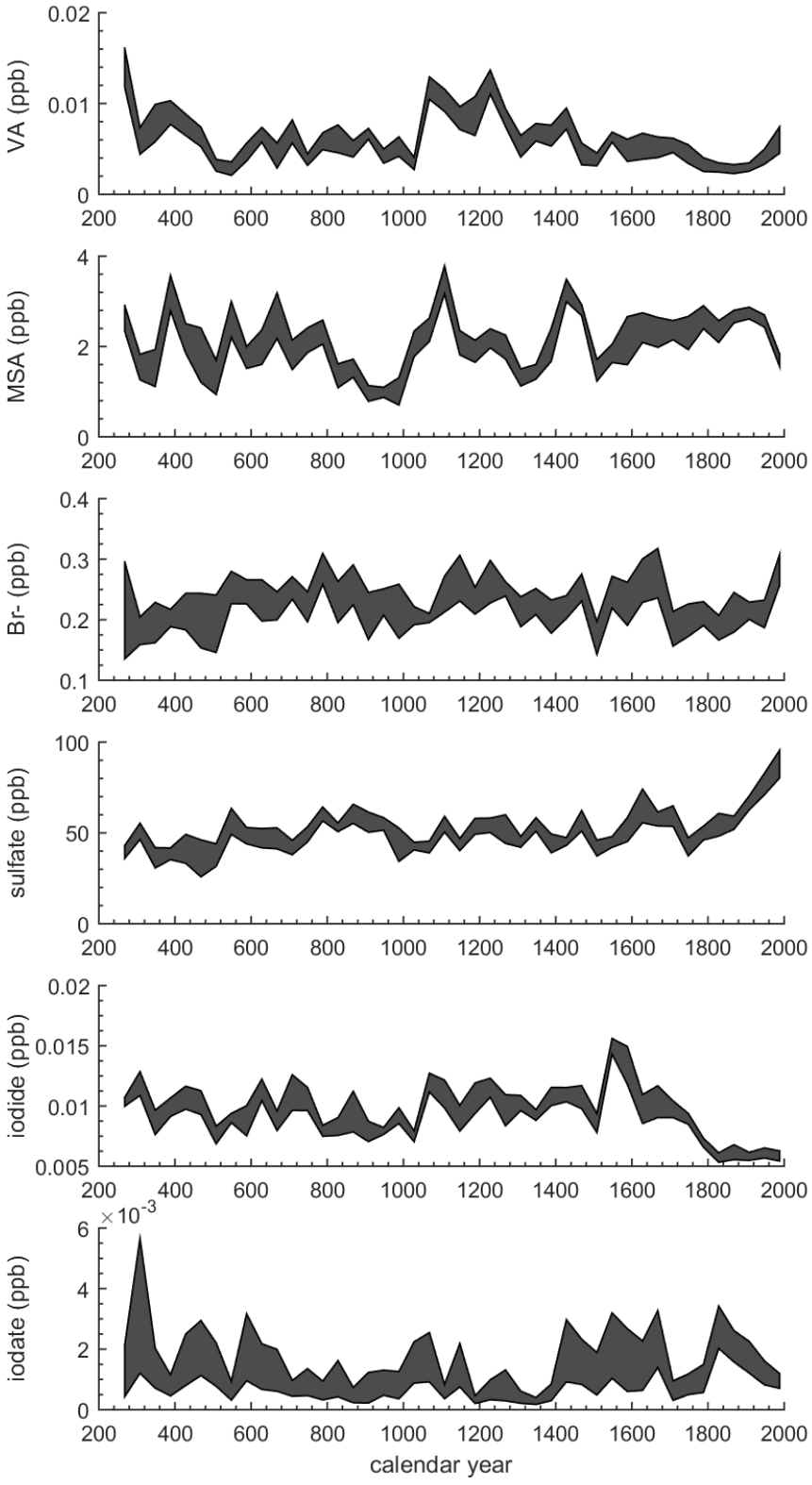

Figure 4.8: Tunu ice core chemistry over the past 1,700 years. Data are 40-year bin-averaged (gray fill is ± 1 standard error of log transform). From top: 1) vanillic acid, 2) methanesulfonate, 3) bromide, 4) sulfate, 5) iodide, and 6) iodate.

4.4.4 Transport

The HYSPLIT Model was used to determine possible biomass burning source locations of Tunu VA (*Stein et al.*, 2015; *Draxler et al.*, 1999; *Draxler and Hess*, 1998, 1997). 10-day back trajectories were started from the Tunu ice core drilling location (78°N, 33°W) at 12:00 AM and 12:00 PM local time (UTC - 2 hours) at 100 m and 500 m above ground level. The trajectories were run for three seasons in the year 2008: spring (trajectories beginning March 1, 2008-May 31, 2008), summer (trajectories beginning June 1, 2008-August 31, 2008), and fall (trajectories beginning September 1, 2008-November 30, 2008). Meteorological data used to produce the trajectories are described in Chapter 3 (*Kalnay et al.*, 1996).

Most of the trajectories stay within Greenland. Some of the trajectories reach Northern Canada starting at both 100 m and 500 m above gound level in all three seasons (Figure 4.9). A few trajectories also reach Siberia in the Spring starting at 500 m above ground level. These HYSPLIT back trajectories suggest that the most likely biomass burning source region to the Tunu site is Canada.

4.5 Conclusion

The VA levels are low enough in the Tunu ice core to suggest that the record cannot be interpreted without accounting for accumulation rate changes and reversible deposition at the ice core site. Further ice core records of VA at nearby locations and comparison to sedimentary charcoal records are necessary to determine if the Tunu record is showing changes in burning emissions or deposition.

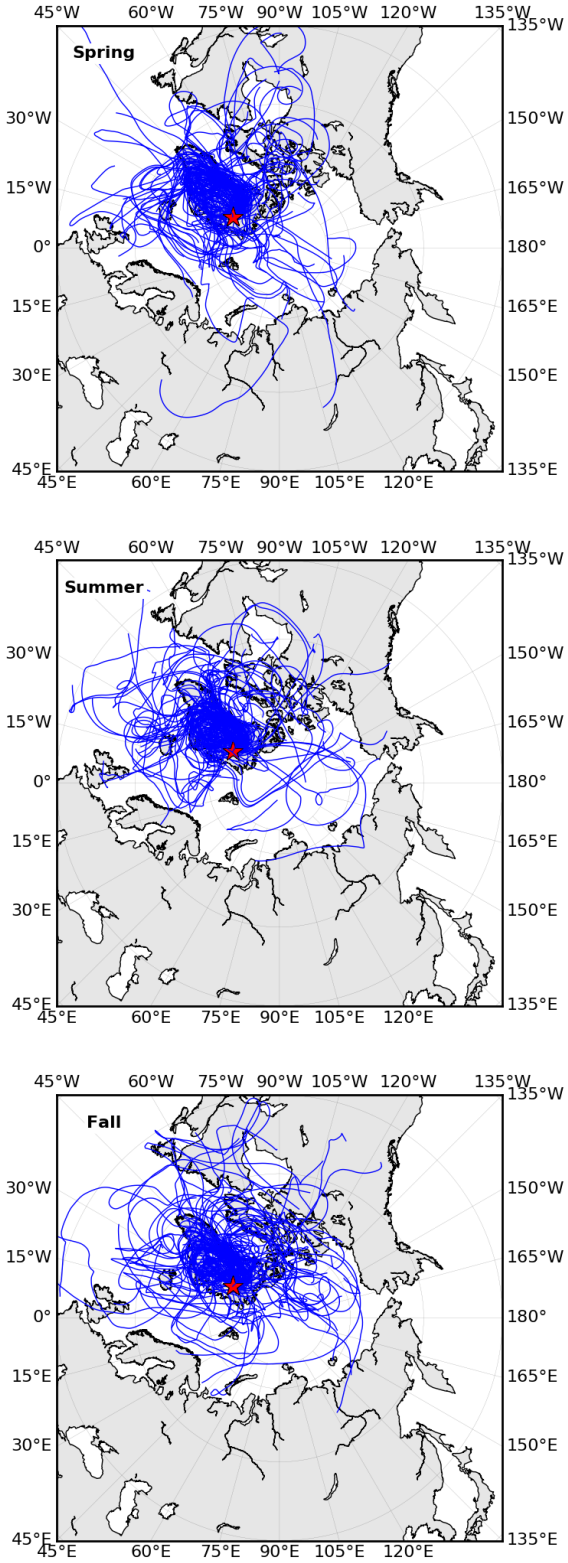

Figure 4.9: 10-day air mass back-trajectories from the Tunu ice core site (red stars) starting at 12:00 PM from 500 m above ground level. From top: 1) spring (trajectories beginning March 1, 2008-May 31, 2008), 2) summer (trajectories beginning June 1, 2008-August 31, 2008), and 3) fall (trajectories beginning September 1, 2008-November 30, 2008).

Chapter 5

Svalbard ice core records of Biomass Burning

5.1 Overview

In this chapter, measurements of the aromatic biomass burning tracers vanillic acid (VA) and *p*-hydroxybenzoic acid (*p*-HBA) in an ice core from Lomonosovfonna in Svalbard covering the past 750 years (1222-2009 CE) are presented. Svalbard is located northward of Scandinavia and northeast of Greenland, at roughly the same latitude as the Akademii Nauk and Tunu ice core drilling sites. Variability in the Lomonosovfonna VA and *p*-HBA records is characterized as large deviations (10x) from the baseline. These large deviations in both records are not confined to particular time periods, but are rather scattered throughout the records. These data are elevated enough to be considered biomass burning signals, but individual measurements are not interpreted due to melt layers throughout the record. 20-year bin averages of the records show that Lomonosovfonna VA and *p*-HBA exhibit a long-term decline over the 750-year period.

5.2 Ice core characteristics, dating, and sample collection

The Svalbard Lomonosovfonna ice core was drilled in 2009 (Figure 5.1; 78°49'24.4"N, 17°25'59.2"E, 1202 m asl.) (*Wendl*, 2014). The Lomonosovfonna ice core was drilled to a depth of 149.5 m (*Wendl*, 2014; *Wendl et al.*, 2015). The Lomonosovfonna ice field is the highest elevation ice field of Svalbard in central Spitsbergen. The current temperature range of the ice field is 0 to -40°C over the year(*Kekonen et al.*, 2005). The annual average temperature is -12°C (*Pohjola et al.*, 2002).

The Lomonosovfonna ice core depth-age scale was determined using annual layer counting based on seasonal $\delta^{18}O$ and Na^{+} measurements, ^{210}Pb decay, 8 volcanic reference horizons identified based on sulfate measurements, a 1963 tritium peak, and a simple glacier flow model (Figure 5.2) (*Wendl*, 2014; *Wendl et al.*, 2015). The Samalas volcanic eruption in 1257/58 was the deepest reference horizon used for dating (*Wendl*, 2014; *Wendl et al.*, 2015). The Lomonosovfonna ice field has radial ice flow (*Kekonen et al.*, 2005). The simple glacier flow model (*Thompson et al.*, 1998) was fitted through the reference horizons to determine the depth-age scale below 79.7 m water equivalent (1750 CE) because annual layer counting was not possible below this point due to ice thinning (*Wendl*, 2014; *Wendl et al.*, 2015). The modeled average accumulation rate is 0.58 m/year. The ice core records the years 1222-2009 CE based on these dating methods (*Wendl*, 2014; *Wendl et al.*, 2015). Dating uncertainty was determined by comparing modeled reference horizon years to known volcanic eruption years. Above 68 m water equivalent (w.eq.) depth, the dating uncertainty is ±1 year near reference horizons (±10 years), and ±3 years between reference horizons. The dating uncertainty is ±3 years between 68-80 m w.eq. depth, and ±10 years below 80 m w.eq. depth (*Wendl*, 2014; *Wendl et al.*, 2015).

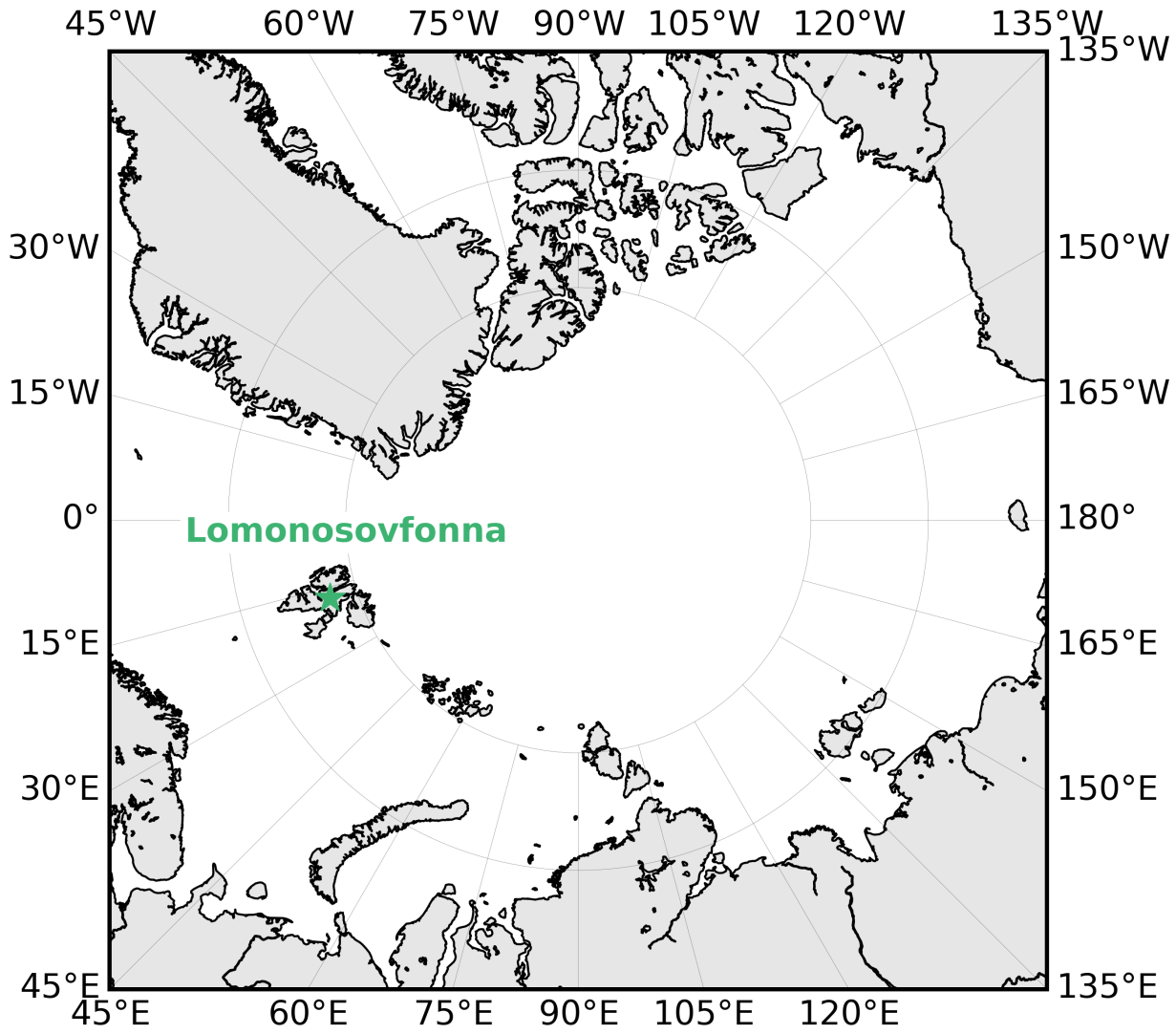

Figure 5.1: Map of Lomonosovfonna ice core drilling site (78°49'24.4" N, 17°25'59.2"E).

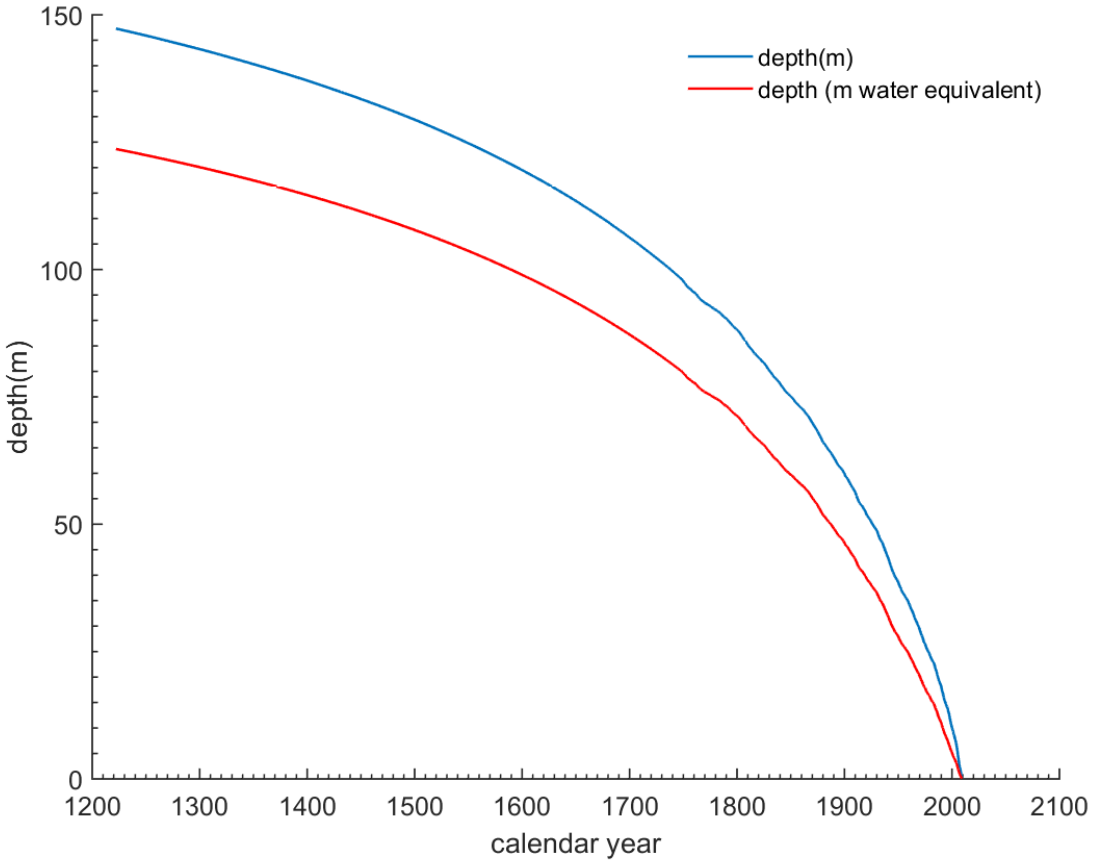

Figure 5.2: Lomonosovfonna ice core depth-age scale (M. Schwikowski, personal communication).

5.3 Methods of sampling and analysis

Meltwater from the Lomonosovfonna ice core was analyzed for vanillic acid (VA) and *p*-hydroxybenzoic acid (*p*-HBA) using the IC/ESI-MS/MS method described in Chapter 2. Discrete ice core samples (1.8 x 1.9 cm cross section, 3-4 cm long) were cut and melted previously for ion chromatographic analysis and stored in polypropylene vials at the Paul Scherrer Institut in Villigen, Switzerland (*Wendl*, 2014; *Wendl et al.*, 2015). For this study, the vials were remelted and sampled at the Paul Scherrer Insitut, combining 4 μl from four adjacent vials into a single sample for analysis of VA and *p*-HBA.

In the Lomonosovfonna ice core, vanillic acid was analyzed at two mass transitions (m/z 167→108 and m/z 167→152) to confirm the identity of the compound and to improve the detection limit (Figure 5.3). The limits of detection for the two transitions were 0.0095 and 0.0057 ppb (n = 80), respectively. The limit of detection for *p*-HBA was 0.012 ppb.

The data were normalized using the mini-max transformation and the z-score. Logarithmic and Box-Cox transformations were used to redistribute the data towards a normal distribution. The logarithmic transformation was the most successful at achieving a normal distribution of the data. These methods are described in chapter 3. The geometric means of the m/z 167→108 VA transition, the m/z 167→152 VA transition, and *p*-HBA were $0.0035^{+0.0078}_{-0.0024}$ ppb, $0.0038^{+.0076}_{-0.0025}$ ppb, and $0.011^{+0.0090}_{-0.0049}$ ppb, respectively. All of these values are below the detection limits of these mass transitions.

20-year bin averaging and LOESS smoothing (described in Chapter 3) were used to find centennial-scale features in the records. Both smoothing treatments reveal the same centennial-scale features in the records (Figure 5.4). The 20-year bin averaged log-transforms of the records are employed here for interpretation of temporal variability.

VA was measured in the same samples using two different methods simultaneously by mea-

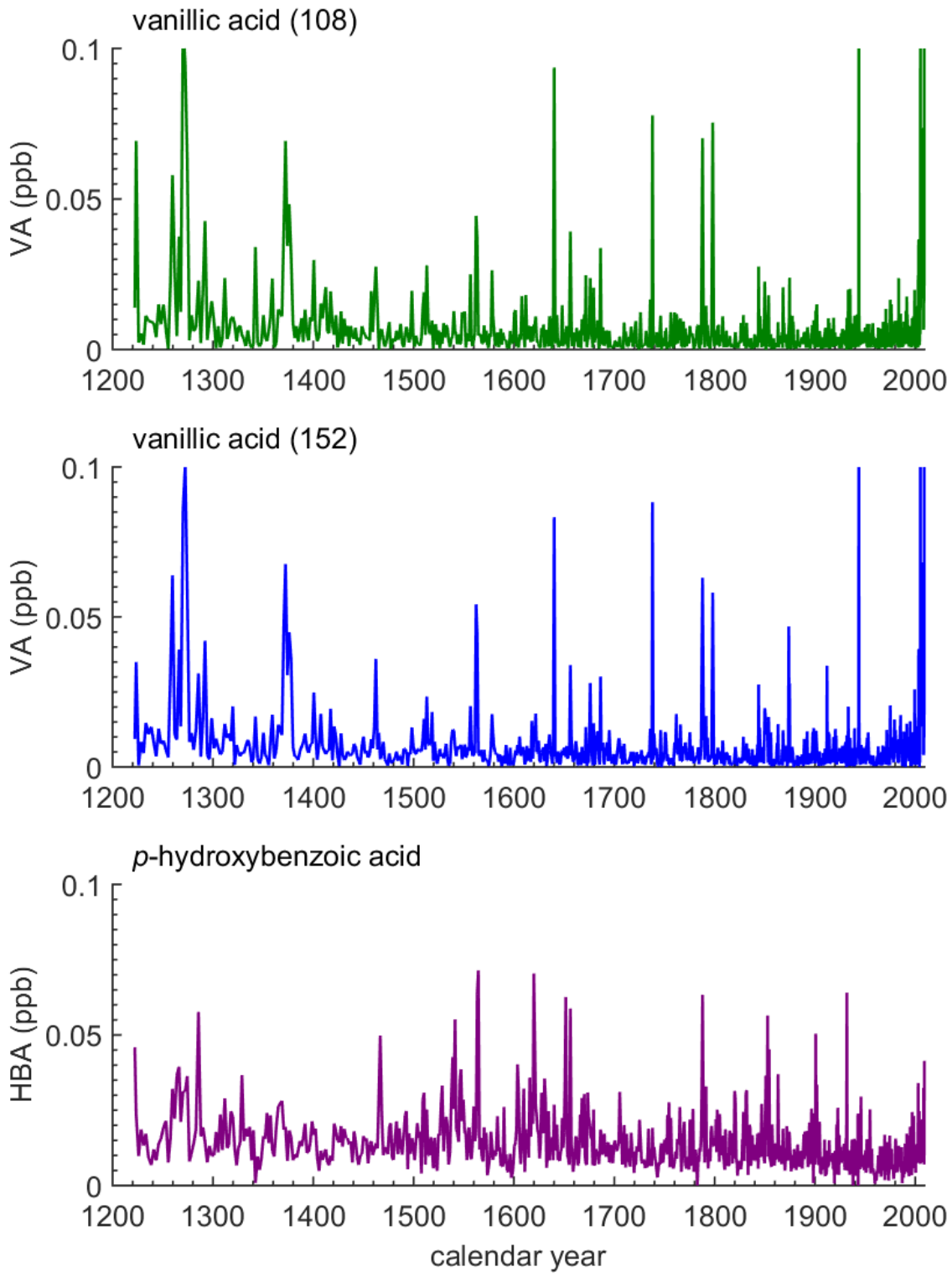

Figure 5.3: Lomonosovfonna VA (top: m/z 167→108, middle: m/z 167→152) and p-HBA (bottom) ice core records.

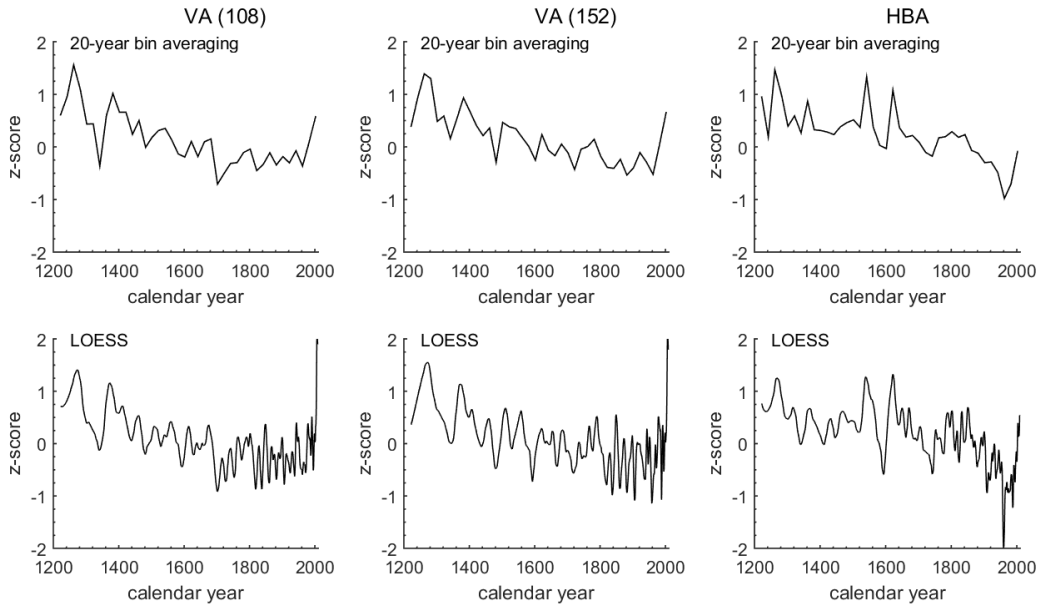

Figure 5.4: Lomonosovfonna VA (left: m/z 167→108, middle: m/z 167→152) and p-HBA (right) using 20-year bin averaging (top) and LOESS smoothing (span = 0.04) (bottom) of the log transforms. Data were normalized using the mini-max transformation and the z-score.

suring VA at two different mass transitions. The level of VA in each sample is expected to be the same using either method of analysis. The two mass transitions were compared using the linear least squares regression of the 20-year bin averages of their log transforms (Figure 5.5). The slope of the linear trend was 0.99 ± 0.065 and the intercept was 0.00036 ± 0.00038 ppb. The relationship is significant ($p < 10^{-6}$) with an r-squared value of 0.86. This result suggests that the VA ion was correctly identified and both mass transitions can be used to measure the level of VA in the ice core.

5.3.1 Temporal variability and trends

Lomonosovfonna VA and p-HBA exhibit large deviations (10x) above the baseline. These deviations are sporadic throughout the records, so multi-decadal periods of elevated VA or p-HBA are not easily discernable in the dataset. 20-year bin averages of the log-transforms of the datasets are used to identify long-term variability. Lomonosovfonna VA and p-HBA bin-

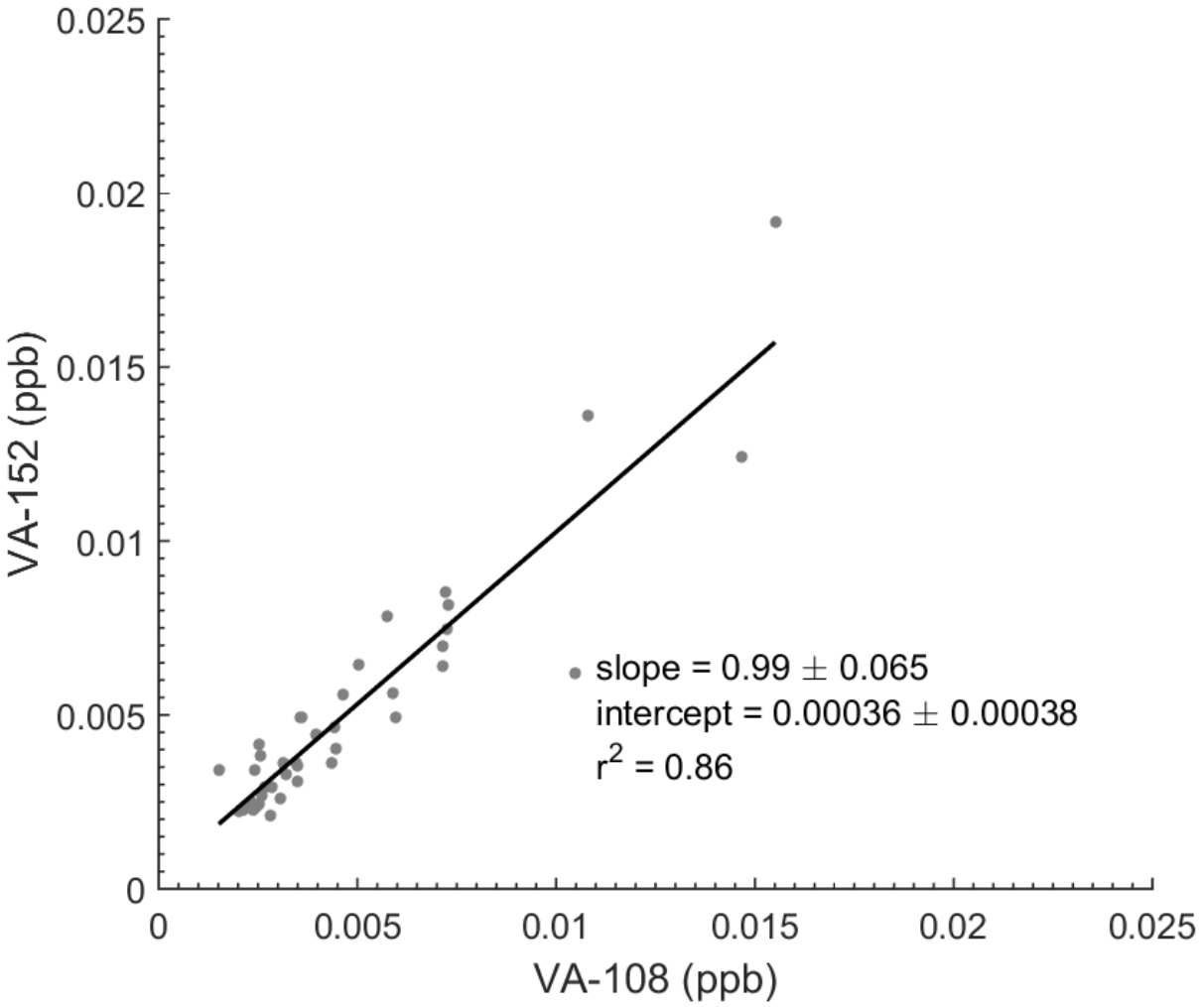

Figure 5.5: Relationship between two VA mass transitions (167→108 and 167→152). 20-year averaged log-transforms of VA were used for the linear fit.

averages decline in the long-term from 1200-1900 CE. Lomonosovfonna VA peaks from 1200-1450 CE. The *p*-HBA record is elevated from 1200-1350 CE and 1500-1650 CE. Lomonosovfonna VA declines from 1500-1650 CE when *p*-HBA is elevated. All three records are elevated from 1900-2000 CE.

Peaks in the VA m/z 167→108 and m/z 167→152 transitions range from below the detection limit to 0.016 ppb and 0.019 ppb, respectively, using the 20-year bin averages of the log transforms. These values are only 68% and 230% increases above the detection limits of the VA m/z 167→108 and m/z 167→152 transitions, respectively. The *p*-HBA peaks range from below the detection limit to 0.023 ppb, using the 20-year bin averages of the log transform. This maximum value is only a 93% increase above the detection limit.

5.3.2 Interpretation of the record

The levels of organic aerosols in the Lomonosovfonna ice core result from the combined effects of emissions, atmospheric transport, and depositional processes. The atmospheric reactivity of VA and *p*-HBA is described in Chapter 3. The levels of these compounds may also be influenced by changes in snow accumulation rate, which would dilute the signal, and possible post-depositional processes, such as chemical reactions in the snowpack (*Grannas et al.*, 2004). In this section, the possible effects of these various processes on the Lomonosovfonna record are discussed.

Individual Lomonosovfonna VA and *p*-HBA measurements deviate strongly (10x) from baseline levels. The amount of time represented by an individual measurement ranges from seasonal to 3.5 years. These individual measurements are not interpreted because the Lomonosovfonna ice core experienced melt due to elevated summer temperatures (Figure 5.6). The average melt index in the Lomonosovfonna ice core is 31% (*Wendl et al.*, 2015). This index means that an average of 31% of an annual layer is affected by melt (*Wendl*,

2014). Maximum percolation of meltwater was likely 8 annual layers (*Wendl et al.*, 2015). Only 20-year bin averages are used for interpretation of the records in this study for this reason.

VA and *p*-HBA levels could be affected by changes in the snow chemistry in the ice core. If VA and *p*-HBA are affected by snow chemistry, then they are expected to be negatively correlated to more acidic conditions and positively correlated to more basic conditions. A positive correlation with seasalt (i.e. Br^- and I^-) or a negative correlation with volcanic sulfate would indicate affects due to changes in snow chemistry. Lomonosovfonna VA, *p*-HBA and bromide exhibit a long-term decline, but iodide increases over the 750-year period (Figure 5.7). The elevated period in Lomonosovfonna VA and *p*-HBA from 1200-1450 is not apparent in the sodium or bromide records. Methanesulfonate and sulfate are steady prior to the 20^{th} century. The lack of correlation between VA, *p*-HBA and these other ions indicates that snow chemistry is likely not an important driver of VA trends in the Lomonosovfonna ice core.

Differences between VA and *p*-HBA measurements reflect possible changes in biomass fuels burned and combustion conditions. VA and *p*-HBA both show a long-term decrease from 1222-2009 CE in the Lomonosovfonna ice core (Figure 5.8). Linear fits between the 20-year bin averaged log transforms of the two VA mass transitions and the *p*-HBA measurements give r-squared values 0.3 (Figure 5.9). These relationships are significant ($p < .001$), and indicate that 30% of the variability in the *p*-HBA measurements can be explained by the VA measurements.

Positive correlation between VA and *p*-HBA and inorganic ions with biomass burning sources would support the interpretation of VA and *p*-HBA as biomass burning signals. Ammonium and nitrate have been used as biomass burning tracers, but they have other sources (*Eichler et al.*, 2011; *Fuhrer et al.*, 1996; *Savarino and Legrand*, 1998; *Taylor et al.*, 1996; *Whitlow et al.*, 1994). Lomonosovfonna ammonium and nitrate are not elevated at the same time

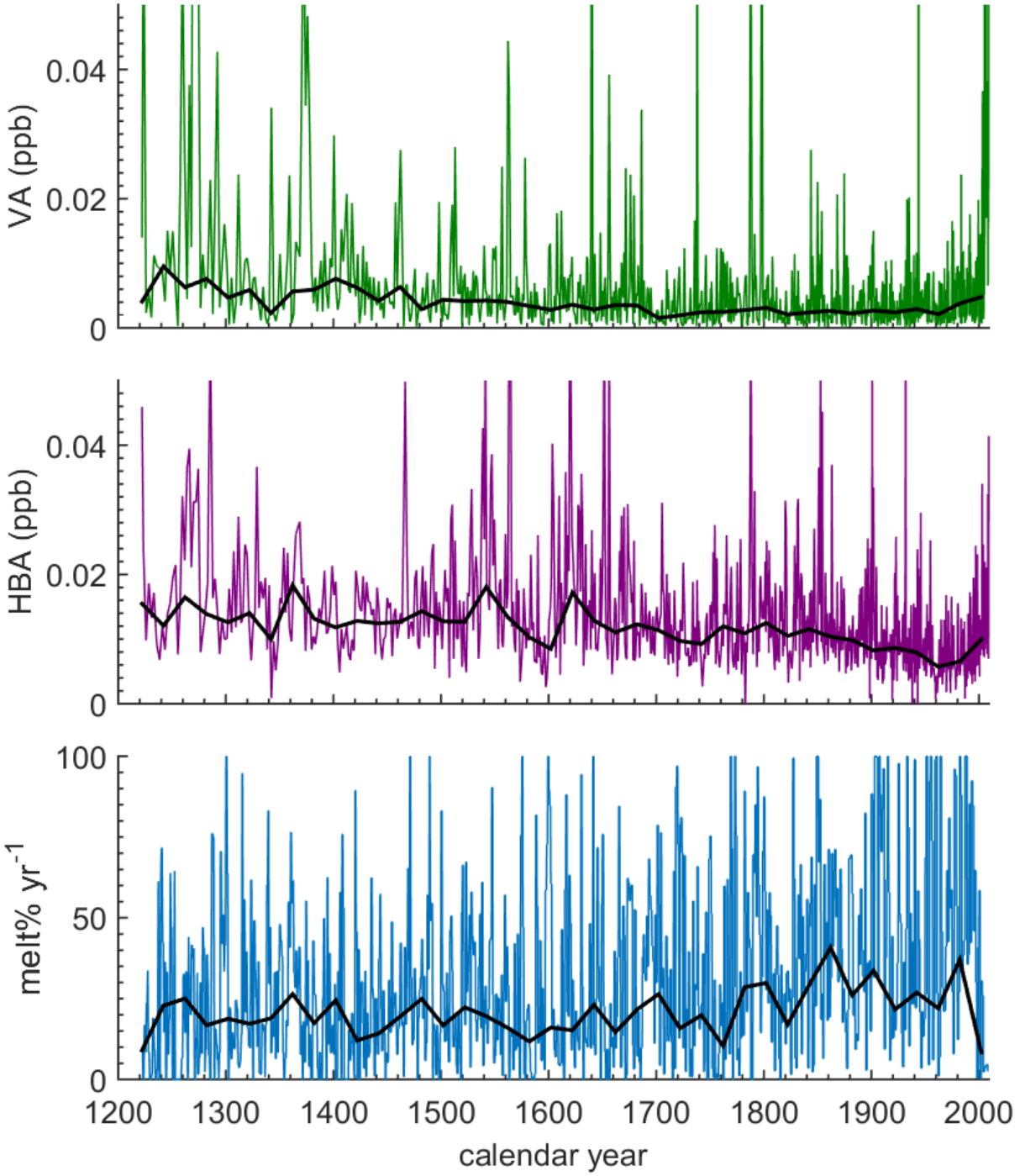

Figure 5.6: Lomonosovfonna melt layers (*Wendl et al.*, 2015). From top: 1) Lomonosovfonna VA (167→108, 2) Lomonosovfonna *p*-HBA, 3) annual average melt percentage. Black lines are 20-year bin averages of the log transforms.

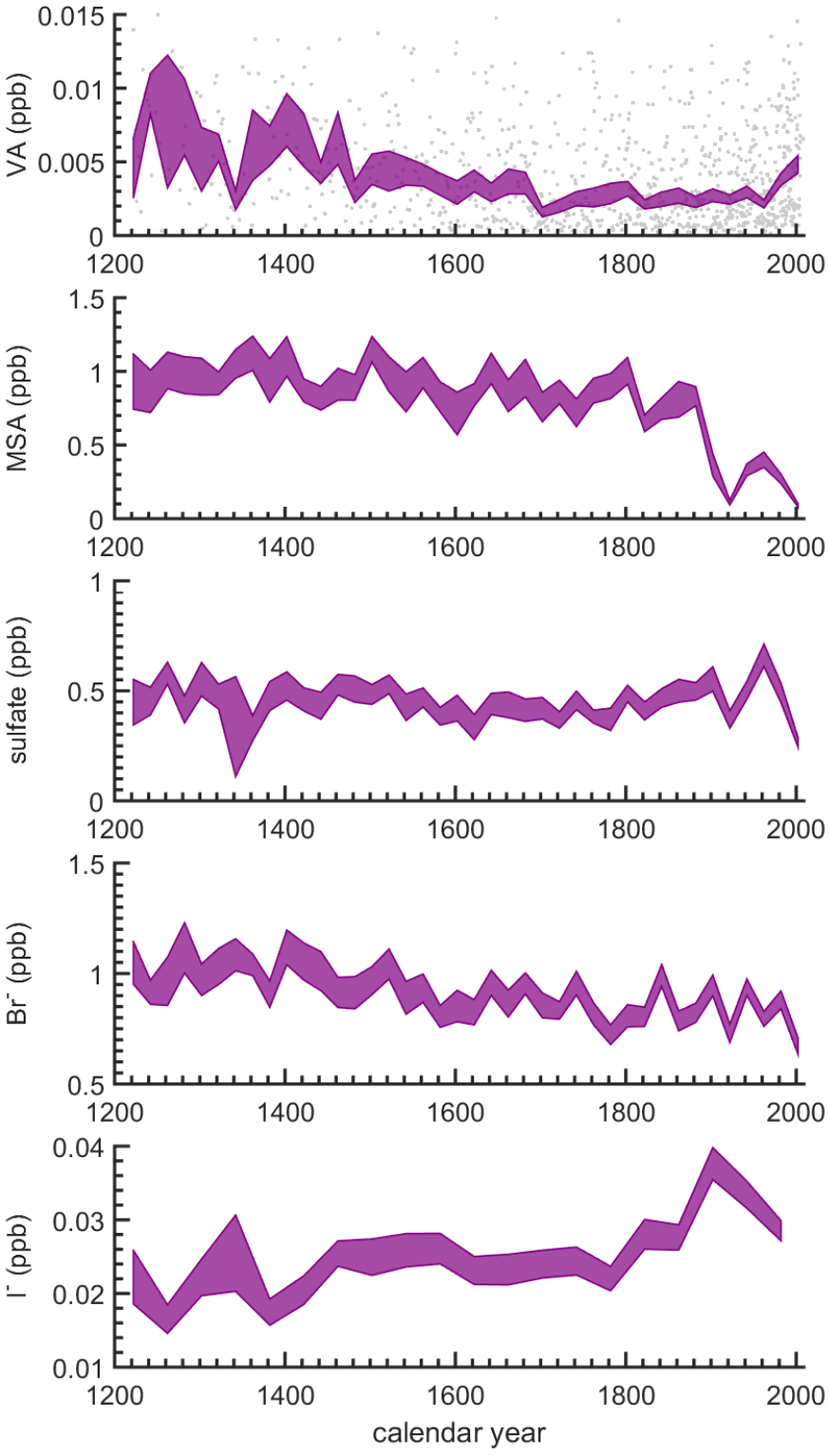

Figure 5.7: Lomonosovfonna ice core measurements (this study). Data are 20-year bin-averages (gray fill is ± 1 standard error of log transform). From top: 1) vanillic acid, 2) methanesulfonate, 3) bromide, 4) sulfate, and 5) iodide.

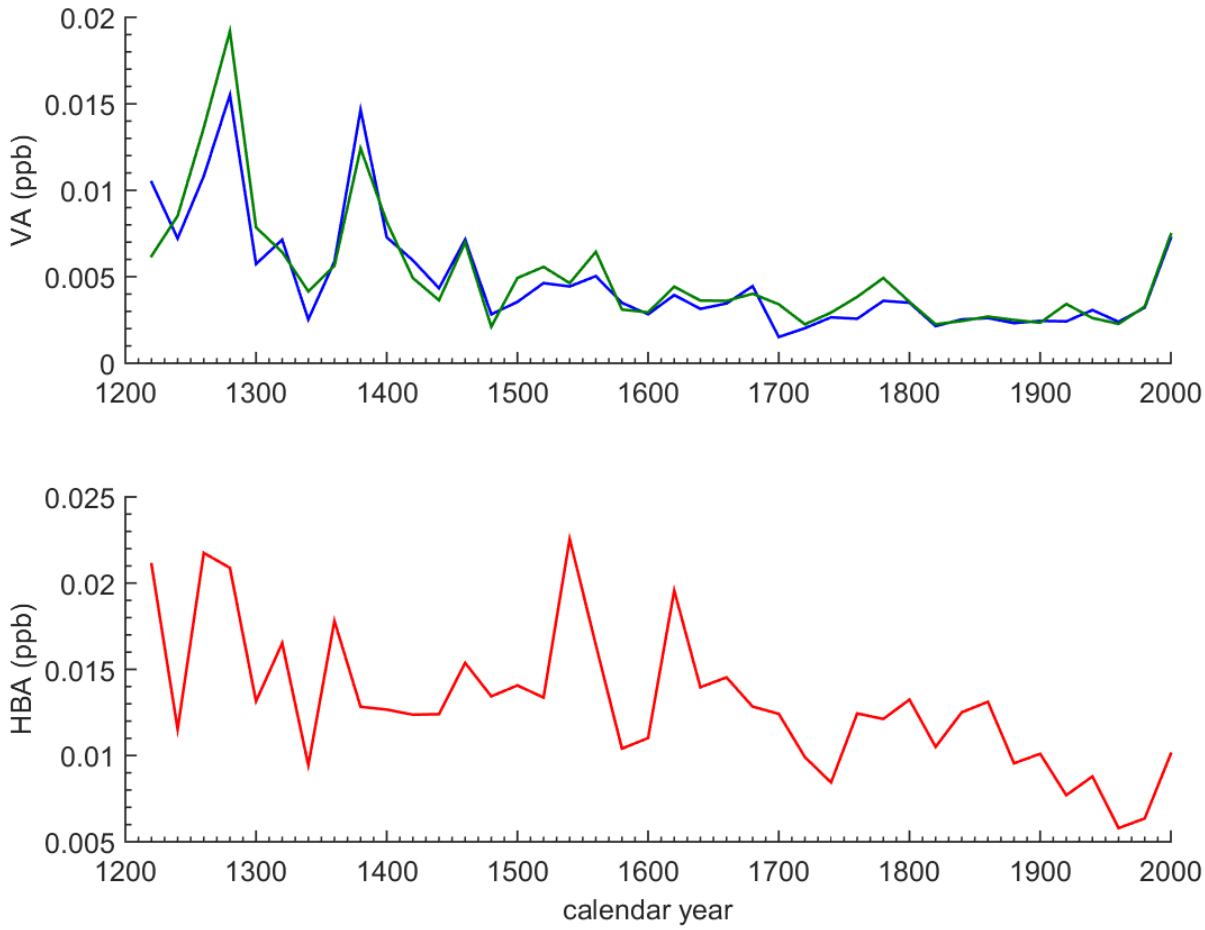

Figure 5.8: Lomonosovfonna VA and p-HBA. Data are 20-year bin averaged log transforms of Lomonosovfonna VA (top; 167→108, blue; 167→152, green) and p-HBA (bottom).

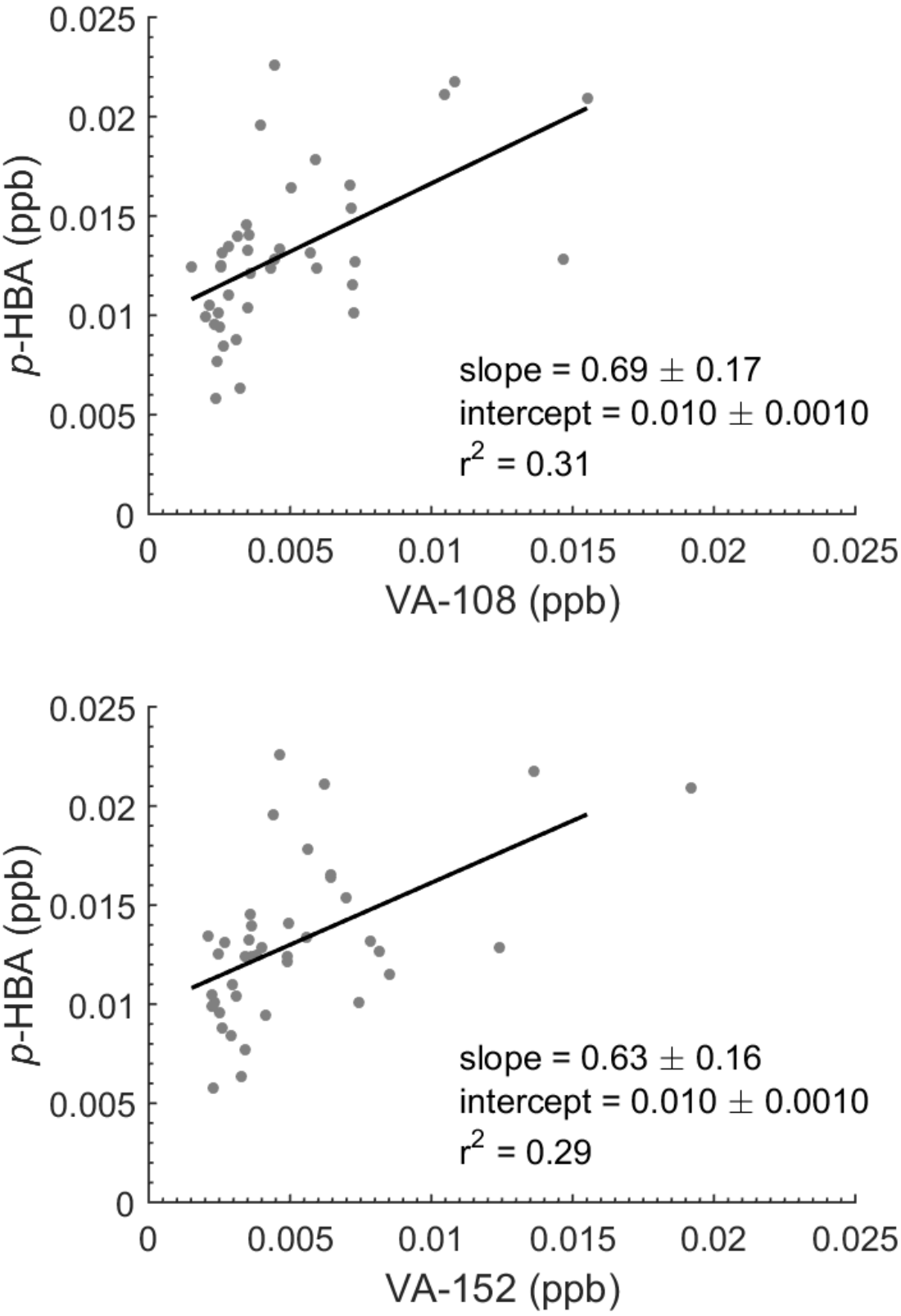

Figure 5.9: Relationship between Lomonosovfonna VA and *p*-HBA. Data are linear fits of the 20-year bin averaged log transforms of VA (167→108, top; 167→152, bottom) and *p*-HBA.

periods as VA and *p*-HBA prior to the 20^{th} century (Figure 5.10). Elevated ammonium and nitrate in the 20^{th} century was likely derived from pollution (*Wendl et al.*, 2015). Principal component analysis indicates that Lomonosovfonna ammonium was likely derived from biogenic sources. Lomonosovfonna nitrate sources have not yet been determined, but the timing of nitrate variability correlates well with Lomonosovfonna methanesulfonate variability (*Wendl et al.*, 2015). Principal componenet analysis and differences between these records and Lomonosovfonna VA and *p*-HBA indicate that it is unlikely that nitrate and ammonium are derived from biomass burning sources in the Lomonosovfonna ice core.

5.3.3 Transport

The HYSPLIT Model was used to determine biomass burning source locations to the Lomonosovfonna ice core site (*Stein et al.*, 2015; *Draxler et al.*, 1999; *Draxler and Hess*, 1998, 1997). 10-day back-trajectories were started from the site (78°49'24.4"N, 17°25'59.2"E) at 100 m and 500 m above ground level. Trajectories were started each day at 12:00 AM and 12:00 PM local time (UTC + 1 hour) for the following three seasons: spring (trajectories beginning March 1, 2008-May 31, 2008), summer (trajectories beginning June 1, 2008-August 31, 2008), and fall (trajectories beginning September 1, 2008-November 30, 2008). The meterological data used are described in Chapter 3 (*Kalnay et al.*, 1996).

Most of the trajectories remain within the Arctic (Figure 5.11). The trajectories reach Northern Siberia in the spring and fall starting at both 100 m and 500 m above ground level and in the summer starting at 500 m above sea level. The back trajectories extend into Fennoscandia in the fall starting from both 100 m and 500 m above ground level. They also reach Northern Canada in all three seasons starting from both 100 m and 500 m above ground level. The biomass burning source regions to the ice core site could be Northern Canada, Siberia, or Fennoscandia.

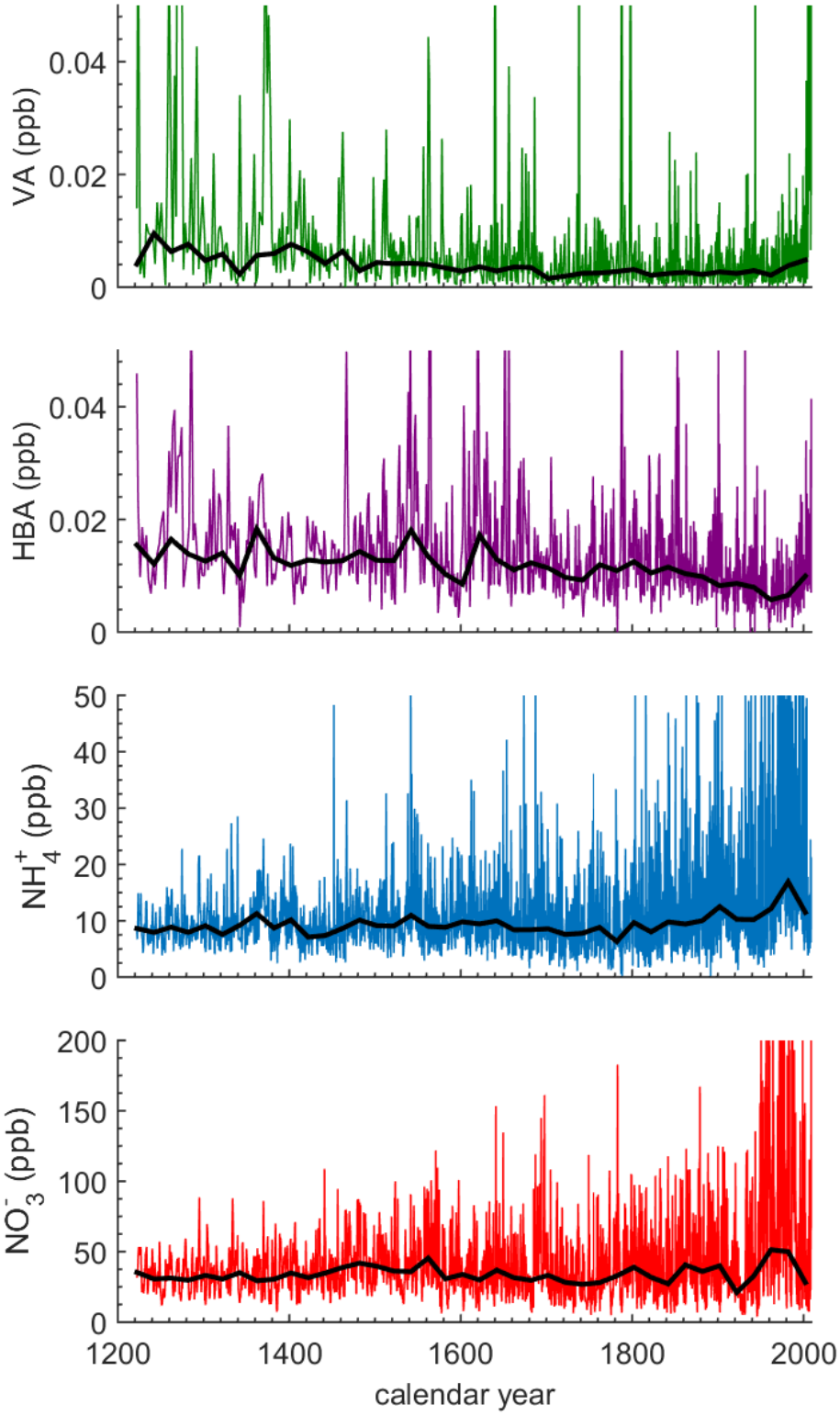

Figure 5.10: Relationship between Lomonosovfonna VA and *p*-HBA and inorganic biomass burning tracers. Black lines are linear fits of the 20-year bin averaged log transforms of the log transforms. From top: 1) VA (167→108) top, 2) *p*-HBA, 3) ammonium (*Wendl et al.*, 2015), and nitrate (*Wendl et al.*, 2015).

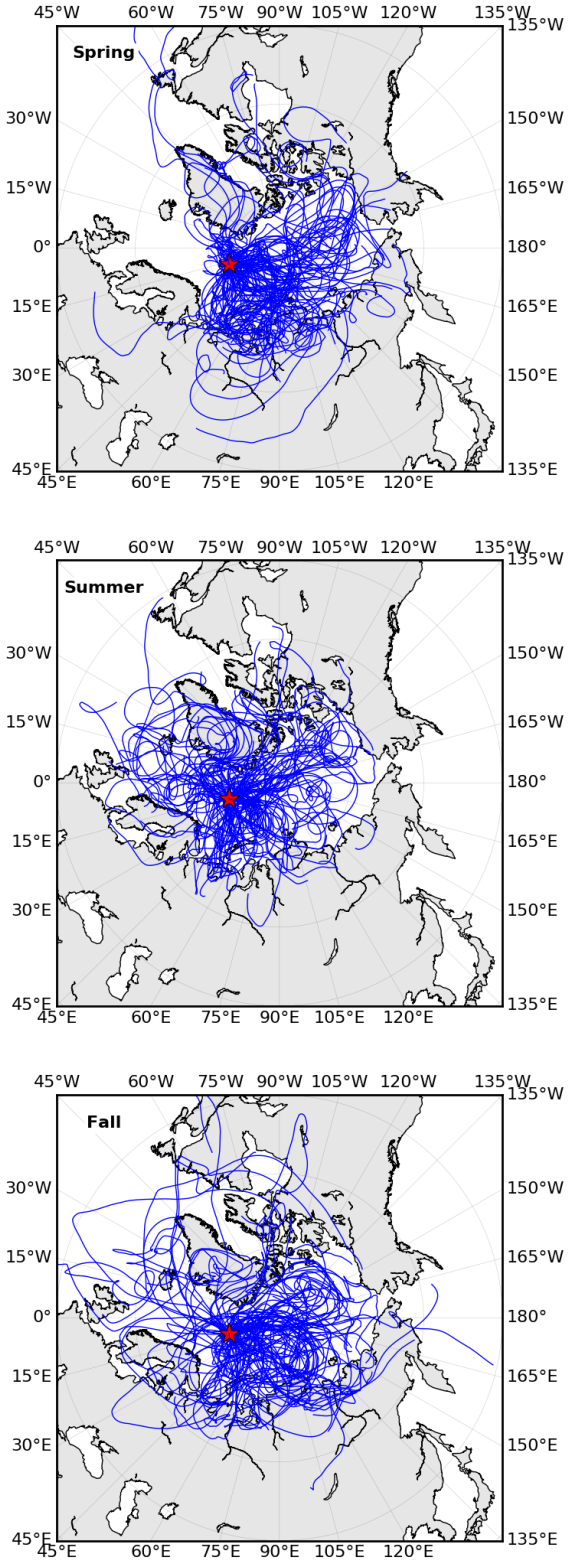

Figure 5.11: 10-day air mass back-trajectories from the Lomonosovfonna ice core site (red stars) starting at 12:00 PM from 500 m above ground level. From top: 1) spring (trajectories beginning March 1, 2008-May 31, 2008), 2) summer (trajectories beginning June 1, 2008-August 31, 2008), and 3) fall (trajectories beginning September 1, 2008-November 30, 2008).

Chapter 6

Comparison of vanillic acid in three Arctic ice cores

6.1 Introduction

In this chapter, the vanillic acid records of the three Arctic ice cores analyzed in this study are compared and contrasted in terms of the magnitude and timing of major features. The similarities and differences between the three records may reflect a number of possible factors, including differences in burning histories at various source regions, atmospheric transport patterns influencing the sites, and different physical conditions at the ice core site. The data are also compared to sedimentary charcoal records and other ice core records in order to assess the extent to which local, regional, or pan-Arctic signals are evident in the data.

6.2 Comparison between records in this study

The characteristics of the Akademii Nauk, Tunu, and Lomonosovfonna vanillic acid (VA) records are quite different. Most notably, the levels of VA in the Akademii Nauk ice core are 10-fold greater than those in the other cores (Figure 6.1). This most likely reflects the proximity of the site to the Siberian tundra and boreal forests (Figure 6.2). The site is also

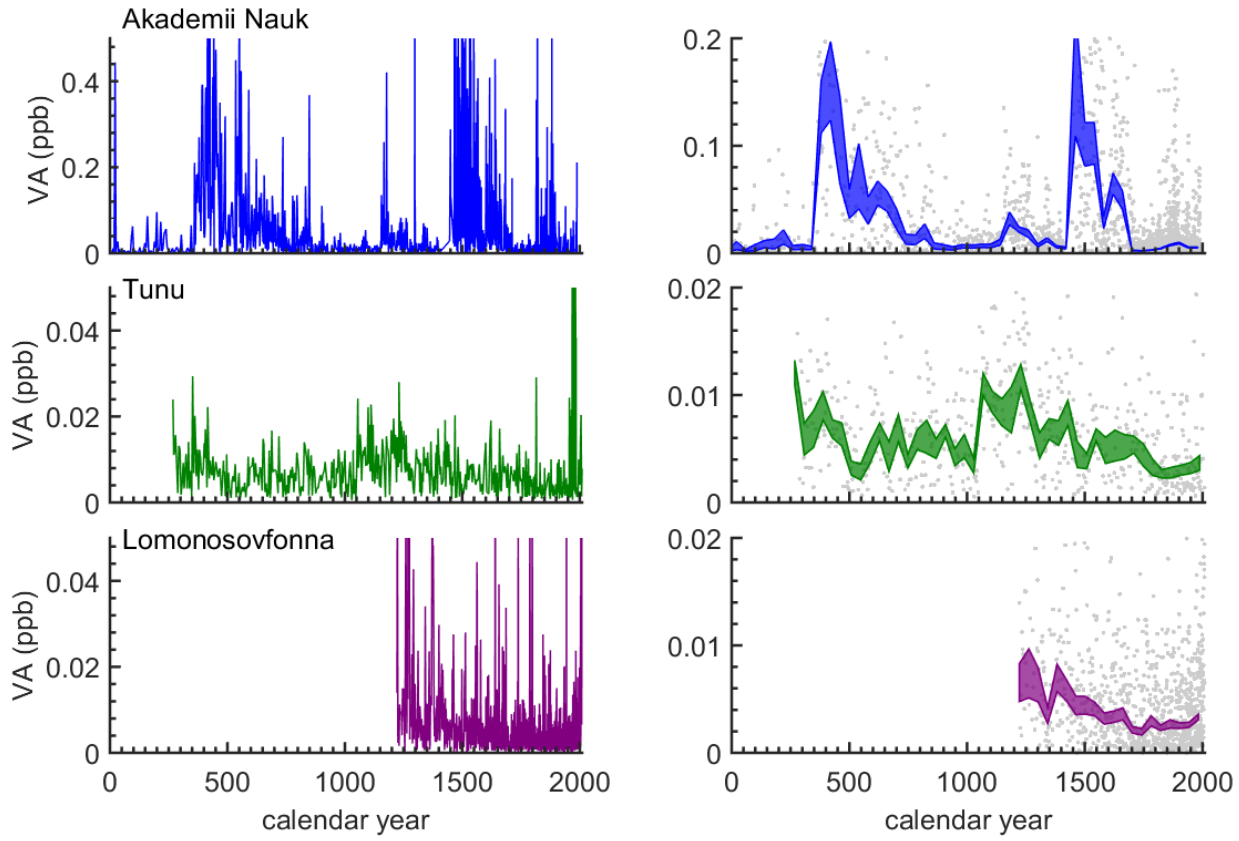

Figure 6.1: Vanillic acid in three Arctic ice cores: Akademii Nauk (top), Tunu (middle) and Lomonosovfonna (bottom) ice cores Left: individual measurements. Right: 40-year bin-averages (fill is ± 1 standard error of log transform).

at the lowest elevation of the three, and at 800 m may be influenced by transport within the boundary layer (Table 6.1). This site also has the largest snow accumulation rate. All of these characteristics favor efficient transport and wet deposition of biomass burning aerosols from Siberian air masses with relatively short transport times.

A second major difference is that the highest levels of VA in Akademii Nauk occur in three major peaks lasting hundreds of years. The possible climatic causes of this millennial-scale variability are discussed in Chapter 7. By contrast, Tunu and Lomonsovfonna show much less centennial or millennial variability (Figure 6.1).

Although the variability in Tunu and Lomonosovfonna VA is small relative to Akademii

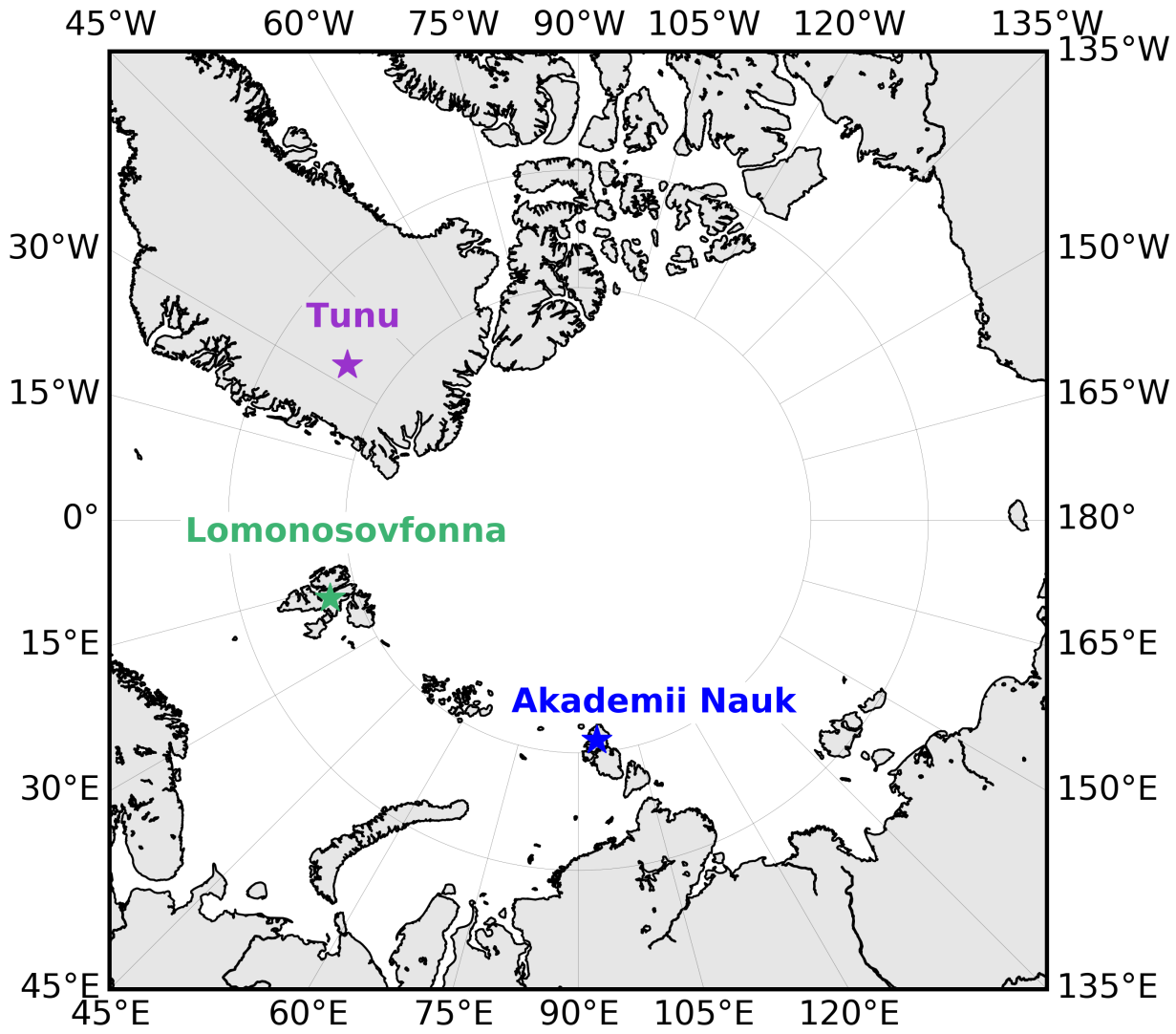

Figure 6.2: Map of the locations of the ice core sites in this study.

Table 6.1: Geographical locations, elevations, and average accumulation rates of the study sites.

	Location	Elevation (m a.s.l.)	Average Accumulation Rate (m.w.e. a^{-1})
Akademii Nauk	80°31'N, 94°49'E	800	0.46
Tunu	78.04°N, 33.88°W	2000	0.10
Lomonosovfonna	78°49'24.4"N, 17°25'59.2"E,	1202	0.58

Nauk VA, these records share some features with Akademii Nauk VA. One similarity is the peak in Tunu VA from 300-500 CE that overlaps the major Akademii Nauk VA peak from 380-660 CE. Similarly, the timing of the Tunu VA peak from 1050-1300 CE overlaps the timing of the minor Akademii Nauk peak from 1150-1300 CE. Lomonosovfonna VA reaches its highest levels from 1220-1300 CE, which may be part of the same peak present in the other cores, but the record is not long enough to determine when the peak begins. The Lomonosovfonna and Tunu VA records exhibit long-term declines from 1500-1800 CE. One could argue that this trend might also be present in the "baseline" of Akademii Nauk, but that it is obscured by the major peak starting at 1460 CE.

Because the very strong VA signals in the three major Akademii Nauk peaks are not shared by the other cores, it seems likely that these signal are derived from Siberian fires. These events clearly did not result in major deposition of burning-derived aerosols across the whole Arctic. By contrast, some of the smaller features and trends shared by the three cores could be derived from sources distal to Akademii Nauk such as Alaska or Canada, and may have undergone widespread transport in the mid-troposphere (Figure 6.2).

Recent forest fires provide some insight into transport of biomass burning aerosols into the Arctic. *Stohl et al.* (2006) showed that fires in Alaska and Canada in 2004 resulted in

increased biomass burning aerosols in Barrow (Alaska). In the largest fires, lower levels of these aerosols also appeared at Alert (Canada), Summit (Greenland), and Zepplin/Ny Alesund on Spitsbergen (Svalbard). It is not unreasonable to hypothesize that the smaller VA peaks shared by all of the Arctic cores in this study could be due to very large fires in North America. This idea could be tested by examining ice cores in Alaska and the Canadian Arctic, where these should appear as very large features.

6.3 Comparison to other ice core biomass burning records

There are relatively few other ice core records of biomass burning suitable for comparison to Akademii Nauk, Tunu, and Lomonosovfonna VA. A 750-year ice core from the Belukha Glacier in the Siberian Altai mountains (49°48'26"N, 86°34'43"E, 4,062 m above sea level) shows a pulse of elevated burning from 1600-1680 CE evidenced by potassium, nitrate, and charcoal particles in the ice core (Figure 6.3; Figure 6.4) (*Eichler et al.*, 2011). This is similar to the timing of the most recent of the major burning peaks in VA in the Akademii Nauk ice core, indicating that either burning was widespread across Siberia at this time, or that atmospheric transport distributed the signal widely.

VA, *p*-HBA, dehydroabietic acid, and levoglucosan in a 300-year ice core from the Kamchatka Peninsula, Northeast Asia (56.07°N, 160.47°E, 4,500 m above sea level) indicate elevated biomass burning from 1700-1800 CE and 1880-2000 CE (*Kawamura et al.*, 2012). The 1700-1800 CE increase in burning is slightly later than the VA peak in the Akademii Nauk ice core. The 1880-2000 CE peak overlaps a small peak in the Akademii Nauk VA record. The similar timing of the VA peaks in both records indicates that both records have the same origin of burning or that the signal was widely distributed by transport processes.

2,000-year levoglucosan and black carbon records from the North Greenland Eemian (NEEM) ice core from Northwest Greenland (77.49° N, 51.2° W, 2,480 m above sea level) show little

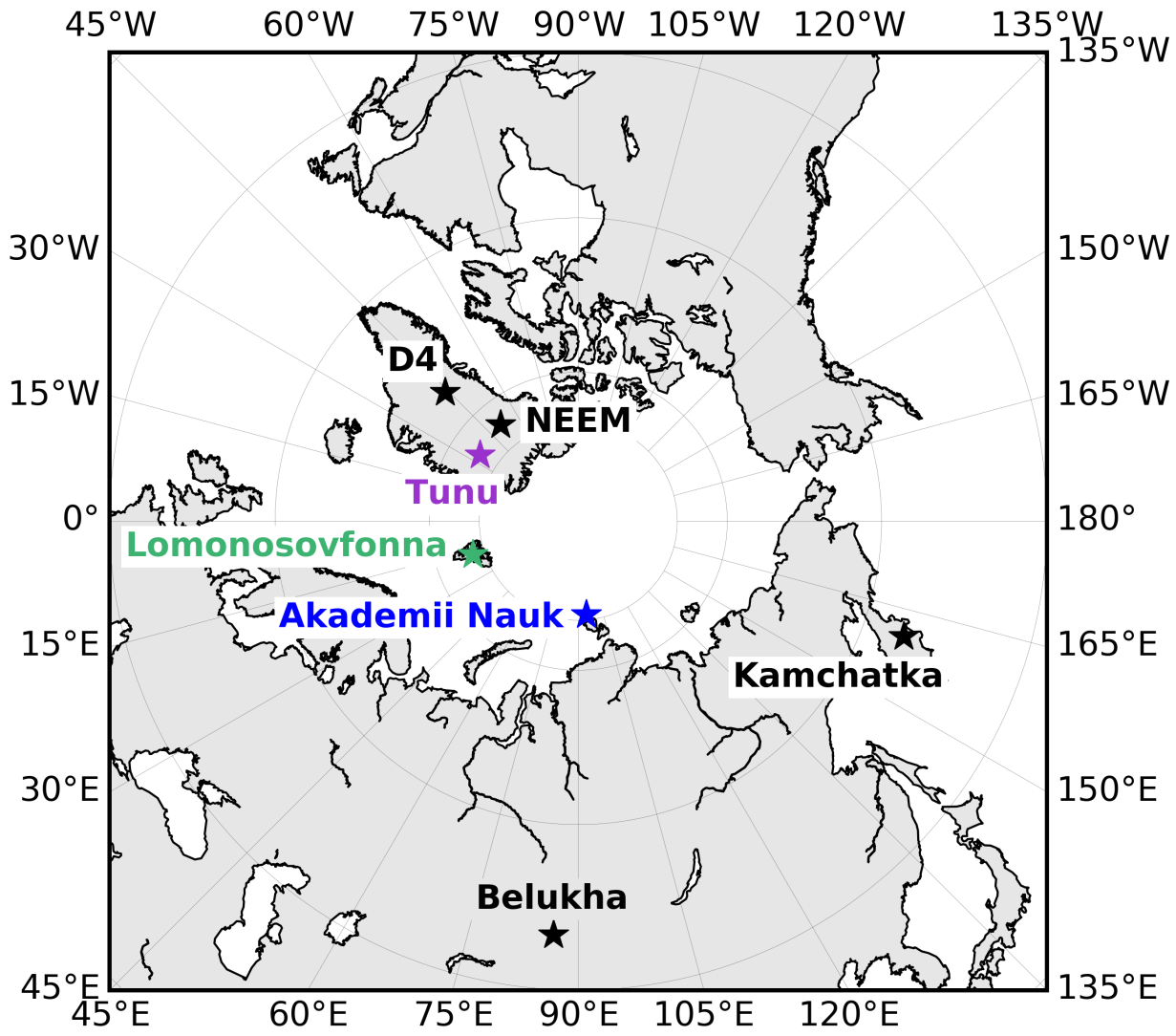

Figure 6.3: Map of the ice core sites in this study and ice core sites compared to this study (*Eichler et al.*, 2011; *McConnell et al.*, 2007; *Kawamura et al.*, 2012; *Zennaro et al.*, 2014; *Sapart et al.*, 2012).

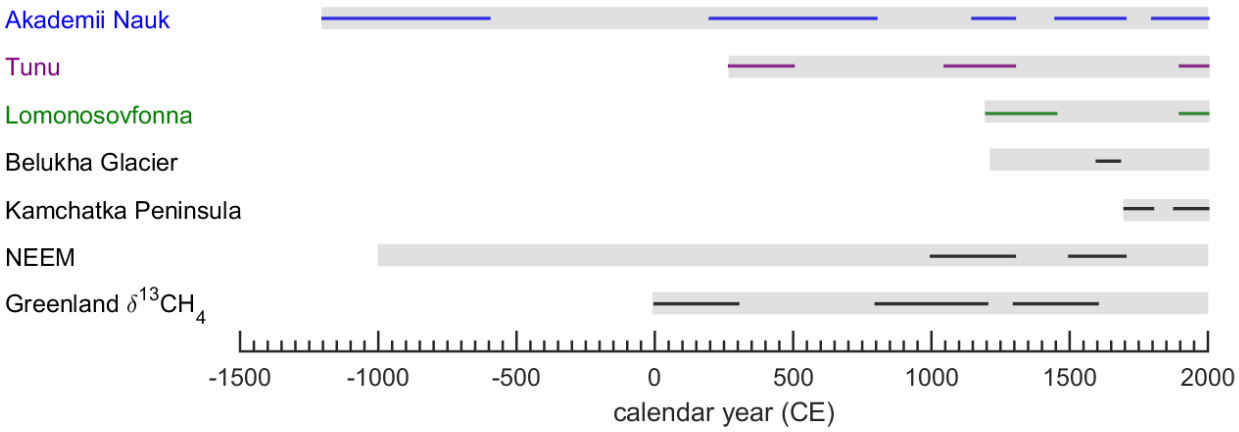

Figure 6.4: Timeline of elevated burning periods in Northern Hemisphere ice core studies (*Ferretti et al.*, 2005; *Eichler et al.*, 2011; *Kawamura et al.*, 2012; *Zennaro et al.*, 2014; *Sapart et al.*, 2012). Lines indicate periods of elevated burning. Gray bars mark the time range analyzed in each core.

variability except for slightly elevated levels above the baseline from 1000-1300 CE and 1500-1700 CE (*Zennaro et al.*, 2014). The timing of the 1500-1700 CE feature is similar to the peak in the Akademii Nauk record. The timing of the 1000-1300 CE feature is similar to the peaks in the Tunu, Lomonosovfonna, and Akademii Nauk records. However, these features are not prominent and are based on very few measurements above the detection limit. They are therefore difficult to interpret as biomass burning signals. The periods of elevated burning are only evident using the z-scores of the levoglucosan record.

VA and black carbon were measured in a 200-year ice core from the D4 site (71.4°N, 44.0°W, 2,713 m above sea level) in west-central Greenland (*McConnell et al.*, 2007). Black carbon in the D4 ice core is elevated from 1900-1950 CE, but surprisinely, VA is near baseline levels. The timing of features in Akademii Nauk VA is also not consistent with the timing of features in Akademii Nauk black carbon (Chapter 3).

Methane isotope measurements in ice cores are a proxy for global biomass burning. $\delta^{13}CH_4$ measurements from Greenland ice cores show periods of increased biomass burning from 1-300 CE, 800-1200 CE, and 1300-1600 CE (*Ferretti et al.*, 2005; *Sapart et al.*, 2012). $\delta^{13}CH_4$ measurements from the Antarctic Law Dome ice core indicate that burning was elevated

globally from 800-1200 CE (*Ferretti et al.*, 2005). The timing of these peaks is similar to the timing of peaks in Akademii Nauk, Tunu, and Lomonosovfonna VA.

6.4 Comparison to sedimentary charcoal records

Ice core VA records are compared to sedimentary charcoal records in order to assess the possible source locations of the burning recorded in the ice cores in this study. Regional high latitude composite charcoal records were constructed using the Global Charcoal Database, the Paleofire R package (*Power et al.*, 2008), and the methodology of *Marlon et al.* (2008). This involves normalizing, smoothing, and combining charcoal influx data from multiple sites.

There is similarity between the Akademii Nauk ice core record and sedimentary charcoal in the Lake Baikal region of Central Siberia (Figure 6.5; 50°-90°N, 100 °-120 °E). Both records show three major periods of burning, although there are some slight differences in their timing. In the charcoal records, the first major burning period is about 50 years longer in duration (1200-550 BCE) and the second burning period starts roughly 100 years later (400-750 CE). The shapes of this second event in the two records are also slightly different, with the VA peaking early and gradually declining, while the charcoal remains high after 500 CE. The third and youngest major burning period occurs later in the ice core (1450-1700 CE) than in the Siberian charcoal record (1300-1650 CE). Overall, the similarity of the records is surprisingly good, given the limited number of sedimentary charcoal records in the region, the high spatial variability, and dating uncertainties characteristic of such records.

Charcoal records from northern Quebec (50-90°N, 20-80 °W) and Fennoscandia (50-90 °N, 0-50 °E) both show peaks in burning with similar timing as the Tunu and Lomonosovfonna records (Figure 6.6). The Tunu ice core record and the charcoal records are all elevated from 200-500 CE. The charcoal records and the Tunu record have peaks centered at 1100

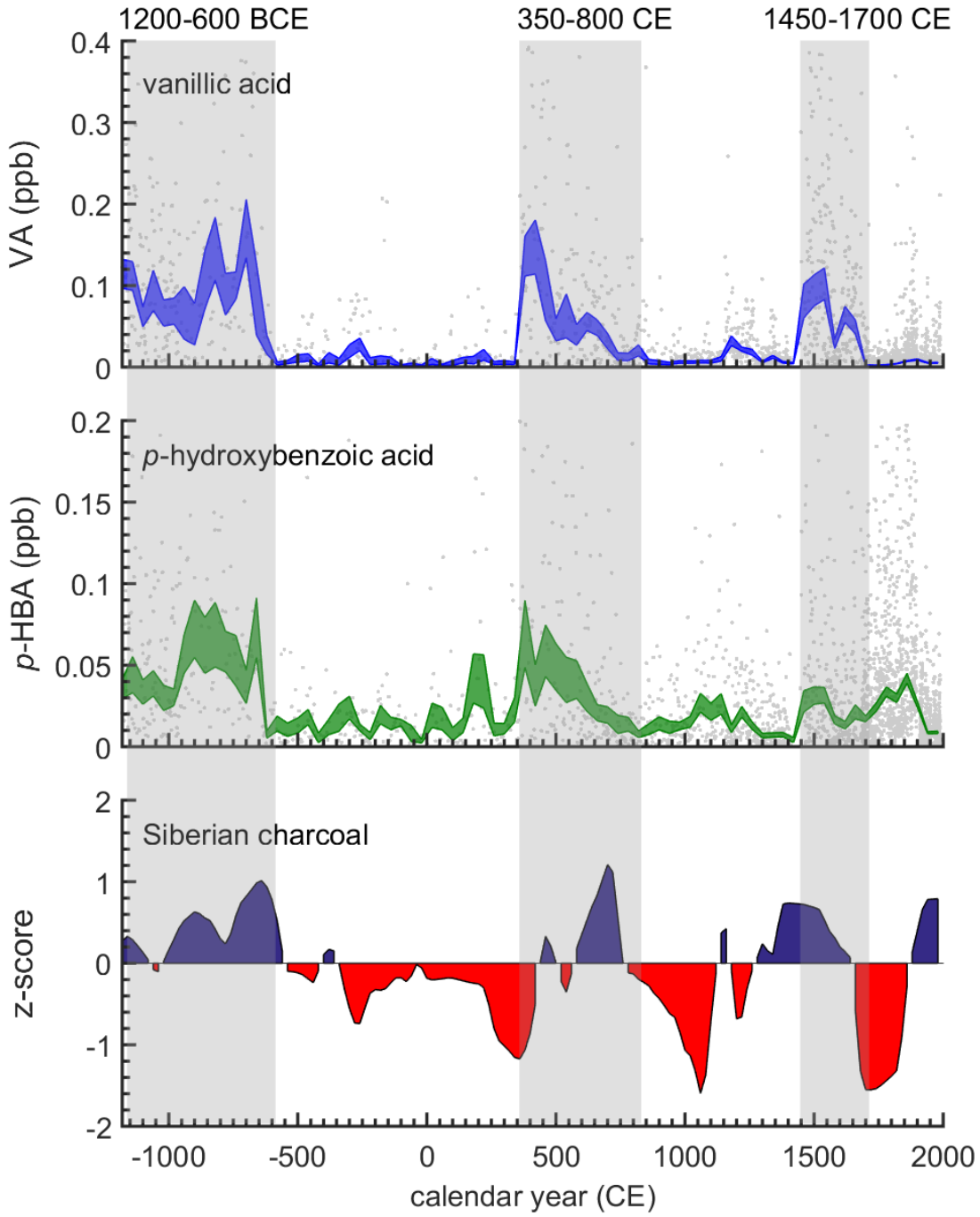

Figure 6.5: Measurements of burning-derived vanillic acid and *p*-hydroxybenzoic acid from Akademii Nauk ice core over the past 3,000 years compared to Siberian charcoal. From top: 40-year averaged Akademii Nauk ice core VA measurements from this study (blue fill is ± 1 standard error of log transform), 40-year averaged Akademii Nauk ice core *p*-HBA measurements from this study (green fill is ± 1 standard error of log transform), and 20-year averaged z-scores of central Siberian charcoal influx (blue > 0, red < 0; 5°0-90°N) (*Power et al.*, 2008). Gray bars are periods of elevated vanillic acid.

CE. The charcoal records are both elevated from 1500-1650 CE, but this peak is only exhibited in the Lomonosovfonna *p*-hydroxybenzoic acid record. These comparisons suggest that either northern Quebec and/or Fennoscandia could be source regions for the Tunu and Lomonosovfonna burning signals.

6.5 Conclusion

Analysis of multiple Arctic ice cores was intended to determine the coherence of timing of biomass burning trends across the Arctic. Surprising, the striking features in the Akademii Nauk VA record are not discernible in the Tunu or Lomonosovfonna VA records. The similarity between the Tunu and Lomonosovfonna records and the smaller features in the Akademii Nauk record suggests that these features could be derived from more distant burning patterns. Clearly, burning signals are not pan-Arctic, and transport plays a major role in determining the ice core signals. Further research is clearly warranted to determine the validity of this hypothesis.

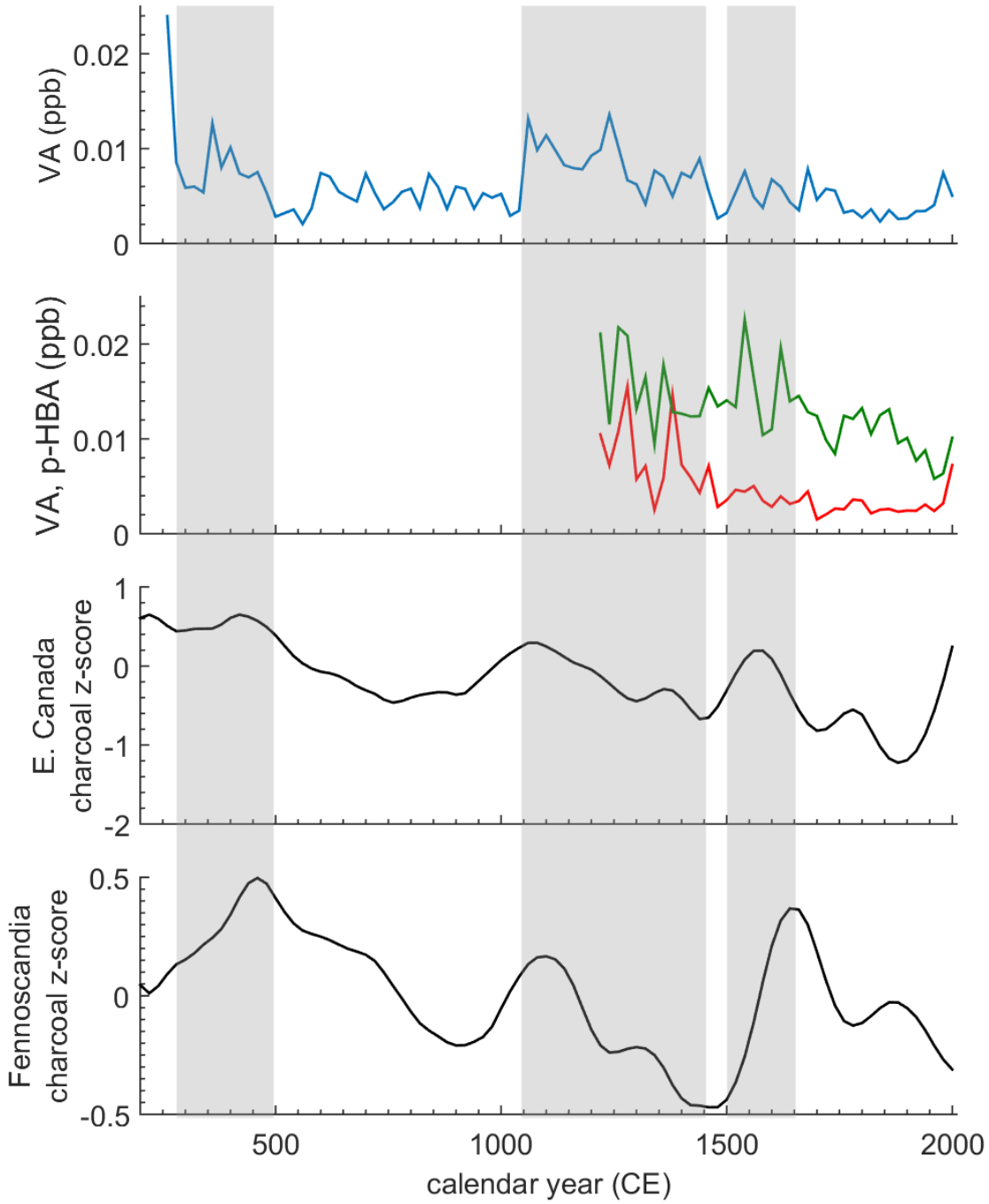

Figure 6.6: Greenland and Svalbard ice core measurements of organic biomass burning-derived aerosols compared to charcoal records. From top: 1) 20-year averaged log transforms of Tunu vanillic acid measurements; 2) 20-year averaged log transforms of Lomonosovfonna vanillic acid (red) and *p*-hydroxybenzoic acid (green) measurements; 3) northern Quebec charcoal influx (50-90°N, 20-80°W); and 4) Fennoscandia charcoal influx (50-90°N, 0-50°E). Charcoal data are 20-year bin-averaged z-scores. Gray bars are periods of elevated vanillic acid or *p*-hydroxybenzoic acid.

Chapter 7

Evidence of climate-driven burning in Siberia

7.1 Overview

In this chapter, Akademii Nauk vanillic acid (VA) and *p*-hydroxybenzoic acid (*p*-HBA) are compared to proxy records of climate variability to determine possible drivers of the biomass burning trends observed in the ice core records. The variability of VA and *p*-HBA in the Akademii Nauk ice core reveals three multi-century periods of extensive fire emissions (1180-660 BCE, 380-620 CE, and 1460-1540 CE). These are periods when VA and *p*-HBA are simultaneously elevated. The timing of these maxima indicates a link between wildfires in Siberia and episodic pulsing of ice-rafted debris in the North Atlantic known as Bond cycles.

7.2 Late Holocene Climate: relationship to Akademii Nauk biomass burning signals

If Akademii Nauk VA and *p*-HBA variability is related to changes in climate, then periods of elevated VA and *p*-HBA would likely be similar to the timing of the major climate modes over the last 3,000 years. Several millennial and centennial-scale climate features have been identified in the Northern Hemisphere using proxy records covering the last 3,000 years.

Regional proxy records show a coherent long-term cooling trend from 2,000 years ago until 19^{th} century. Temperatures began to rise in the 19^{th} century to the present. The two most discernable centennial-scale features in temperature proxy records are the Medieval Climate Anomaly and the Little Ice Age. The Medieval Climate Anomaly is a warm period lasting from about 830 to 1100 CE. The Little Ice Age is a cooling period lasting from about 1580 to 1880 CE (*Ahmed et al.*, 2013). The Little Ice Age is the most recent of Holocene cooling events known as "Bond events."

Bond events are episodes of increased ice rafted debris in North Atlantic sediment cores throughout the Holocene at intervals of 1,470±500 years with durations from 200-500 years. The three most recent Bond events were centered at: 2,800, 1,400, and 500 years BP (850 BCE, 550 CE, and 1450 CE, Figure 7.1) (*Bond et al.*, 1997). Storm activity in the North Atlantic also increased with this same 1,500-year cycle. Holocene storm periods have been identified from: 3,300-2,400, 1,900-1050, and 600-250 years BP (1350-450 BCE, 50-900 CE, and 1350-1700 CE) (*Sorrel et al.*, 2012). Sea surface temperatures (SSTs) in both the North Atlantic and North Pacific oceans were anomalously low during Bond Events. Lower SSTs are linked to the migration of the jet stream, and reduced meridional moisture transport that resulted in east central North America droughts (*Springer et al.*, 2008).

The three major periods of increased Siberian burning found in the Akademii ice core are similar in timing to the three most recent Bond Events. Simultaneous changes in climate are also observed in the Chinese speleothem record from Dongge Cave, centered at: 2,700, 1,600, and 500 years BP (750 BCE, 350 CE, and 1450 CE) (*Wang et al.*, 2005). The speleothem record shows three 100-500 year periods of increased δ^{18}O, indicating decreased East Asian summer monsoon intensity (*Wang et al.*, 2005; *Dykoski et al.*, 2005; *Yuan et al.*, 2004). In the Lake Baikal region of southern Siberia, shifts from Taiga to steppe vegetation occurred with similar timing, indicating widespread climate and associated ecosystem changes across Asia (Figure 7.1) (*Tarasov et al.*, 2007). The similarity in timing between the Siberian biomass

burning pulses, the Bond events, and the monsoonal changes strongly suggests a link between fires and large-scale climate variability on millennial time scales. These North Atlantic and East Asian climate events were originally attributed to reduced solar radiation, as evidenced by increased cosmogenic ^{14}C (*Bond et al.*, 2001; *Wang et al.*, 2005; *Stuiver and Braziunas*, 1998). However, recent studies have demonstrated that there is not a simple quantitative relationship between solar variability and the amplitude of these climate signals (*Wanner et al.*, 2011).

The most recent period of elevated aromatic acids in the Akademii Nauk record from 200-50 years BP (1750-1900 CE) is clearly different from the other three. It does not appear to be related to the Bond events or other known large scale climate events. It is also distinct in having a much higher ratio of *p*-HBA to VA, suggesting that the burning conditions, fuel types, source regions, or transport mechanisms could be different from the earlier burning periods.

7.3 Late Holocene Arctic Oscillation variability: relationship to Akademii Nauk biomass burning signals

Over recent decades, Siberian wildfire burned area correlates with changes in the Arctic Oscillation, with increased biomass burning during the positive phase of the Arctic Oscillation when Siberian summers are warmest (*Balzter et al.*, 2007). It seems logical that changes in the phase and strength of the Arctic Oscillation might also play a role in modulating Siberian fires on long time scales. Arctic sediment cores record variations in transport of ice rafted debris from the Kara Sea to the Beaufort-Chukchi Seas region. This debris transport is caused by changes in wind-driven Arctic Ocean circulation associated with variations in the phase of the Arctic Oscillation (*Darby et al.*, 2012). An 8 kyr Holocene proxy record of

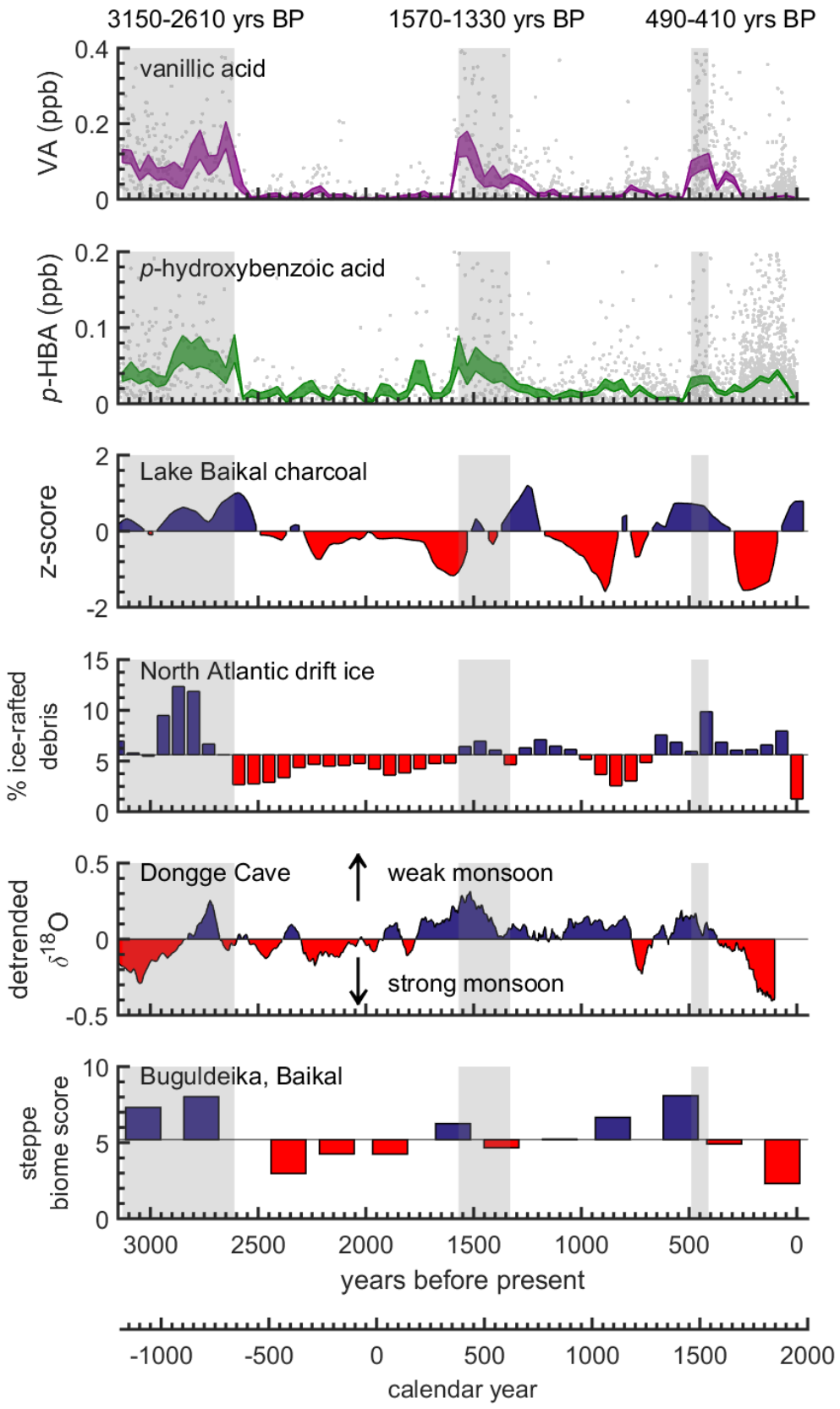

Figure 7.1: (Caption on next page.)

Figure 7.1: (Previous page.) Measurements of burning-derived VA and *p*-HBA from Akademii Nauk ice core over the past 3,000 years compared to other burning- and climate-related proxy records. The similarity in these records shows that Siberian fires changed in concert with large-scale changes in climate.
From top: **a** 40-year bin-averaged (gray fill is ± 1 standard error of log transform) Akademii Nauk ice core VA measurements from this study, **b** 40-year bin-averaged (gray fill is ± 1 standard error of log transform) AN ice core *p*-HBA measurements from this study, **c** 20-year averaged z-scores of central Siberian charcoal influx (blue > 0, red < 0; 5°0-90°N), **d** North Atlantic ice-rafted debris indicating Bond Events (blue $>$ mean; red $<$ mean) (*Bond et al.*, 2001), **e** smoothed Dongge Cave climate record from Asia showing changes in the monsoon using a moving average (blue > 0, red < 0; window size $= 15$) (*Wang et al.*, 2005), **f** Pollen record from Baikal showing changes in vegetation(blue $>$ mean; red $<$ mean) (*Tarasov et al.*, 2007). The gray bands are periods when VA and *p*-HBA are both elevated.

Arctic Oscillation shows a 1,500-year cycle (*Darby et al.*, 2012), but it is not synchronous with increased biomass burning in the AN ice core (Figure 7.2). This sedimentary proxy evidence does not support the Arctic Oscillation as the primary mode of climate variability controlling Siberian burning on millennial time scales. The differences between these records show that Siberian fires were not driven by changes in atmospheric circulation alone.

7.4 Conclusion

This study presents the first clear evidence of major climate-modulated episodes of Siberian wildfire activity on millennial time scales. The timing of the the three striking features in the Akademii Nauk record surprisingly appears to be related to the timing of Bond Events. Biomass burning can be driven by warmer temperatures. Biomass burning in central Siberia has been related to Arctic Oscillation variability in the 20^{th} century (*Balzter et al.*, 2005). The biomass burning signals in the Akademii Nauk record were therefore expected to be related to warm periods in the Northern Hemisphere climate record, such as the Medieval Climate Anomaly, or millennial-scale Arctic Oscillation changes rather than abrupt Holocene cooling events. Further research is needed to determine the physical mechanism linking biomass burning to these periods of increased ice-rafted debris in the North Atlantic.

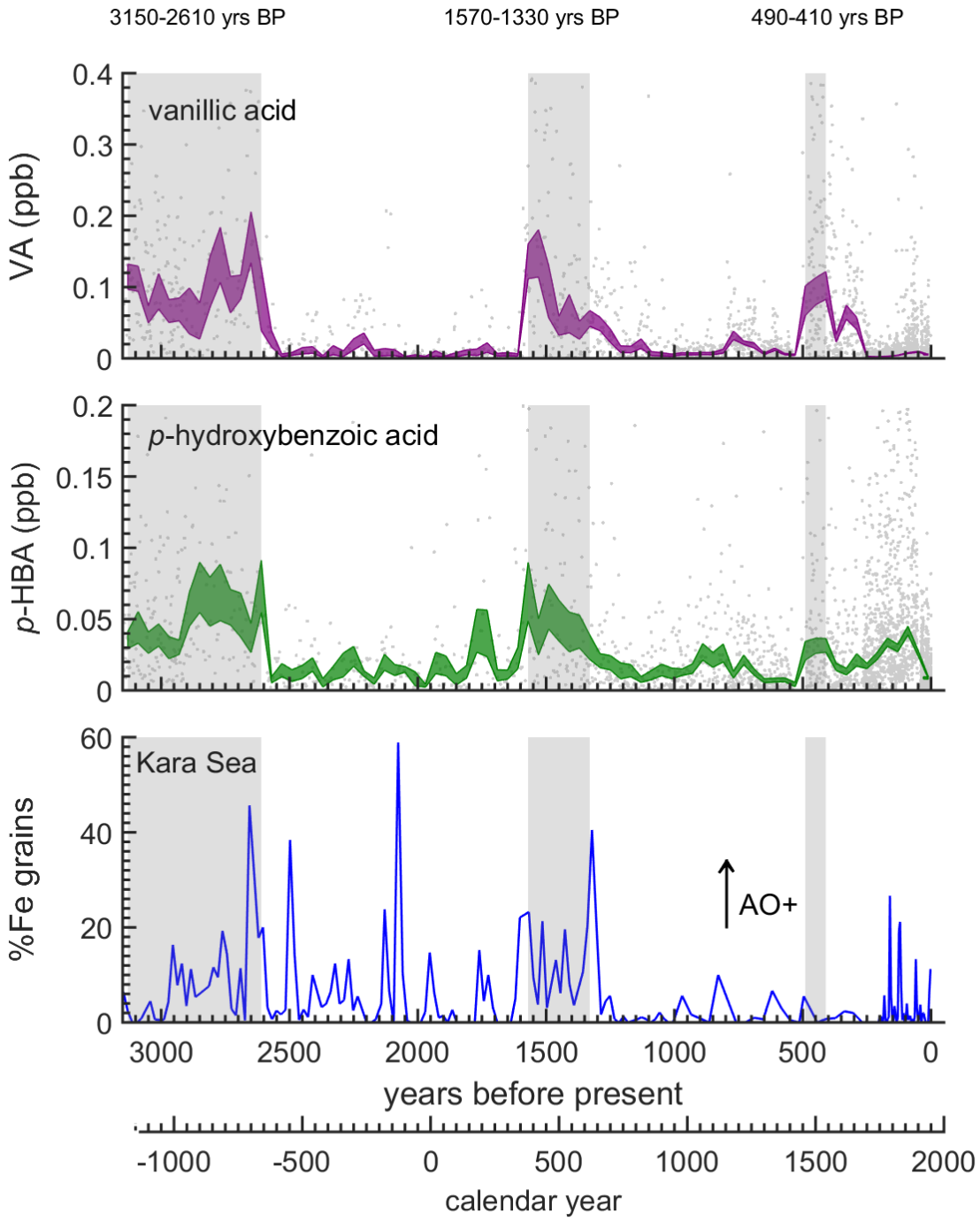

Figure 7.2: Measurements of burning-derived VA and *p*-HBA from the Akademii Nauk ice core over the past 3,000 years compared to Arctic Oscillation record. From top: **a** 40-year bin-averaged (gray fill is ±1 standard error of log transform) Akademii Nauk ice core VA measurements from this study, **b** 40-year bin-averaged (gray fill is ±1 standard error of log transform) Akademii Nauk ice core VA measurements from this study, **b** Alaskan sediment core Kara Sea Fe grain record showing Arctic Oscillation changes (*Darby et al.*, 2012). The gray bands are the periods when VA and *p*-HBA are both elevated.

Chapter 8

Conclusions

This thesis investigated aromatic acids as a class of biomass burning tracers in polar ice cores. These chemicals are significantly different from prior ice core tracers in that they are exclusively derived from burning and retain some information about the precursor biological material burned. This study advanced the field by developing a new method for analyzing these tracers, allowing for the first time the automated analysis of small volume ice core samples with high sensitivity and high selectivity (Chapter 2). This study showed that two common burning-derived aromatic acids (vanillic acid and *p*-hydroxybenzoic acid) are detectable in Arctic ice cores from different sites (Chapters 3,4, and 5). Previous studies of biomass burning proxies in ice cores have struggled to identify events or trends superimposed on large non-burning related signals. This study showed that the organic tracers can exhibit large variability in polar ice cores that is likely dominated by historical variations in biomass burning (chapter 6).

An exciting result of this study is the observation of three major periods of burning in the first millennial time scale record of vanillic acid and *p*-hydroxybenzoic acid in a Siberian ice core. The timing of these features is unexpectedly synchronous to large-scale climate phenomena known as Bond Events (Chapter 7). This discovery is an example of how combining organic tracers with the precise and accurate dating of ice cores may allow for investigation of the connections between variations in burning to patterns of climate change. It is likely

that many discoveries about the relationship between climate and wildfire will be made as additional ice cores are analyzed.

An important next step in this field of research is to analyze these tracers in North American ice cores. It would interesting to examine the phase relationship in burning between the Western and the Eastern Hemispheres to improve the understanding of the modes of climate variability that influence biomass burning on millennial timescales. Understanding the variability of biomass burning in North America will also help to explain the burning signals in the Greenland and Svalbard ice cores in this study.

Comparing North American to Eurasian ice cores would also help to investigate the role of humans on biomass burning variability in the past. Studies of sedimentary charcoal records have concluded that humans were not the primary driver of burning in North America after 1500 CE (*Power et al.*, 2013). Ice core analyses of biomass burning tracers could validate this conclusion. Similar timing between biomass burning variability exhibited in North American ice cores and North American population or land use change would indicate a relationship between humans and biomass burning.

The successful analysis of vanillic acid and *p*-hydroxybenzoic acid in polar ice cores suggests that there is potential for analyzing a suite of the many compounds derived from different species of plants in the future. Analysis of a suite of phenols is needed to determine the ratios of vanillyl, syringyl, cinnamyl, and *p*-hydroxyl structures in a record in order to resolve which plant type burned. Comparison between these compounds and the pollen types in ice cores will also provide information about the types of plants that were present during high/low burning periods. The type of plant material burned could not be determined in this study because only two compounds were analyzed.

In this study, the assertion that aromatic acids in ice cores are "proxies" for biomass burning is based on the following: 1) these molecules are major products of biomass burning in

laboratory experiments, 2) burning is the only known source of these molecules in ambient aerosols, and 3) long distance aerosol transport of these compounds has been observed. These chemicals are not yet proxies in a quantitative sense. In other words, there is no quantitative, calibrated relationship between the levels of vanillic acid in an ice core and regional burning emissions or extent. Any such relationship would be empirical at best, and subject to many uncertainties. Detailed time series studies comparing ice core records to historical records have not yet been carried out. These are needed in order to validate the notion that the ice core variations of these compounds quantitatively reflect biomass burning emissions from various regions. Such studies could be done for the satellite era by carefully comparing ice core records to satellite-based regional estimates of burning.

This thesis advanced the study of how biomass burning changed in the past, and provides a new approach to study the long term history of fire. Records of the patterns of burning helps to understand the relationship between climate and fire. Understanding this relationship is important for developing models that simulate the role of fire in the earth system.

Bibliography

Ahmed, M., K. J. Anchukaitis, A. Asrat, H. Borgaonkar, M. Braida, B. M. Buckley, U. Büntgen, B. M. Chase, D. A. Christie, E. R. Cook, et al. (2013), Continental-scale temperature variability during the past two millennia, *Nature Geoscience*, *6*(5), 339–346.

Balzter, H., F. F. Gerard, C. T. George, C. S. Rowland, T. E. Jupp, I. McCallum, A. Shvidenko, S. Nilsson, A. Sukhinin, A. Onuchin, et al. (2005), Impact of the Arctic Oscillation pattern on interannual forest fire variability in Central Siberia, *Geophysical Research Letters*, *32*(14), doi:10.1029/2005GL023027.

Balzter, H., F. Gerard, C. George, G. Weedon, W. Grey, B. Combal, E. Bartholomé, S. Bartalev, and S. Los (2007), Coupling of vegetation growing season anomalies and fire activity with hemispheric and regional-scale climate patterns in central and east Siberia, *Journal of Climate*, *20*(15), 3713–3729, doi:10.1175/JCLI4226.

Bond, G., W. Showers, M. Cheseby, R. Lotti, P. Almasi, P. deMenocal, P. Priore, H. Cullen, I. Hajdas, and G. Bonani (1997), A Pervasive Millennial-Scale Cycle in North Atlantic Holocene and Glacial Climates, *Science*, *278*(5341), 1257–1266, doi:10.1126/science.278.5341.1257.

Bond, G., B. Kromer, J. Beer, R. Muscheler, M. N. Evans, W. Showers, S. Hoffmann, R. Lotti-Bond, I. Hajdas, and G. Bonani (2001), Persistent Solar Influence on North Atlantic Climate During the Holocene, *Science*, *294*(5549), 2130–2136, doi:10.1126/science.1065680.

Bouwman, A. F., D. S. Lee, W. A. H. Asman, F. J. Dentener, K. W. Van Der Hoek, and J. G. J. Olivier (1997), A global high-resolution emission inventory for ammonia, *Global Biogeochemical Cycles*, *11*(4), 561–587, doi:10.1029/97GB02266.

Bowman, D. M., J. K. Balch, P. Artaxo, W. J. Bond, J. M. Carlson, M. A. Cochrane, C. M. DAntonio, R. S. DeFries, J. C. Doyle, S. P. Harrison, et al. (2009), Fire in the Earth system, *science*, *324*(5926), 481–484, doi:10.1126/science.1163886.

Brown, T. J., B. L. Hall, and A. L. Westerling (2004), The impact of twenty-first century climate change on wildland fire danger in the western United States: an applications perspective, *Climatic change*, *62*(1-3), 365–388, doi:10.1023/B:CLIM.0000013680.07783.de.

Chylek, P., B. Johnson, P. A. Damiano, K. C. Taylor, and P. Clement (1995), Biomass burning record and black carbon in the GISP2 Ice Core, *Geophysical Research Letters*, *22*(2), 89–92, doi:10.1029/94GL02841.

Crutzen, P. J., and M. O. Andreae (1990), Biomass burning in the tropics: Impact on atmospheric chemistry and biogeochemical cycles, *Science*, *250*(4988), 1669–1678, doi:10.1126/science.250.4988.1669.

Dai, A., W. Washington, G. Meehl, T. Bettge, and W. Strand (2004), The ACPI climate change simulations, *Climatic Change*, *62*(1-3), 29–43, doi:10.1023/B:CLIM.0000013679.74883.e6.

Darby, D. A., J. D. Ortiz, C. E. Grosch, and S. P. Lund (2012), 1,500-year cycle in the Arctic Oscillation identified in Holocene Arctic sea-ice drift, *Nature geoscience*, *5*(12), 897–900, doi:10.1038/ngeo1629.

Dibb, J. E., R. W. Talbot, S. I. Whitlow, M. C. Shipham, J. Winterle, J. McConnell, and R. Bales (), Biomass burning signatures in the atmosphere and snow at Summit, Greenland: An event on 5 August 1994, *Atmospheric Environment*, *30*(4), 553–561.

Donahue, N., W. Chuang, S. Epstein, J. Kroll, D. Worsnop, A. Robinson, P. Adams, and S. Pandis (2013), Why do organic aerosols exist? Understanding aerosol lifetimes using the two-dimensional volatility basis set, *Environmental Chemistry*, *10*(3), 151–157, doi:10.1071/EN13022.

Draxler, R. R., and G. Hess (1997), Description of the HYSPLIT4 modeling system, *Tech. rep.*, US Department of Commerce, National Oceanic and Atmospheric Administration, Environmental Research Laboratories, Air Resources Laboratory.

Draxler, R. R., and G. Hess (1998), An overview of the HYSPLIT_4 modelling system for trajectories, *Australian meteorological magazine*, *47*(4), 295–308.

Draxler, R. R., B. Stunder, G. Rolph, and A. Taylor (1999), HYSPLIT4 user's guide, *NOAA Technical Memorandum ERL ARL*, *230*, 35.

Dykoski, C. A., R. L. Edwards, H. Cheng, D. Yuan, Y. Cai, M. Zhang, Y. Lin, J. Qing, Z. An, and J. Revenaugh (2005), A high-resolution, absolute-dated holocene and deglacial asian monsoon record from dongge cave, china, *Earth and Planetary Science Letters*, *233*(12), 71 – 86, doi:http://dx.doi.org/10.1016/j.epsl.2005.01.036.

Eichler, A., W. Tinner, S. Brtsch, S. Olivier, T. Papina, and M. Schwikowski (2011), An ice-core based history of Siberian forest fires since AD 1250, *Quaternary Science Reviews*, *30*(910), 1027–1034, doi:http://dx.doi.org/10.1016/j.quascirev.2011.02.007.

Ferretti, D. F., J. B. Miller, J. W. C. White, D. M. Etheridge, K. R. Lassey, D. C. Lowe, C. M. M. Meure, M. F. Dreier, C. M. Trudinger, T. D. van Ommen, and R. L. Langenfelds (2005), Unexpected changes to the global methane budget over the past 2000 years, *Science*, *309*(5741), 1714–1717, doi:10.1126/science.1115193, 10.1126/science.1115193.

Fritzsche, D., F. Wilhelms, L. M. Savatyugin, J. F. Pinglot, H. Meyer, H.-W. Hubberten, and H. Miller (2002), A new deep ice core from akademii nauk ice cap, severnaya zemlya, eurasian arctic: first results, *Annals of Glaciology*, *35*, 25–28.

Fritzsche, D., R. Schutt, H. Meyer, H. Miller, F. Wilhelms, T. Opel, and L. M. Savatyugin (2005), A 275 year ice core record from akademii nauk ice cap, severnaya zemlya, russian arctic, *Annals of Glaciology*, *42*, 361–366.

Fu, P., K. Kawamura, and L. A. Barrie (2008), Photochemical and other sources of organic compounds in the canadian high arctic aerosol pollution during winter-spring, *Environmental Science and Technology*, *43*(2), 286–292.

Fuhrer, K., A. Neftel, M. Anklin, T. Staffelbach, and M. Legrand (1996), High-resolution ammonium ice core record covering a complete glacial-interglacial cycle, *Journal of Geophysical Research: Atmospheres*, *101*(D2), 4147–4164, doi:10.1029/95JD02903.

Gambaro, A., R. Zangrando, P. Gabrielli, C. Barbante, and P. Cescon (2008), Direct determination of levoglucosan at the picogram per milliliter level in antarctic ice by high-performance liquid chromatography/electrospray ionization triple quadrupole mass spectrometry, *Analytical Chemistry*, *80*(5), 1649–1655.

Generoso, S., I. Bey, J.-L. Atti, and F.-M. Bron (2007), A satellite- and model-based assessment of the 2003 Russian fires: Impact on the Arctic region, *Journal of Geophysical Research: Atmospheres*, *112*(D15), doi:10.1029/2006JD008344, d15302.

Gower, S., O. Krankina, R. Olson, M. Apps, S. Linder, and C. Wang (2001), Net primary production and carbon allocation patterns of boreal forest ecosystems, *Ecological Applications*, *11*(5), 1395–1411.

Grannas, A. M., P. B. Shepson, and T. R. Filley (2004), Photochemistry and nature of organic matter in Arctic and Antarctic snow, *Global Biogeochem. Cycles*, *18*(1), GB1006, doi:10.1029/2003GB002133.

Grannas, A. M., A. E. Jones, J. Dibb, M. Ammann, C. Anastasio, H. J. Beine, M. Bergin, J. Bottenheim, C. S. Boxe, G. Carver, G. Chen, J. H. Crawford, F. Dominé, M. M. Frey, M. I. Guzmán, D. E. Heard, D. Helmig, M. R. Hoffmann, R. E. Honrath, L. G. Huey, M. Hutterli, H. W. Jacobi, P. Klán, B. Lefer, J. McConnell, J. Plane, R. Sander, J. Savarino, P. B. Shepson, W. R. Simpson, J. R. Sodeau, R. von Glasow, R. Weller, E. W. Wolff, and T. Zhu (2007), An overview of snow photochemistry: evidence, mechanisms and impacts, *Atmospheric Chemistry and Physics*, *7*(16), 4329–4373, doi:10.5194/acp-7-4329-2007.

Hedges, J. I., and D. C. Mann (1979), The characterization of plant tissues by their lignin oxidation products, *Geochimica et Cosmochimica Acta*, *43*(11), 1803–1807, doi:10.1016/0016-7037(79)90028-0.

Hedges, J. I., and P. L. Parker (1976), Land-derived organic matter in surface sediments from the Gulf of Mexico, *Geochimica et Cosmochimica Acta*, *40*(9), 1019–1029, doi:10.1016/0016-7037(76)90044-2.

Hennigan, C. J., A. P. Sullivan, J. L. Collett, and A. L. Robinson (2010), Levoglucosan stability in biomass burning particles exposed to hydroxyl radicals, *Geophysical Research Letters*, *37*(L09806), L09,806, doi:10.1029/2010GL043088.

Hessl, A. E. (2011), Pathways for climate change effects on fire: Models, data, and uncertainties, *Progress in Physical Geography*, *35*(3), 393–407, doi:10.1177/0309133311407654.

Higuera, P. E., L. B. Brubaker, P. M. Anderson, T. A. Brown, A. T. Kennedy, and F. S. Hu (2008), Frequent Fires in Ancient Shrub Tundra: Implications of Paleorecords for Arctic Environmental Change, *PLoS ONE*, *3*, e0001,744, doi:10.1371/journal.pone.0001744.

Hoffmann, D., A. Tilgner, Y. Iinuma, and H. Herrmann (2010), Atmospheric stability of levoglucosan: a detailed laboratory and modeling study., *Environmental Science and Technology*, *44*, 694–699.

Jaffrezo, J. L., C. I. Davidson, H. D. Kuhns, M. H. Bergin, R. Hillamo, W. Maenhaut, J. W. Kahl, and J. M. Harris (1998), Biomass burning signatures in the atmosphere of central Greenland, *Journal of Geophysical Research: Atmospheres*, *103*(D23), 31,067–31,078, doi:10.1029/98JD02241.

Kalnay, E., M. Kanamitsu, R. Kistler, W. Collins, D. Deaven, L. Gandin, M. Iredell, S. Saha, G. White, J. Woollen, Y. Zhu, A. Leetmaa, B. Reynolds, M. Chelliah, W. Ebisuzaki, W. Higgins, J. Janowiak, K. Mo, C. Ropelewski, J. Wang, R. Jenne, and D. Joseph (1996), The NCEP/NCAR 40-Year Reanalysis Project, *Bulletin of the American Meteorological Society*, *77*(3), 437–471.

Kasischke, E. S., N. Christensen Jr, and B. J. Stocks (1995), Fire, global warming, and the carbon balance of boreal forests, *Ecological applications*, pp. 437–451.

Kawamura, K., Y. Izawa, M. Mochida, and T. Shiraiwa (2012), Ice core records of biomass burning tracers (levoglucosan and dehydroabietic, vanillic and p-hydroxybenzoic acids) and total organic carbon for past 300 years in the kamchatka peninsula, northeast asia, *Geochimica et Cosmochimica Acta*, *99*(null), 317–329, doi:10.1016/j.gca.2012.08.006.

Kehrwald, N., R. Zangrando, A. Gambaro, and C. Barbante (2010), Fire and climate: Biomass burning recorded in ice and lake cores, *EPJ Web of Conferences*, *9*, 105–114, doi:10.1051/epjconf/201009008.

Kehrwald, N., R. Zangrando, P. Gabrielli, J.-L. Jaffrezo, C. Boutron, C. Barbante, and A. Gambaro (2012), Levoglucosan as a specific marker of fire events in Greenland snow, *Tellus B*, *64*, 18,196, doi:10.1002/2013EO460001.

Kehrwald, N. M., C. Whitlock, C. Barbante, V. Brovkin, A.-L. Daniau, J. O. Kaplan, J. R. Marlon, M. J. Power, K. Thonicke, and G. R. Werf (2013), Fire research: linking past, present, and future data, *Eos, Transactions American Geophysical Union*, *94*(46), 421–422.

Kekonen, T., J. Moore, P. Permki, R. Mulvaney, E. Isaksson, V. Pohjola, and R. S. W. van de Wal (2005), The 800 year long ion record from the Lomonosovfonna (Svalbard) ice core, *Journal of Geophysical Research: Atmospheres*, *110*(D7), doi:10.1029/2004JD005223, d07304.

Laj, P., J. M. Palais, and H. Sigurdsson (1992), Changing sources of impurities to the Greenland ice sheet over the last 250 years, *Atmospheric Environment. Part A. General Topics*, *26*(14), 2627–2640, doi:10.1016/0960-1686(92)90114-Z.

Legrand, M., M. De Angelis, T. Staffelbach, A. Neftel, and B. Stauffer (1992), Large perturbations of ammonium and organic acids content in the summit-Greenland Ice Core. Fingerprint from forest fires?, *Geophysical Research Letters*, *19*(5), 473–475, doi: 10.1029/91GL03121.

Mack, M. C., M. S. Bret-Harte, T. N. Hollingsworth, R. R. Jandt, E. A. G. Schuur, G. R. Shaver, and D. L. Verbyla (2011), Carbon loss from an unprecedented Arctic tundra wildfire, *Nature*, *475*, 489–492, doi:10.1038/nature10283.

Marlon, J. R., P. J. Bartlein, C. Carcaillet, D. G. Gavin, S. P. Harrison, P. E. Higuera, F. Joos, M. J. Power, and I. C. Prentice (2008), Climate and human influences on global biomass burning over the past two millennia, *Nature Geosci*, *1*(10), 697–702, 10.1038/ngeo313.

Matsui, H., Y. Kondo, N. Moteki, N. Takegawa, L. Sahu, Y. Zhao, H. Fuelberg, W. Sessions, G. Diskin, D. Blake, et al. (2011), Seasonal variation of the transport of black carbon aerosol from the Asian continent to the Arctic during the ARCTAS aircraft campaign, *Journal of Geophysical Research: Atmospheres*, *116*(D5), doi:10.1029/2010JD015067.

McConnell, J. R., G. W. Lamorey, S. W. Lambert, and K. C. Taylor (2001), Continuous ice-core chemical analyses using inductively coupled plasma mass spectrometry, *Environmental Science and Technology*, *36*(1), 7–11.

McConnell, J. R., R. Edwards, G. L. Kok, M. G. Flanner, C. S. Zender, E. S. Saltzman, J. R. Banta, D. R. Pasteris, M. M. Carter, and J. D. W. Kahl (2007), 20th-century industrial black carbon emissions altered arctic climate forcing, *Science*, *317*(5843), 1381–1384, 10.1126/science.1144856.

Mernild, S. H., E. Hanna, J. R. McConnell, M. Sigl, A. P. Beckerman, J. C. Yde, J. Cappelen, J. K. Malmros, and K. Steffen (2015), Greenland precipitation trends in a long-term instrumental climate context (18902012): evaluation of coastal and ice core records, *International Journal of Climatology*, *35*(2), 303–320, doi:10.1002/joc.3986.

Mischler, J. A., T. Sowers, R. Alley, M. Battle, J. McConnell, L. Mitchell, T. Popp, E. Sofen, and M. Spencer (2009), Carbon and hydrogen isotopic composition of methane over the last 1000 years, *Global Biogeochemical Cycles*, *23*(4), doi:10.1029/2009GB003460.

Nolte, C. G., J. J. Schauer, G. R. Cass, and B. R. T. Simoneit (2001), Highly polar organic compounds present in wood smoke and in the ambient atmosphere, *Environmental Science and Technology*, *35*(10), 1912–1919.

Opel, T., D. Fritzsche, and H. Meyer (2013), Eurasian Arctic climate over the past millennium as recorded in the Akademii Nauk ice core (Severnaya Zemlya), *Clim. Past*, *9*(5), 2379–2389, doi:10.5194/cp-9-2379-2013.

Opsahl, S., and R. Benner (1995), Early diagenesis of vascular plant tissues: lignin and cutin decomposition and biogeochemical implications, *Geochimica et Cosmochimica Acta*, *59*(23), 4889–4904, doi:10.1016/0016-7037(95)00348-7.

Oros, D. R., and B. R. Simoneit (2001a), Identification and emission factors of molecular tracers in organic aerosols from biomass burning Part 1. Temperate climate conifers, *Applied Geochemistry*, *16*(13), 1513–1544, doi:10.1016/S0883-2927(01)00021-X.

Oros, D. R., and B. R. Simoneit (2001b), Identification and emission factors of molecular tracers in organic aerosols from biomass burning Part 2. Deciduous trees, *Applied Geochemistry*, *16*(13), 1545–1565, doi:10.1016/S0883-2927(01)00022-1.

Oros, D. R., M. R. bin Abas, N. Y. M. Omar, N. A. Rahman, and B. R. Simoneit (2006), Identification and emission factors of molecular tracers in organic aerosols from biomass burning: Part 3. grasses, *Applied Geochemistry*, *21*(6), 919 – 940, doi:http://dx.doi.org/10.1016/j.apgeochem.2006.01.008.

Pechony, O., and D. T. Shindell (2010), Driving forces of global wildfires over the past millennium and the forthcoming century, *Proceedings of the National Academy of Sciences*, *107*(45), 19,167–19,170, doi:10.1073/pnas.1003669107.

Pohjola, V. A., J. C. Moore, E. Isaksson, T. Jauhiainen, R. S. W. van de Wal, T. Martma, H. A. J. Meijer, and R. Vaikme (2002), Effect of periodic melting on geochemical and isotopic signals in an ice core from Lomonosovfonna, Svalbard, *Journal of Geophysical Research: Atmospheres*, *107*(D4), ACL 1–1–ACL 1–14, doi:10.1029/2000JD000149.

Power, M., J. Marlon, N. Ortiz, P. Bartlein, S. Harrison, F. Mayle, A. Ballouche, R. Bradshaw, C. Carcaillet, C. Cordova, S. Mooney, P. Moreno, I. Prentice, K. Thonicke, W. Tinner, C. Whitlock, Y. Zhang, Y. Zhao, A. Ali, R. Anderson, R. Beer, H. Behling, C. Briles, K. Brown, A. Brunelle, M. Bush, P. Camill, G. Chu, J. Clark, D. Colombaroli, S. Connor, A. L. Daniau, M. Daniels, J. Dodson, E. Doughty, M. Edwards, W. Finsinger, D. Foster, J. Frechette, M. J. Gaillard, D. Gavin, E. Gobet, S. Haberle, D. Hallett, P. Higuera, G. Hope, S. Horn, J. Inoue, P. Kaltenrieder, L. Kennedy, Z. Kong, C. Larsen, C. Long, J. Lynch, E. Lynch, M. McGlone, S. Meeks, S. Mensing, G. Meyer, T. Minckley, J. Mohr, D. Nelson, J. New, R. Newnham, R. Noti, W. Oswald, J. Pierce, P. Richard, C. Rowe, M. Sanchez Goi, B. Shuman, H. Takahara, J. Toney, C. Turney, D. Urrego-Sanchez, C. Umbanhowar, M. Vandergoes, B. Vanniere, E. Vescovi, M. Walsh, X. Wang, N. Williams, J. Wilmshurst, and J. Zhang (2008), Changes in fire regimes since the Last Glacial Maximum: an assessment based on a global synthesis and analysis of charcoal data, *Climate Dynamics*, *30*(7), 887–907–907, doi:10.1007/s00382-007-0334-x.

Power, M., F. Mayle, P. Bartlein, J. Marlon, R. Anderson, H. Behling, K. Brown, C. Carcaillet, D. Colombaroli, D. Gavin, D. Hallett, S. Horn, L. Kennedy, C. Lane, C. Long,

P. Moreno, C. Paitre, G. Robinson, Z. Taylor, and M. Walsh (2013), Climatic control of the biomass-burning decline in the Americas after AD 1500, *The Holocene*, *23*(1), 3–13, doi:10.1177/0959683612450196.

Randerson, J. T., H. Liu, M. G. Flanner, S. D. Chambers, Y. Jin, P. G. Hess, G. Pfister, M. C. Mack, K. K. Treseder, L. R. Welp, F. S. Chapin, J. W. Harden, M. L. Goulden, E. Lyons, J. C. Neff, E. A. G. Schuur, and C. S. Zender (2006), The Impact of Boreal Forest Fire on Climate Warming, *Science*, *314*(5802), 1130–1132, 10.1126/science.1132075.

Rubino, M., A. D'Onofrio, O. Seki, and J. A. Bendle (2015), Ice-core records of biomass burning, *The Anthropocene Review*, p. 2053019615605117, doi:10.1177/2053019615605117.

Ryan, K. C. (2002), Dynamic Interactions between Forest Structure and Fire Behavior in Boreal Ecosystems, *Ecosystems*, *36*(1), 13–39.

Saltzman, E. S., P.-Y. Whung, and P. A. Mayewski (1997), Methanesulfonate in the Greenland Ice Sheet Project 2 Ice Core, *Journal of Geophysical Research: Oceans*, *102*(C12), 26,649–26,657, doi:10.1029/97JC01377.

Sapart, C. J., G. Monteil, M. Prokopiou, R. S. W. van de Wal, J. O. Kaplan, P. Sperlich, K. M. Krumhardt, C. van der Veen, S. Houweling, M. C. Krol, T. Blunier, T. Sowers, P. Martinerie, E. Witrant, D. Dahl-Jensen, and T. Rockmann (2012), Natural and anthropogenic variations in methane sources during the past two millennia, *Nature*, *490*(7418), 85–88, 10.1038/nature11461.

Savarino, J., and M. Legrand (1998), High northern latitude forest fires and vegetation emissions over the last millennium inferred from the chemistry of a central Greenland ice core, *Journal of Geophysical Research: Atmospheres*, *103*(D7), 8267–8279, doi:10.1029/97JD03748.

Sigl, M., J. R. McConnell, L. Layman, O. Maselli, K. McGwire, D. Pasteris, D. Dahl-Jensen, J. P. Steffensen, B. Vinther, R. Edwards, R. Mulvaney, and S. Kipfstuhl (2013), A new bipolar ice core record of volcanism from WAIS Divide and NEEM and implications for climate forcing of the last 2000 years, *Journal of Geophysical Research: Atmospheres*, *118*(3), 1151–1169, doi:10.1029/2012JD018603.

Sigl, M., M. Winstrup, J. McConnell, K. Welten, G. Plunkett, F. Ludlow, U. Büntgen, M. Caffee, N. Chellman, D. Dahl-Jensen, et al. (2015), Timing and climate forcing of volcanic eruptions for the past 2,500 years, *Nature*, pp. 543–549, doi:10.1038/nature14565.

Simoneit, B., J. Schauer, C. Nolte, D. Oros, V. Elias, M. Fraser, W. Rogge, and G. Cass (1999), Levoglucosan, a tracer for cellulose in biomass burning and atmospheric particles, *Atmospheric Environment*, *33*(2), 173–182.

Simoneit, B. R. T. (2002), Biomass burning – a review of organic tracers for smoke from incomplete combustion, *Applied Geochemistry*, *17*(3), 129–162.

Simoneit, B. R. T., V. O. Elias, M. Kobayashi, K. Kawamura, A. I. Rushdi, P. M. Medeiros, W. F. Rogge, and B. M. Didyk (2004), Sugars dominant water-soluble organic compounds in soils and characterization as tracers in atmospheric particulate matter, *Environmental Science and Technology*, *38*(22), 5939–5949.

Slade, J. H., and D. A. Knopf (2013), Heterogeneous oh oxidation of biomass burning organic aerosol surrogate compounds: assessment of volatilisation products and the role of oh concentration on the reactive uptake kinetics., *Physical Chemistry Chemical Physics*, *15*, 5898–915.

Solomon, S., D. Qin, M. Manning, Z. Chen, M. Marquis, K. Averyt, M. Tignor, and H. Miller (2007), The physical science basis, *Contribution of working group I to the fourth assessment report of the intergovernmental panel on climate change*, pp. 235–337.

Sorrel, P., M. Debret, I. Billeaud, S. L. Jaccard, J. F. McManus, and B. Tessier (2012), Persistent non-solar forcing of Holocene storm dynamics in coastal sedimentary archives, *Nature Geoscience*, *5*(12), 892–896, doi:10.1038/ngeo1619.

Springer, G. S., H. D. Rowe, B. Hardt, R. L. Edwards, and H. Cheng (2008), Solar forcing of Holocene droughts in a stalagmite record from West Virginia in east-central North America, *Geophysical Research Letters*, *35*(17), doi:10.1029/2008GL034971.

Stein, A., R. Draxler, G. Rolph, B. Stunder, M. Cohen, and F. Ngan (2015), NOAAs HYSPLIT atmospheric transport and dispersion modeling system, *Bulletin of the American Meteorological Society*, *96*(12), 2059–2077, doi:10.1175/BAMS-D-14-00110.1.

Stocks, B., B. Wotton, M. Flannigan, M. Fosberg, D. Cahoon, and J. Goldammer (2001), Boreal forest fire regimes and climate change, in *Remote Sensing and Climate Modeling: Synergies and Limitations*, pp. 233–246, Springer, doi:10.1007/0-306-48149-9_10.

Stohl, A. (2006), Characteristics of atmospheric transport into the Arctic troposphere, *Journal of Geophysical Research: Atmospheres*, *111*(D11), n/a–n/a, doi:10.1029/2005JD006888, d11306.

Stohl, A., E. Andrews, J. F. Burkhart, C. Forster, A. Herber, S. W. Hoch, D. Kowal, C. Lunder, T. Mefford, J. A. Ogren, S. Sharma, N. Spichtinger, K. Stebel, R. Stone, J. Strm, K. Trseth, C. Wehrli, and K. E. Yttri (2006), Pan-Arctic enhancements of light absorbing aerosol concentrations due to North American boreal forest fires during summer 2004, *Journal of Geophysical Research: Atmospheres*, *111*(D22), n/a–n/a, doi:10.1029/2006JD007216, d22214.

Stuiver, M., and T. F. Braziunas (1998), Anthropogenic and solar components of hemispheric 14C, *Geophysical Research Letters*, *25*(3), 329–332, doi:10.1029/97GL03694.

Tarasov, P., E. Bezrukova, E. Karabanov, T. Nakagawa, M. Wagner, N. Kulagina, P. Letunova, A. Abzaeva, W. Granoszewski, and F. Riedel (2007), Vegetation and climate dynamics during the holocene and eemian interglacials derived from lake baikal pollen records, *Palaeogeography, Palaeoclimatology, Palaeoecology*, *252*(34), 440 – 457, doi:http://dx.doi.org/10.1016/j.palaeo.2007.05.002.

Taylor, K., P. Mayewski, M. Twickler, and S. Whitlow (1996), Biomass burning recorded in the GISP2 ice core: a record from eastern Canada?, *The Holocene*, *6*(1), 1–6, doi: 10.1177/095968369600600101.

Thompson, L. G., M. E. Davis, E. Mosley-Thompson, T. A. Sowers, K. A. Henderson, V. S. Zagorodnov, P.-N. Lin, V. N. Mikhalenko, R. K. Campen, J. F. Bolzan, J. Cole-Dai, and B. Francou (1998), A 25,000-Year Tropical Climate History from Bolivian Ice Cores, *Science*, *282*(5395), 1858–1864, doi:10.1126/science.282.5395.1858.

Thonicke, K., A. Spessa, I. Prentice, S. P. Harrison, L. Dong, and C. Carmona-Moreno (2010), The influence of vegetation, fire spread and fire behaviour on biomass burning and trace gas emissions: results from a process-based model., *Biogeosciences*, *7*(6), 1991–2011, doi:10.5194/bg-7-1991-2010.

Vanholme, R., B. Demedts, K. Morreel, J. Ralph, and W. Boerjan (2010), Lignin biosynthesis and structure, *Plant Physiology*, *153*(3), 895–905, doi:10.1104/pp.110.155119.

Wang, Y., H. Cheng, R. L. Edwards, Y. He, X. Kong, Z. An, J. Wu, M. J. Kelly, C. A. Dykoski, and X. Li (2005), The Holocene Asian Monsoon: Links to Solar Changes and North Atlantic Climate, *Science*, *308*(5723), 854–857, doi:10.1126/science.1106296.

Wanner, H., O. Solomina, M. Grosjean, S. P. Ritz, and M. Jetel (2011), Structure and origin of Holocene cold events, *Quaternary Science Reviews*, *30*(21), 3109–3123, doi:10.1016/j.quascirev.2011.07.010.

Warneke, C., K. D. Froyd, J. Brioude, R. Bahreini, C. A. Brock, J. Cozic, J. A. de Gouw, D. W. Fahey, R. Ferrare, J. S. Holloway, A. M. Middlebrook, L. Miller, S. Montzka, J. P. Schwarz, H. Sodemann, J. R. Spackman, and A. Stohl (2010), An important contribution to springtime Arctic aerosol from biomass burning in Russia, *Geophysical Research Letters*, *37*(1), n/a–n/a, doi:10.1029/2009GL041816, l01801.

Weiler, K., H. Fischer, D. Fritzsche, U. Ruth, F. Wilhelms, and H. Miller (2005), Glaciochemical reconnaissance of a new ice core from Severnaya Zemlya, *J. Glaciology*, *51*, 64–74.

Wendl, I., A. Eichler, E. Isaksson, T. Martma, and M. Schwikowski (2015), 800-year ice-core record of nitrogen deposition in Svalbard linked to ocean productivity and biogenic emissions, *Atmospheric Chemistry and Physics*, *15*(13), 7287–7300.

Wendl, I. A. (2014), High Resolution Records of Black Carbon and Other Aerosol Constituents from the Lomonosovfonna 2009 Ice Core, Ph.D. thesis, University of Bern.

Whitlow, S., P. Mayewski, J. Dibb, G. Holdsworth, and M. Twickler (1994), An ice-core-based record of biomass burning in the arctic and subarctic, 1750-1980, *Tellus B*, *46*(3), 234–242.

Yuan, D., H. Cheng, R. L. Edwards, C. A. Dykoski, M. J. Kelly, M. Zhang, J. Qing, Y. Lin, Y. Wang, J. Wu, J. A. Dorale, Z. An, and Y. Cai (2004), Timing, Duration, and Transitions of the Last Interglacial Asian Monsoon, *Science*, *304*(5670), 575–578, doi:10.1126/science.1091220.

Zangrando, R., E. Barbaro, P. Zennaro, S. Rossi, N. M. Kehrwald, J. Gabrieli, C. Barbante, and A. Gambaro (2013), Molecular Markers of Biomass Burning in Arctic Aerosols, *Environmental Science & Technology*, *47*(15), 8565–8574, doi:10.1021/es400125r.

Zennaro, P., N. Kehrwald, J. R. McConnell, S. Schpbach, O. Maselli, J. Marlon, P. Vallelonga, D. Leuenberger, R. Zangrando, and A. Spolaor (2014), Fire in ice: two millennia of Northern Hemisphere fire history from the Greenland NEEM ice core, *Climate of the Past Discussions*, *10*(1), 809–857.